FACULTY OF AGRICULTURAL SCIENCES

Institute of Agricultural Sciences in the Tropics (Hans-Ruthenberg-Institute)

University of Hohenheim

Agronomy in the Tropics and Subtropics

Prof. Dr. Georg Cadisch

Compound-specific ^{13}C fingerprinting for sediment source allocation in intensely cultivated catchments

Dissertation

Submitted in fulfillment of the requirements for the degree

"Doktor der Agrarwissenschaften"

(Dr.sc.agr. / Ph.D. in Agricultural Sciences)

to the

Faculty of Agricultural Sciences

presented by

Christian Brandt

Wolfen

2018

This thesis was accepted as doctoral dissertation in fulfilment of the requirements for the degree "Doktor der Agrarwissenschaften" (Dr. sc. Agr. / PhD in Agricultural Sciences) by the Faculty of Agricultural Sciences at University of Hohenheim on April 25, 2018.

Date of oral examination: November 23, 2018

Examination Committee

Head of the committee	Prof. Dr. Stefan Böttinger
Supervisor and Reviewer	Prof. Dr. Georg Cadisch
Co-Reviewer	Prof. Dr. ir. Pascal Boeckx
Co-Supervisor	PD Dr. Frank Rasche

Acknowledgements

I am hugely indebted to the many wonderful individuals who played indispensable (though often underappreciated) roles in the creation and completion of this thesis. I am utterly amazed that I finished this thing at all and simply cannot imagine how I would have ever finished it without your encouragement and support that kept me going.

I wholeheartedly thank Georg Cadisch for having accepted me as his student, providing the unique opportunity to dive deep into an unknown area of knowledge and giving me the hand that is needed to emerge again. The level of trust and the generosity of time he gave me are extraordinary. The thought of his words that: "finishing a doctoral thesis has a value that is much greater than a pure career building block", has motivated me again and again and will always stick with me. I am very grateful to Frank Rasche for encouraging me to take on this project in the first place but also for his constant trust and backing, profound scientific and editorial advice, as well as his unwavering enthusiasm and confidence that the work will be finished sometime. I've been very fortunate to have Frank as my direct supervisor.

For introducing me to the strangely beautiful world of R, I'd like to thank Holger Fröhlich. Without Holger's inspiring enthusiasm, data analysis would have been a much more daunting experience. I very much appreciate the fruitful discussions with Thomas Hilger and Carsten Marohn. Their expertise and encouragement have helped me in various ways. I thank Gerd Dercon, who, with his great and contagious enthusiasm has given me the feeling of being an important part of something bigger. I wish to express my gratitude also to Moncef Benmansour. Without his great expertise, downright helpfulness and friendliness we would not have been able to conduct research work with radionuclides in such a short time. I am very glad and grateful that I had the opportunity to talk to Max Gibbs about the actual application-based history of the CSSI fingerprinting method in New Zealand. His tremendous knowledge and commitment to improving water quality is inspiring. I want to thank Pascal Boeckx, Samuel Bodé and Dries Huygens for allowing us to work with their data and for their constructive feedback and inspiration on method development. I am grateful to Pascal for acting as my external reviewer and examiner. I thank Nguyen Thanh Lam for his great support in planning and organizing the two field campaigns in Vietnam. I am grateful to Elke Dachtler for her steadfastly humorous handling of a very obstinate isotope measuring device and her everlasting helpfulness. Wolfgang Armbruster literally always took the time when I needed him to answer

my newbie questions or allow me to make isotope measurements on short notice possible. I greatly benefited from his expertise and generosity. Although Julia Pöhlitz and Leander Walz have sometimes troubled me with their critical questions, their unbiased view has greatly improved this work, for which I am grateful to both. I thank Gabi Kircher for being the big-hearted person in the world. We can all be very grateful for having her in our institute. A life without a well-organized laboratory is possible but meaningless. Therefore, I would like to express my thanks to Stefan Becker-Fazekas who kept the lab running when I started and to Carolin Röhl who has taken on this difficult task. A big hug and heartfelt thanks goes to Linh Phan, who incredibly assisted me during my second field campaign. Linh, with her charming way, has made sure that I eat and drink enough and do not work under the blazing sun for too long. She kept me organized in the chaos that field work can be and told me how to cook Bánh cuốn. While I cannot begin to thank everybody, I am utterly grateful to all the people, friends and colleagues who made and continue to make this institute such a welcoming, solidary and uniquely human environment, where I can look forward each day to learning something from someone smarter than me.

Finally, I want to thank my parents and family who gave me the freedom and encouragement to pursue a life guided by interest in everything. Without Sabine's persuasive powers and exceptional support and encouragement, I might well not have had the fortitude or patience to persist with this thesis. That acknowledgement goes further than gratitude. Thanks also to my smart, brave and humorous daughter Carla, who is a living marvel in herself. You two make my world more beautiful and interesting.

Table of contents

Abbreviations

^{137}Cs	caesium-137
$^{210}Pb_{ex}$	unsupported lead-210
Bq	becquerel is the SI derived unit of radioactivity
C_3	Calvin cycle
C_4	Hatch–Slack cycle
CAM	Crassulacean acid metabolism
CFCS	constant flux constant sedimentation dating model
CHK	Chieng Khoi catchment in Vietnam
CSSI	compound-specific stable isotope analysis
CRS	constant rate of supply dating model
CV	coefficient of variance
$\delta^{13}C$	$^{13}C/^{12}C$ ratio (in ‰)
DCM	dichloromethane
EA-IRMS	elemental analysis-isotope ratio mass spectrometer
FA	fatty acids
FAME	fatty acid methyl ester
FRN	fallout radionuclides
GC-C-IRMS	gaschromatography-combustion-isotope ratio mass spectrometer
LOESS	locally weighted scatterplot smoothing
LOS	Los Ulmos catchment in Chile
LUC	land use category
LUT	land use type
Mcf	1000 cubic feet, a unit of measure in the oil and gas industry
MCMC	Markov chain Monte Carlo
MYB	My Bouchta catchment in Morocco
NAC	Nacimiento catchment in Chile
NER	net erosion rates
POP	Popovskiy Pond catchment in Russia
SIAR	Stable Isotope Analysis in R (statistical computing package)
SIMM	stable isotope mixing models
VPDB	Vienna Peedee Belemnite (^{13}C standard)
XIN	Xinzheng catchment in China

Chapter I General Introduction

1.1 Overview

In view of population growth in less developed countries, the consequences of global warming, depletion of useable freshwater resources, loss of arable land due to soil degradation, erosion and pollution, many regions of the world will encounter serious challenges to the maintenance or achievement of sustainable food security (WWAP (UN *World Water Assessment Programme)*, 2012). Increased rural population density is generally associated with smaller farm size which leads to agricultural intensification by increased fertilizer use per hectare, which ultimately results in a lasting decline in soil fertility (Leigh Josephson et al., 2014, Ricker-Gilbert et al., 2014). This soil crisis is worsened when crop production is expanded to shallow soil of greater vulnerability. Soil erosion is one of the most important constraints on food security in less economically developed countries (Pimentel, 2006; Scherr, 1999). Soil erosion caused by rain not only leads to a loss of fertile topsoil (on-site effects) but also to detrimental consequences far from the site of eroding soil, such as siltation of reservoirs and disruption of aquatic ecosystems (off-site effects).

In particular, in upland regions of Southeast Asia (e.g., Northwest Vietnam), intensified agriculture has been induced by political incentives, demographic shifts and increasing pressure of a global market for agricultural products. Hence, farmers expanded crop cultivation into marginal forested upland regions, where large scale cultivation of high yielding maize and cassava varieties was introduced (Valentin et al., 2008). As a consequence of resulting loss of soil cover and intensive soil tillage, severe erosion on steep slopes was induced resulting in associated soil degradation through soil relocation (e.g., SOC, nutrients) from uplands to lowlands (Dung et al., 2008; Lam et al., 2005; Pansak et al., 2008; Tuan et al., 2014). Soil relocation processes increased sedimentation yields in paddy rice fields and local reservoirs and enhanced sediment loads in aquatic waterways (Dung et al., 2009; Lippe et al., 2014; Schmitter et al., 2012).

1.2 Land use transformation

1.2.1 Disruption of ecosystem integrity as consequence of land use transformation

Humans have been interacting with their environment in the most complex way to satisfy their basic needs and to improve their standard of living since we have evolved. Over many millennia anthropogenic interactions have greatly altered the biosphere. The clearing of forests for farmland, firewood and building materials is one of the most obvious and consequential anthropogenic land-use changes (Hughes and Thirgood, 1982). The Neolithic Revolution, when agriculture originated independently in multiple areas around the globe, allowed hunter-gatherer communities to become sedentary and harvest more calories per area compared to their previous lifestyle. Early civilizations typically developed along the fertile banks and valleys of rivers (e.g. Tigris, Euphrat, Jordan, Nile, Indus, Yangtze and Yellow River) were it was easy to divert water for irrigation or pursue trade with other settlements along the waterways. For example, when wet rice agriculture was introduced to the Red River Plain, in present day Vietnam, during the Neolithic, shifts in the locations of settlements occurred from highlands to the fertile lowlands, which extended seawards with alleviation (Nishimura, 2005). The fertile soil in this area has not only made the Red River Plain the densest but also the longest populated of all the lowland plains of Mainland Southeast Asia (Nishimura, 2005). The Neolithic Revolution was a pivotal event in humanity that, however, came with high costs for the natural environment, including removal of natural vegetation and deforestation, loss of biodiversity and an increase in soil degradation and erosion.

The integrity of an ecosystem encompasses a wide set of criteria, including by stresses from human activity unimpaired structure, composition and function of the ecosystem; intact and self-sustaining natural ecological processes; the capacity for self-renewal and the maintenance of biodiversity. When an ecosystem loses the ability to sustain its organization in changing environmental conditions, its integrity is at risk. The conversion of natural ecosystems has multiple, complex and often harmful effects on ecosystem integrity and consequently ecosystem functions, i.e. biotic and abiotic processes that take place in an ecosystem and are intrinsically worth protecting. The impairment of ecosystem functions may yield in negative consequences on the provisioning capacity of supporting services (e.g. primary production and nutrient cycling), provisioning services (e.g. raw materials, genetic resources), regulating services (e.g. carbon sequestration and waste decomposition), and cultural services (e.g.

recreational experiences and heritage value). Essentially ecosystem services provide life support services necessary for the survival of both humans and animals and should at least be preserved for reasons of human self-preservation. In the past unsustainable rates of resource consumption, have had serious consequences for the well-being of the people, sometimes resulting in the collapse of societies (e.g., Diamond, 2005). Today, globalization and trade have much reduced the risk of social breakdown as a result of ecological degradation (Raudsepp-Hearne et al., 2010). Contrastingly, the Millennium Ecosystem Assessment (MA) found that although most ecosystem services are deteriorating, globally human well-being is increasing (MA 2005). Raudsepp-Hearne et al. (2010) suggested three hypotheses to explain this paradox, (i) human well-being is dependent on food services, which are increasing, and not on other services that are declining; (ii) technology has decoupled well-being from nature and (iii) time lags may lead to future reductions in well-being.

Changes in land-use not only impact on-site ecosystem function but also those off-site, which are always external and often at great distance to the land directly affected by the decision (Sinclair, 1999, van Noordwijk et al., 2004). Off-site effects of land-use change, especially soil erosion may have serious consequences at the landscape, regional or global scale. Re-allocation of sediment can lead to siltation of natural watercourses, irrigation systems and reservoirs as well as the disruption of aquatic ecosystems and contamination of drinking water. Suspended sediments can block out the sunlight that is vital to the submerged aquatic vegetation, which produces oxygen and provides a habitat for aquatic organisms. Detrimental eutrophic conditions are created when suspended sediments in conjunction with excessive nutrients lead to hypoxic conditions in freshwater or coastal marine ecosystems. Suspended sediments also have detrimental effects on the survivorship of juvenile corals.

A negative on-site effect of an ecosystem function is the degradation of soil fertility through continuous mono-cultural cropping and an associated increase in soil erosion. Soil organic carbon (SOC), a key determinant of soil structure, water infiltration capacity and therefore a risk-reducing factor of soil erosion is central to soil quality and soil fertility (Young, 1997). The SOC content is determined by numerous factors, such as geologic parent material, temperature and moisture conditions, clay content and cation exchange capacity (Dawson and Smith, 2007). Quantity and quality of carbon inputs are mainly controlled by the type of land use and consequently greatly affected by land-use changes and fragmentation. Highest input rates of carbon to the soil are often found in forest systems and grasslands, while low input

rates are common for crop lands. Carbon inputs in crop lands are restricted by various factors. In contrast to forests and grasslands that have year-round carbon inputs, the potential duration of carbon inputs in crop lands is limited to the crop growing season. The removal of harvest products and crop residue further depletes the potential carbon inputs. Tillage further increases SOC loss by altering the temperature and moisture conditions of the soil. It may also break up soil aggregates and exposes protected organic C to weathering and microbial breakdown (Smith, 2008).

1.2.2 Land use transformation in the Northwest of Vietnam

The mountainous northwestern part of Vietnam, also known as Tây Bắc ("Northwest") is one of the country's eight administrative regions. The Northwest is home to many ethnic groups, including Kinh, Tay, Thai, Muong, H'Mong and Dao. Chieng Khoi, the community where the main part of this study was conducted, is the home of the Tai Dam.

The Tai Dam (engl. *Black Thai*), are an ethnic group predominantly from northwest Vietnam and Laos. The name is a reference to the traditional black clothing. Being descendents of the Tai peoples of Thailand and Laos, the Tai Dam settled in the northwestern highlands in the first centuries AD. With an estimated 400,000 people, this group represents a large population share in northwest Vietnam (Sikor, 2004). Before the independence from French colonization in 1954 the Tai Dam lived exclusively from subsistence agriculture. Composite swiddening cultivation, a relatively sustainable and resilient form of land use, was used for centuries (Rambo and Vien, 2001; Sikor, 2004; Lam et al., 2005, Dung et al., 2008). Terraced paddy rice cultivation was practiced in the valleys, while upland rice and supplementary crops were cultivated on the surrounding slopes. When soil fertility declined, old upland fields were abandoned, and forest was cleared for the establishment of new fields. Hard-to-reach highlands and lack of transport infrastructure made it very difficult to trade with distant villages or even neighboring regions. After independence in 1954, the Vietnamese government integrated Tai Dam villages into the state structure, nationalized forests in 1955 and promoted agricultural collectivization in 1960 (Sikor, 2004). The state decreed that slope areas with more than 20 degrees incline would only need to be used for forestry under state-management. That included extensive upland areas that were previously managed freely by the Tai Dam. During the coming decades, it became increasingly clear that across northwestern Vietnam state restrictions on the use of the highlands have been unsuccessful. In the late 1980s, as a result of the economic

problems that are the result of agricultural-collectivization and the growing influence of the free-market economy, a government policy of liberalization known as doi moi has emerged (Sikor, 2004). In the early 1990s, when land relations resembled those that had existed before agricultural collectivization, a new legislation promoting exclusive and territorial land rights was introduced. Contradicting the very notion of people's lived land relations, the implementation of this legislation was fiercely resisted by the Tai Dam (Sikor, 2004; Fforde and de Vylder, 1996). As a result of failed enforcement of land allocation and forest protection contracts, the further expansion of agricultural land into forestry areas could not be prevented. During the 1990s, market expansion and lifting of domestic trade barriers resulted in significantly increased agricultural production and living standards. Villagers gained access to new seed varieties of rice and maize, increasingly affordable and available mineral fertilizer and were permitted to trade the harvest to lowland feed mills (Sikor and Truong, 2002). Lippe et al. (2011) suggested that the use of fertilizers and hybrid crop varieties were masking the effect of ongoing soil fertility decline and indicating a resource overuse that may become increasingly irreversible without external interventions.

The agricultural intensification that followed *doi moi* led to a renewed regeneration of forests during the 1990s. In 1998, along with other pivotal regions of Vietnam, commercial logging in natural forests in the northern highlands was banned (Sikor, 2004). Although Vietnam has seen a total increase in forest cover since the early 1990s, the rate of decline in old primary forest between 1990 and 2015 was the second highest worldwide and was only surpassed by Nigeria (FAO, 2015).

Today, rainfall and surface runoff induced soil erosion is one of the most pressing environmental and agricultural challenges in the mountainous northwestern part of Vietnam (Lal, 2004; Valentin et al., 2008). The abandonment of shifting cultivation in favor of extensive mono-cultural cropping systems, primarily maize (*Zea maize* L.), has led to soil retrogression and degradation in these regions (Yen et al., 2013, Podwojewski et. al., 2008; MSEC, 2000). Rainfall and surface runoff produce staggering soil erosion rates resulting in fast declining soil fertility and water availability on intensively cultivated slopes (Lal, 2004; Valentin et al., 2008). For example, in the Chieng Khoi catchment, erosion on steep slopes causes a loss of fertile top soil of up to 174 t $ha^{-1}yr^{-1}$ (Dung et al., 2008; Lam et al., 2005; Pansak et al., 2008; Tuan et al., 2014), along with accelerated sedimentation of paddy fields, local reservoirs and rivers (Dung et al., 2009; Lippe et al., 2014; Schmitter et al., 2012). Quang et al. (2014) suggested that reducing soil losses of 30 t $ha^{-1}yr^{-1}$ for maize fields and 27 t $ha^{-1}yr^{-1}$ for cassava fields would

require incentive payments to farmers of about 12–16 USD per ton of soil saved, which equals to 180–250 USD $ha^{-1}yr^{-1}$.

1.3 Carbon stable isotopes

1.3.1 Stable isotope chemistry

Isotopes are nuclides that have the same number of protons (*Z*) and position in the periodic table and virtually identical chemical behavior but with differing numbers of neutrons (*N*) and physical properties. Frequently used natural carbon isotopes exist in three species. Carbon-12 (^{12}C) contains six neutrons in addition to its six protons, while carbon-13 (^{13}C) has an additional neutron. Both ^{12}C and ^{13}C are energetically stable and exhibit no tendency to decay if left alone and are therefore referred to as stable isotopes or stable nuclides. The rarely occurring and energetically unstable Carbon-14 (^{14}C) isotope consists of eight neutrons in its nucleus. Unlike the stable isotopes ^{12}C and ^{13}C, ^{14}C decays voluntarily into other elements and is therefore referred to as radioisotope or radionuclide. The 84 naturally existing elements occur as 339 isotopes, including 269 stable isotopes, and 70 radioisotopes. Although many allegedly stable isotopes have never been observed to decay, theory suggests that they are radioactive, with very long half-lives. Isotopes tend to be unstable when *N* and *Z* are comparatively disparate ($N/Z \geq 1.5$). The more abundant isotopes of a chemical element have one or two neutrons less than protons, and thus are lighter than the less abundant isotopes of the same element. While light and heavy isotopes can react freely with one another in chemical and physical processes, the strength of intra- and intermolecular forces differ causing different reaction times. Consequently, isotopic fractionation of the light and heavy isotopes occurs between the reactant and product in physical and biological reactions. Fractionation creates shifts in the isotope ratio and thus provides an isotopic signal that can reveal the existence or magnitude of key processes in elemental cycles. Isotopes of lighter, biologically prevailing compounds are predestined for ecological research, since the relative increase in mass caused by the addition of a single neutron is greatest for these elements (Sulzman, 2008).

The most profound and consistent source of variation in the carbon stable isotopic composition of plants derives from the different photosynthetic CO_2 fixation pathways. These are the Calvin cycle (C_3), Hatch–Slack cycle (C_4) and Crassulacean acid metabolism (CAM) photosynthetic pathways (O'Leary, 1988). C_3 plants generally have $^{13}C/^{12}C$ isotope ratios, referred to as $\delta^{13}C$ values of around −35‰ to −20‰, whereas C_4 plants have a $\delta^{13}C$ range of about −18‰ to −7‰,

with the resulting soil organic $\delta^{13}C$ reflecting the respective photosynthetic process (Smith and Epstein, 1971).

Furthermore, the ratio of intercellular CO_2 pressure to ambient atmospheric air pressure determines the degree of ^{13}C discrimination during photosynthetic CO_2 fixation (Farquhar et al., 1989). When stomatal conductance decreases, intercellular CO_2 pressure decreases resulting in less negative $\delta^{13}C$ values (Farquhar et al., 1989; Wang et al., 2010). Stomatal closing during dry stress results in less CO_2 pressure within the leaf, resulting in less discrimination of $^{13}CO_2$ to the preferred $^{12}CO_2$ by Ribulose-1,5-bisphosphate carboxylase oxygenase (Rubisco) (Ainsworth and Long, 2004; Farquhar et al., 1989; Wang et al., 2010). Global surveys of ^{13}C over altitudinal gradients have shown an increase of ^{13}C with increasing altitude (Körner et al. 1988). A possible explanation might be the decrease in atmospheric pressure of CO_2 and O_2, as well as temperature, resulting in greater evaporation and finally in stomata closing (Hultine and Marshall, 2000; Wei and Jia, 2009; Wang et al., 2010).

Another factor for carbon isotope discrimination is increased soil strength, i.e. the capacity of soil to resist deformation measured in megapascals (MPa), as a result of reduced soil moisture levels and external pressure to the soil. Masle and Farquar (1988) reported that carbon isotope discrimination decreases with increasing soil strength because of both an increase in photosynthetic capacity and a decrease in stomatal conductance.

1.3.2 Compound-specific stable isotope analysis

Isotopic measurements of organic matter employing elemental analyzers coupled to isotope ratio mass spectrometers are fast and reproducible. There is, however, a crucial inherent limitation associated with analyzing bulk samples that derives from the chemical heterogeneity of organic matter. Even simple organic samples contain a variety of chemical compounds, e.g. phospholipid fatty acids, long-chain n-alkanes and lignin phenols. The conversion of complex samples to simple and equalized analyte gases (CO_2 and N_2) by high temperature combustion of bulk samples results in a complete loss of information on differences in isotopic composition between different chemical compounds. While an abundance of valuable data is being revealed by this process, much potential information is also concealed (Glaser, 2005). The compound-specific stable isotope (CSSI) analysis provides a solution to the limitations of bulk isotopic analysis. This technique typically consists of a chromatograph (gas or liquid) coupled to a mass spectrometer via a combustion interface (GC-C-IRMS) (Hayes et al., 1978). Samples are separated using task-specific capillary columns and identified based on their retention times.

Instead of the information of a single measurement, obtaining the values of a suite of compounds, as provided by CSSI, enables a more comprehensive insight of each individual sample.

The specific steps for preparing and analyzing soil and sediment samples for CSSI analysis as performed for this study are detailed in Chapter 2. The general steps are: (i) drying and sieving of samples; (ii) extraction of soil lipids; (iii) fractionation; (iv) derivatization of fatty acids (FAs) to fatty acid methyl esters (FAMEs) to allow a chromatographic detection of FAs; (v) analysis of FAMEs by GC-C-IRMS.

1.3.3 Stable isotope mixing models

In addition to the improvement of analytical techniques, the continuing progress of the capabilities and sophistication of stable isotope mixing models has also contributed to this. Isotope mixing models convert the isotopic data into estimates of proportional contributions of the different components of a source (Phillips et al., 2014). The earliest isotope mixing models were only capable of providing a single solution, neglecting uncertainty to account for variability of isotopic values and measurement error. Phillips and Gregg (2001) introduced sources of uncertainty and variation in the IsoError mixing model to provide propagation of error calculations. To account for significant differences in elemental concentrations between sources, concentration-dependent equations were later featured in the IsoConc model (Phillips and Koch, 2002). A constraint of early stable isotope mixing models was their ability to only partitioning two or three sources. This restriction was overcome by the development of the IsoSource mixing model (Phillips and Gregg, 2003), which enabled the partition of numerous sources.

Stable isotope mixing models that are based on Bayesian inference allow incorporating uncertainties, concentration-dependence and larger number of sources, which generates potential dietary solutions as true probability distributions (Phillips et al., 2014). Bayesian stable isotope mixing models are based on a Markov chain Monte Carlo (MCMC) model fitting. MCMC algorithms draw many random samples from a normal distribution, and calculate the sample mean of those. This is achieved by constructing a Markov chain. Each random sample acts as chain link to generate the next random sample. While each new sample depends on the one before it, new samples do not depend on any samples before the previous one. The quality of the sample increases with increasing number of steps (Ravenzwaaij et al., 2018). The estimated values of the parameters are known as posterior distributions,

representing a true probability density for the parameters of interest. Phillips et al. (2014) provide a comprehensive overview Bayesisan stable isotope mixing models including MixSIR (Moore and Semmens, 2008; Ward et al., 2010), SIAR (Parnell et al., 2010), MixSIAR (Stock and Semmens, 2013), IsotopeR (Hopkins and Ferguson, 2012), and FRUITS (Fernandes et al. 2014).

1.3.4 Carbon stable isotopes for ecological applications

Many biological and geochemical processes are accompanied by fractionation, i.e., changes in stable isotope ratios. Thus, distinct gradients of stable isotopes are maintained between components in any ecosystem as well as between ecosystems making them effective tracers of ecological processes (Michener and Lajtha, 2007). Ecological investigations may use the natural abundance of stable isotopes, i.e. naturally occurring levels; and at enriched levels. As their isotopic value is determined by abiotic conditions and the biochemical discrimination against $^{13}CO_2$ during photosynthesis $\delta^{13}C$ values are especially valuable as an ecological index of plant function. Therefore, $\delta^{13}C$ tracer are particularly useful to study the dynamics of soil carbon from years to centuries and thus to understand the consequences of anthropogenic land use change (e.g. Cadisch et al., 1996). C and O isotopes allow tracing the CO_2 flux in the soil-plant-atmosphere continuum (Flanagan and Ehleringer, 1998). This application requires sufficiently contrasting isotopic signatures of the sources and sinks in question. When using $\delta^{13}C$ values of bulk SOC this method is restricted to systems where plants of different CO_2 fixation pathways (i.e. C_3, C_4 and CAM) are present or have recently been present (Dawson et al., 2002). The compound-specific stable isotope (CSSI) analysis provides a solution to the limitations of bulk SOC isotopic analysis. Instead of the information of a single measurement, obtaining the values of a suite of compounds, as provided by CSSI, enables a more comprehensive insight of each individual sample.

1.4 Sediment fingerprinting

Sediment fingerprinting is based on the principle that different soil properties reflect the origin of sediments and soils. A wide range of physical (e.g. color, grain-size distribution), chemical (clay mineralogy, mineral-magnetism, geochemistry, fallout radionuclides, cosmogenic radionuclides, bulk stable isotopes and compound specific stable isotopes) and biological (pollen, enzymes) tracer properties have been tested either individually or in combination as

an integrated fingerprinting approach (Owens et al., 2016; Collins et al, 2017). Collins et al. (2016) provide a comprehensive overview of the development and current status of fingerprinting methods. For example, spectrometric quantification of sediment color is a rapid and inexpensive technique for indentifying sediment sources (e.g Grimshaw and Lewin, 1980; Barthod et al., 2015). Grain-size distribution is used to extract palaeoclimate information of deep-sea sediments by discriminating biogenic components of pedominantly intrabasinal origin, i.e. sediments form inside the basin; including chemical precipitates and most carbonate rocks, and of terrigenous origin (e.g. Kurashige and Fusejima, 1997; Weltje, 2012). Clay minerals in combination with trace elements and isotopic signatures ($^{87}Sr/^{86}Sr$; $^{143}Nd/^{144}Nd$) were used to discriminate the provenances of sediments in the Murray–Darling Basin, Australia, and to quantify the contribution of each tributary to the system (Gingele and De Deckker, 2005). A widely used method of choice to quantify sediment source contributions at the catchment scale uses geochemical properties of soils and sediments such as major elements (e.g. Douglas et al., 2003), trace metals metalloids, i.e. Cd, Cu, Pb, Zn, As (e.g Collins et al., 2013, Zhang et al., 2012), elemental ratios (e.g., Cu/Pb; Si/Al; Pb/Al) (Wang et al., 2009, Rowan et al., 2012) or rare earth elements (Xu et al., 2009; Collins et al., 2013). Fallout radionuclides (FRN; e.g., Cesium-137 (^{137}Cs), excess lead-210 ($^{210}Pb_{ex}$)) and also the cosmogenic radionuclide Beryllium-7 (^{7}Be) have proven most suitable for generating soil redistribution patterns at the catchment scale (Dercon et al., 2012; Mabit et al., 2008; Zapata, 2003). Bulk stable isotopes of carbon ($\delta^{13}C$) and nitrogen ($\delta^{15}N$) and the carbon to nitrogen atomic ratio (C/N) are indicators of the vegetation covering the landscape as well as plant management and can be used to distinguish sediments derived from sources with unique land-uses, land management, geomorphology and depth in the soil column (Fox and Papanicolaou, 2008). Nosrati et al. (2011) showed that soil enzymes, i.e. β-glucosidase and dehydrogenase, provide a complementary tool to currently existing sediment fingerprinting approaches. Brown (1985) suggested the use of pollen and spore concentrations to trace suspended sediment sources, e.g. eroding bedrock, channel banks, or hillslopes that have specific vegetation covers. The compound specific stable isotope (CSSI) technique uses land use cover-dependent differences in the $\delta^{13}C$ isotopic values of specific organic compounds (i.e., soil fatty acids (FA), *n*-alkenes) to estimate the proportional sediment contributions of different land use types (Chikaraishi and Naraoka, 2003; Gibbs, 2008; Mead et al., 2005; Ratnayake et al., 2011, Alewell et al. 2016, Blake et al., 2012; Brandt et al., 2016; Hancock and Revill, 2013, Reiffarth et al., 2016, Upadhayay et al., 2017).

Apart from the identification of pollen and spore concentrations (Brown, 1985), CSSI-fingerprinting is the only sediment fingerprinting approach that allows to trace sediment sources based on their specific vegetation cover. While pollen and spores fulfill some preconditions for suitable tracer, such as the transfer from plants onto soil, recalcitrance to microbial degradation and high mobility from source to sink, they have also significant shortcomings. A decisive disadvantage of pollen and spores against CSSI-fingerprinting using fatty acids or *n*-alkenes is the lack of aggregate formation with fine soil particles, which provides a clear link between sediment source and sink. Land use characteristic pollen and spores may also be carried away by wind, which possibly alters their concentrations on the land uses under investigation.

1.5 Objectives and Hypotheses

The main goal of this thesis was to further develop the CSSI – fingerprinting approach and statistical methods to identify land use types of heightened soil erosion in an intensely cultivated, tropical mountainous watershed, in order to provide a scientific basis for focused soil conservation measures. The specific objectives were to:

(i) Develop a statistical procedure to identify erosion prone land use types based on their proportional isotopic contribution to sediment deposition areas in a heterogeneous small agricultural catchment,

(ii) Evaluate the global applicability of the FA-based CSSI technique, using an aligned protocol, to detect hot spots of soil erosion across catchments of different agro-ecologies,

(iii) Integrate CSSI and FRN ($^{210}Pb_{ex}$, ^{137}Cs) to estimate past net erosion rates linked to land use types.

Corresponding to these objectives, the hypotheses tested in this thesis are:

(i) The CSSI analysis approach is suited to derive significant differences of individual soil FA $\delta^{13}C$ values in source soils allowing the clear distinction of various upland land use types. When bound to clay minerals and translocated by erosion, FAs with land use type specific $\delta^{13}C$ values enable the identification of source soil composition of sediments and hence the determination of SOC-related source-sink relationships at catchment levels smaller than one hectare.

(ii) Using an aligned protocol to distinguish major land use categories (i.e., forest, cultivated, non-cultivated land) allows a comparison of catchments of contrasting agro-ecologies. Further resolving of categories into specific land use types allows assessing the potential resolution threshold of the CSSI technique.

(iii) Integrating FRN-derived quantitative past sediment budgets with CSSI-calculated proportional soil contributions to the layers of a sediment profile would permit estimation of land use type-specific past net erosion rates. We further hypothesized that knowledge about past net erosion rates would provide critical insights into past soil redistribution, providing a way to evaluate the accelerating impact of specific land use change on soil degradation in heterogeneous agricultural catchments.

1.6 Outline of thesis

This thesis consists of five chapters. Following the general introduction (Chapter 1), the method development and testing of the CSSI technique will be described based on the example of the intensely cultivated Chieng Khoi catchment in Northwest Vietnam (Chapter 2). In Chapter 3 it will be discussed of whether the CSSI technique is applicable to catchments of contrasting agro-ecological zones and how to compare their often very different land use types. The combined use of CSSI and FRN (^{210}Pbex, ^{137}Cs) to estimate past net erosion rates linked to land use change will be explored in Chapter 4. Finally, the thesis closes with a general discussion (Chapter 5).

Chapter II Compound-specific $\delta^{13}C$ isotopes and Bayesian inference for erosion estimates under different land use in Vietnam[1]

Christian Brandt[a], Georg Cadisch[a], Lam T. Nguyen[b], Tran D. Vien[c], Frank Rasche[a]

[a]Institute of Plant Production and Agroecology in the Tropics and Subtropics, University of Hohenheim, Stuttgart, Germany

[b]Department of Environmental Management, Vietnam National University of Agriculture, Hanoi, Vietnam

[c]Center for Agricultural Research and Environmental Studies (CARES), Vietnam National University of Agriculture, Hanoi, Vietnam

[1]A version of this chapter was published as:

Brandt, C., Cadisch, G., Nguyen, L.T., Vien, T.D., Rasche, F., 2016. Compound-specific $\delta^{13}C$ isotopes and Bayesian inference for erosion estimates under different land use in Vietnam. Geoderma Regional 7, 311–322.

2.1 Abstract

Recent studies have pointed out the potential of the compound specific stable isotope (CSSI) technique based on long-chain fatty acids methylester (FAME) to identify hot spots of soil erosion by means of land use types. We tested the applicability of the CSSI technique on the basis of soil and sediment samples derived from a small agriculturally used catchment in Vietnam which is exemplary for many mountainous areas in Southeast Asia. Following CSSI analysis we set up a statistical decision sequence to identify hot spots of soil erosion by i) testing for significant differences between $\delta^{13}C$ values of fatty acids (FA) of different contributing land use types and thereafter ii) examining the data using a Monte Carlo simulation of mixing polygons to provide a quantitative basis for model rejection and exclusion for sediment samples which violate the point-in-polygon assumption and iii) applying a Bayesian model with a Markov chain Monte Carlo (MCMC) model fitting using "SIAR" (Stable Isotope Analysis in R), which produces simulations of plausible values and therefore representing a true probability density for the proportional contribution of source soils. Our results confirmed that there were significantly different $\delta^{13}C$ values for identical FAMEs extracted from soils under different land uses. Most fatty acids with significantly different $\delta^{13}C$ values were found between soils under C_3 (protected and secondary forest, teak and fruit plantations) and C_4 (maize) plants but also within different soils of land use types which consisted only of C_3 plants (e.g. protected forest, fruit plantation and teak). The resulting soil proportions were plausible for the six investigated sedimentation areas and suggested that fields under crop production such as maize and cassava, but also teak plantations were the main sources of eroding soil in the upland area surrounding the Chieng Khoi reservoir. Based on our data, we can conclude that the developed integrated Bayesian SIAR-CSSI approach represents a unique tool to identify and apportion soil sources to major land use types in small heterogeneous catchments by linking biomarkers of land use types to the sediment in deposition zones.

2.2 Introduction

Water erosion and accompanying loss of soil organic carbon (SOC) is a global driver of land degradation (Lal, 2003). Water erosion leads to a serious decline in soil productivity and crop production in intensively managed tropical mountainous catchments, where exceptional topographical and climatic conditions prevail (El-Swaify et al., 1982). In particular, in

mountainous regions of Southeast Asia (e.g., Vietnam, Thailand), land use intensification has been promoted by increased population pressure and agricultural commercialization. Hence, farmers expanded crop cultivation into marginal forested upland regions, where large scale cultivation of maize and cassava as cash crops was introduced (Valentin et al., 2008). As a consequence of resulting loss of soil cover and intensive soil tillage, severe erosion on steep slopes (up to 174 Mg $ha^{-1}yr^{-1}$) was induced resulting in associated soil degradation through soil relocation (e.g., SOC, nutrients) from uplands to lowlands (Dung et al., 2008; Lam et al., 2005; Pansak et al., 2008; Tuan et al., 2014). This soil relocation process increased sedimentation yields in paddy fields and in local reservoirs as well as enhanced sediment loads in rivers (Dung et al., 2009; Lippe et al., 2014; Schmitter et al., 2012).

To counteract this development and to design soil conservation measures at designated soil erosion hot spots, accurate analytical methods are required to trace predominant sources of soil erosion. So far, fallout radionuclides (FRN; e.g., caesium-137, excess lead-210, beryllium-7) proved to be most suitable for generating soil redistribution patterns at catchment scale (Dercon et al., 2012; Mabit et al., 2008). Although FRNs estimate accurately the quantitative sediment budget for a specific location, they do not assign a denudation rate to a specific upland land use type (Blake et al., 2012; Hancock et al., 2012).

Alternatively, lipid biomarkers (e.g., fatty acids (FA)) were recently introduced as promising indicators for tracking land use types (i.e., sources) that contribute to downstream sediment materials (Benowetz et al., 2006; Mead et al., 2005; Ratnayake et al., 2011). FAs are ubiquitous in soil and originate from root exudates, above ground plant biomass and microorganisms (Badri and Vivanco, 2009; Ibekwe and Kennedy, 1995; Wiesenberg et al., 2010). Due to their polarity, FAs are partially water soluble and after percolation into soil, they can form associations with clay minerals (Williams et al., 2006). The newly formed FA-clay mineral associations serve as a biomarker, which, after surface run-off and deposition in sedimentation areas, provide the link between eroding soil material from distinct land use types and respective sediments. An important criterion to use FAs as erosion biomarkers is their individual $\delta^{13}C$ isotopic signature creating a unique fingerprint which allows identifying erosion sources without relying on the amount of FAs present. It is worthwhile emphasizing that this isotopic signature does not alter to a great extent over time as non-degradative processes including volatilization, dilution, dispersion, and equilibrium sorption do not cause significant isotope fractionation (Blessing et al., 2008). Hence, it can be manifested that compound specific stable

isotope (CSSI) analysis based on long-chain FAs (i.e., C12:0 to C24:0) represents a major advancement to tackle source-sink relationships at catchment level (e.g., Chikaraishi and Naraoka, 2003; Gibbs, 2008).

Gibbs (2008) using the CSSI approach successfully assessed the contributions of soils under natural forest, pine forest, pasture, agricultural land and urban areas to sediment bodies in an estuary of the Mahurangi catchment (117 km²) in New Zealand. Blake et al. (2012) applied the CSSI approach in a small agricultural catchment (i.e., 145 ha, Furze Brook, UK) to successfully apportion the relative sediment contribution of harvested fields (maize, wheat), grasslands and forests to downstream sediments. Moreover, Hancock and Revill (2013) investigated the sediment provenances of the Logan River Basin in Australia (3860 km²).

Although these examples justify the successful application of FA-based CSSIs at larger catchment scales, their applicability was never corroborated in erosion prone small tropical catchments which are characterized by very heterogeneous land use types. Hence, we used a representative catchment in Northwest Vietnam with various annual and perennial crops, fruit trees and commercial and natural forests to test the hypothesis if the CSSI analysis approach is suited to derive significant differences of individual soil FA $\delta^{13}C$ values in source soils allowing the clear distinction of various upland land use types. We further hypothesized that, when bound to clay minerals and translocated by erosion, FAs with land use type specific $\delta^{13}C$ values enable the identification of source soil composition of sediments and hence the determination of SOC-related source-sink relationships at catchment levels smaller than one hectare. Our objective was thus to develop a statistical procedure to identify erosion prone land use types based on their proportional isotopic contribution to sediment deposition areas in a heterogeneous small agricultural catchment.

2.3 Materials and methods

2.3.1 Study area

The model catchment was located in the Chieng Khoi commune (21°7´60´´N, 105°40´0´´E), Son La province in Northwest Vietnam. The climate is characterized by tropical monsoons, with a rainy season from May to October and a relatively dry, cold season from November to April. The average annual temperature is 21°C, with a maximum of 27°C in August and a

minimum of 16°C in February (Thao, 1997). Average annual precipitation amounts to 1,110 mm (Hien et al., 1995).

The commune covers a total area of 3,189 ha and has an altitudinal range of 320 to 1,600 m above sea level (a.s.l.). Steep mountain limestone ridges and areas of more undulating hills characterize the topography of the catchment. The geological bedrock material derived from the Yen Chau Formation deposited during the upper Cretaceous period. The dominating bedrocks are made of limestone and schist (Bao, 2004). Upland soils in the Yen Chau area belong mostly to Ferralsols and Leptosols (FAO classification) (Wezel et al., 2002). Clemens et al. (2010) reported that the most common soil types within the upland area of the Chieng Khoi commune were characterized as Luvisols and Alisols (FAO classification). Leptosols were mostly found on top-slope position and showed considerable signs of severe soil erosion, especially on hills under maize production. Exposed parent rocks on hilltops as well as sheet and gully erosion on the upper and middle slopes are common for maize fields in the region. An irrigation lake was constructed to regulate the supply of water to downstream paddy rice fields in the catchment. It covers approximately 12% of the Chieng Khoi catchment. Originating from the dammed stream Doi Ban, the Chieng Khoi Lake of about 26 ha is situated in a karstic depression, surrounded by a chain of calcareous mountains and has a catchment area of about 207 ha. The stream was initially dammed in 1963, while the present concrete dam was finished in 1974. Elevation of the area around the Chieng Khoi Lake ranges from 429 to 493 m a.s.l. with slope steepness up to 86%. Since 1963, the primary forest decreased by more than 50% and nowadays almost 25% of the total catchment area is under agricultural use.

The Chieng Khoi catchment has been characterized by traditional shifting cultivation and secondary forests. The latter are 10 to 30 years of age and consist mainly of small deciduous broad-leaved trees mixed with bamboo and bushes. The remnants of the protected natural forests were never cultivated. In the last decades, most traditional shifting cultivation systems with fallow periods were replaced by permanent crop monocultures and commercial fruit trees and forests.

2.3.2 Sample collection

Characteristic land use types of the upland area surrounding the Chieng Khoi Lake were identified as potential soil source sites. These land use types included field crops such as maize (M; *Zea mays* L.) and cassava (C; *Manihot esculenta* Crantz) as well as commercial forests (T) consisting of teak (*Tectona grandis* L.) or Chukrasia (*Chukrasia tabularis* A. JUSS.).

Moreover, fruit tree plantations (FP) including mango (*Mangifera indica* L.), jackfruit (*Artocarpus heterophyllus* LAM.), tamarind (*Tamarindus indica* L.), and longan (*Dimocarpus longan* LOUR.) were determined. Furthermore, secondary (SF) and protected natural (PF) forests surrounding the lake were considered as potential sources of soil erosion.

Soil and sediment samples were collected in July to September 2010 and March to May 2012. At the time of sampling maize and cassava were cultivated either as mono crops or as maize-cassava intercrop. We obtained soil samples only from fields with monocrops. Crop-fallow rotation systems and also maize-cassava rotation systems were abandoned in favor for permanent cropping systems with high yield varieties in the 1990s. Top soil (0-2 cm) samples of each individual land use type were collected from at least 3 discrete plots of each land use type within the upland area around the Chieng Khoi Lake. In each plot, soil samples were obtained from 3 different positions (e.g., lower, middle, upper slope). At each position, 20 sub-samples from an area of 20 m^2 were combined to a composite sample of each land use. Collecting spatially-integrated mixtures allowed us to obtain representative soil samples of each land use type but the degree of variability in the source samples might still be under-estimated in most cases. Analyzing all individual sub-samples would have provided better insight on the variability of each CSSI value from that explicit land use type and improved most likely the interpretation and statistics using SIAR. However, these advantages stand in contrast to the analytical costs which would have been soared. Using spatially-integrated mixtures is therefore a trade-off between the determination of the degree of spatial variability of CSSI values and analytical costs which are necessary to meet the research objectives.

At 7 distinct deposition areas (Fig. 2.1; Area A to F) top sediment layer samples (0-2 cm) were obtained by combining 20 sub-samples from an area of 20 m^2 to ensure a representative sample. Bulked soil and sediment samples were dried at 50°C directly after sampling, disaggregated, sieved (2-mm) and maintained under dry and dark conditions. **Area A.** This part of the Chieng Khoi Lake was surrounded by extended M, C, M x C intercropping systems as well as M x FP agroforestry systems. At higher elevations, SF and T were predominant. T was present only to a minor extent and showed pronounced rill erosion. **Area B.** The central area of the western part of the lake was surrounded by cropping systems (M, C, M x C intercropping), SF and T. **Area C.** This area was dominated by cropping systems (M, C, M x C intercropping), but is also partly influenced by T, FP and SF. To allow a more detailed observation of different erosion pathways, area C was split into sub-areas C_1 and C_2. **Area D.** An extended part of FP and SF

characterized the north and west slopes of this area. The east slopes were dominated by M, C, and M x C intercropping as well as agroforestry systems with FP. T was only of minor importance. **Area E.** This area was mostly surrounded by SF and only to a minor extent by M x C intercropping systems as well as T and FP. **Area F.** Located in the southwestern part of the lake, this area was closest to the remaining parts of PF. Cropping (M, C, M x C intercropping) was dominating. Areas of the defined land use types were estimated using the "Google Maps Area Calculator Tool" (http://www.daftlogic.com/projects-google-maps-area-calculator-tool.htm, 2015).

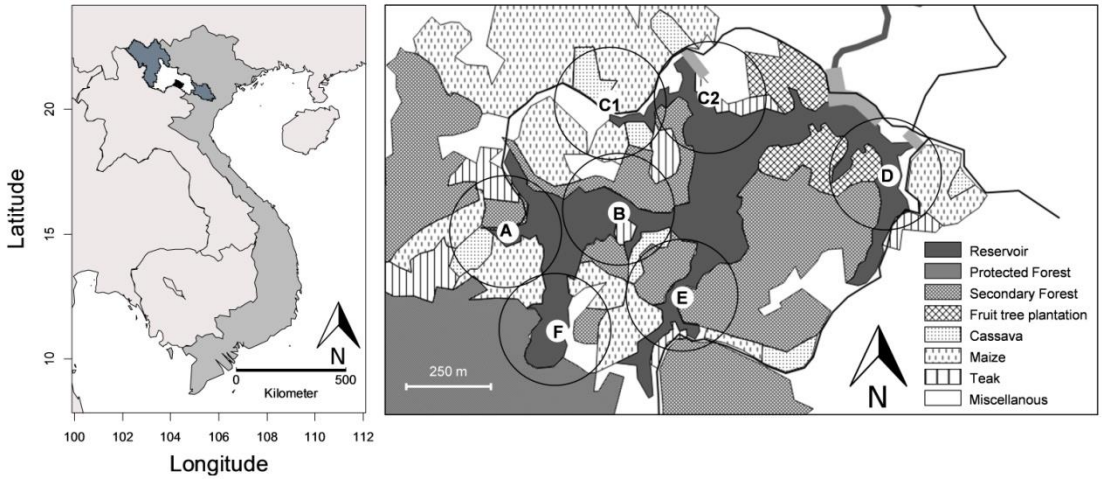

Fig. 2.1 Location map of Chieng Khoi Catchment in Son La Province, Northwest Vietnam. Encircled and labelled from A to E are the investigated sedimentation areas.

2.3.3 EA-IRMS analysis

Bulk carbon (C) isotopic ratios ($\delta^{13}C/^{12}C$) and organic C content of soil and sediment samples were determined using a Euro EA 3000 elemental analyzer (Hekatech, Wegberg, Germany) connected to a Delta plus XP mass spectrometer via a Conflo III Interface (Thermo Finnigan MAT, Bremen, Germany). Inorganic carbonates were removed previously with 1 M hydrochloric acid to detect only the $\delta^{13}C$ values of organic C components in soil and sediment samples. Samples were then oven-dried at 70°C until constant weight, ball-milled and analyzed. $\delta^{13}C$ was calculated by expressing the measured ratios (R_{sample}) against the international Pee Dee Belemnite (PDB) standard (R_{PDB}):

$$\delta^{13}\,C_{sample}(‰) = \left\{\left(\frac{R_{sample}}{R_{PDB}}\right) - 1\right\} x10^3 \qquad (2.1)$$

2.3.4 Extraction, fractionation and derivatization of fatty acids

Extraction and analysis of fatty acids (FAs) was performed according to Blake et al. (2012) with some modifications. All glassware, evaporation needles and pipette tips were thoroughly degreased by double rinsing with dichloromethane (DCM) prior to use. Total lipids were extracted from 25 g dried and soil samples, sieved to <2 mm, using a 25 ml solvent mixture of DCM/methanol (9:1, v/v). Mixtures were shaken (Universal Shaker SM-30, Edmund Bühler GmbH, Hechingen, Germany) for 12 h. Extraction process was repeated to maximize lipid recovery. After each extraction step, the sample mixture was centrifuged at 1000 rpm for 10 min and the solvent mixture was decanted. Subsequently, the solvent mixture containing the extracted lipids was evaporated at 45°C under a gentle nitrogen stream (Techne, Bibby Scientific Limited, Staffordshire, UK). Solid phase extraction (SPE; Bond Elute-aminopropyl bonded silica gel cartridges, Agilent Technologies, Santa Clara, USA) was used to segregate the total lipids into an acid and neutral fraction (Blake et al., 2012). Prior to fractionation, cartridges were conditioned with 2 ml DCM followed by 2 ml of DCM:isopropanol (2:1 v/v). Concentrated extracts were re-dissolved in 3x 300 µl DCM/isopropanol (2:1, v/v) and transferred into the cartridges. The eluted neutral fraction was discarded, while the acid fraction was collected after re-extraction from the aminopropyl cartridge with 10 ml of 2% acetic acid in diethyl ether. After evaporation, the acid fraction was re-dissolved in 200 µl toluene and 1.5 ml of methanol. To allow a chromatographic detection of FAs, they were methylated with methanolic HCl (0.39 M) at 45°C for 14 h (Ichihara and Fukubayashi, 2010). After methylation, 1 ml H_2O and 2x 1 ml hexan was added and mixed. The subsequently formed hexane layer was transferred to a glass test tube and evaporated. Finally, the methylated FA fraction was re-dissolved in 200 µl isooctane for analysis by gas chromatograph mass spectrometry (GC-C-IRMS).

2.3.5 GC-C-IRMS analysis

A gas chromatograph (Agilent 6890, Agilent Technologies Inc, Santa Clara, USA) coupled to a Delta plus XP mass spectrometer via a Conflo III Interface (Thermo Finnigan MAT) was used to measure $\delta^{13}C$ signatures of methylated FAs (FAMEs). Samples were injected into a splitless injector at 250°C and separated using a Varian Factor Four VF23-MS fused silica capillary column (high cyanopropyl modified methyl polysiloxane; 30 m, 0.25 mm internal diameter, 0.25 µm film thickness; Varian Inc., Santa Clara, CA, USA). Hydrogen was used as

carrier gas, and the oven temperature was programmed from 50 to 100°C at 15°C min^{-1}, from 100 to 220°C at 1°C min^{-1}, and from 220 to 240°C at 15°C min^{-1}. FAMEs were identified based on their retention times using the *Supelco® 37 Component FAME Mix and the Supelco®* C8 – C24 FAME Mix (Sigma-Aldrich, St. Louis, USA).

2.3.6 Data processing and analysis

Sediment source ascription using CSSIs (e.g., FAMEs) requires that naturally abundant $\delta^{13}C$ values of FAMEs differ significantly between the source soils representing distinct land use types. The Tukey's HSD test was applied to determine these significant differences between $\delta^{13}C$ values of identical FAMEs among different source soils. The proportional contribution of each source soil to respective sediments was estimated by use of the mixing model SIAR (Stable Isotope Analysis in R) software package (Parnell et al., 2010). Initially, SIAR was developed for food web studies (e.g., Chouvelon et al., 2014; Kürten et al., 2014) and was used to apportion sources of nitrate in surface water (e.g., Gaouzi et al., 2013; Xue et al., 2012). To our knowledge, SIAR has, however, never been applied in the context of CSSI-based erosion studies.

SIAR uses a Bayesian model with a Markov chain Monte Carlo (MCMC) model fitting, which produces simulations of plausible values. The estimated values of the parameters are known as posterior distributions, representing a true probability density for the parameters of interest. A detailed description of SIAR can be found in Parnell et al. (2010).

An important advancement to precursory stable isotope mixing models in CSSI approaches (e.g., IsoSource; Blake et al., 2012; Gibbs, 2008; Hancock and Revill, 2013) is that the Bayesian approach of SIAR allows for uncertainty in all parameters including proportional contribution. Another important advantage is the calculation of diagnostic matrix plots which indicate the quality of source discrimination. A strong negative correlation between two posterior values strengthens the possibility of a close relationship of two sources. This negative correlation further indicates that only one of both sources contributes to the sediment mixture at the same time. Strong positive correlations show that apart from one particular source, another source is required to provide a reasonable modeling result (Inger et al., 2010; Parnell et al., 2010).

Prior to each model run, we assessed if it was likely that in SIAR every source contributed to the sediment mixtures. When this assumption was violated, it was traced back to an unknown soil source. Linear mixing models (e.g., IsoSource; Phillips and Gregg, 2003) use a discrete

mixing polygon to assess for point-in-polygon conditions. Consequently, the isotopic signature of the mixture must be located within a polygon enclosing the signatures of sources (Phillips and Gregg, 2003). SIAR, however, will always attempt to fit a model, even if the sources lie outside of the isotopic mixing polygon (Parnell et al., 2010). Thus, to enhance the plausibility of results, we examined the data prior to the SIAR runs using a Monte Carlo simulation of mixing polygons for the point-in-polygon test (Smith et al., 2013). Convex hulls ('mixing polygons') were iterated using the distributions of the CSSI values of FAMEs of the intended source soils. The proportion of polygons, which provide a solution (i.e., meet the point-in-polygon assumption), was then calculated. This provided a quantitative basis for model rejection and exclusion for sediments which lay outside the 95% mixing region. For source apportioning of the 7 sedimentation areas (i.e., Areas A to F), we included only those $\delta^{13}C$ values of FAMEs which were present in all sedimentation areas and which showed significant differences for as many as possible pair wise land use comparisons. Sediment samples which did not meet the point-in-polygon assumption were rejected from further analysis, i.e. sediment area F. Finally, the isotopic proportions of FAMEs were corrected to soil proportions (Equation 2.2). This conversion uses a linear correction equation based on the bulk C content of each source soil:

$$\%source_n = \frac{I_n / \%C_n}{\sum_n^1 (I_n / \%C_n)} x100 \qquad (2.2)$$

where I_n is the mean proportion of source n in the mixture as estimated from isotopic values of C by SIAR, and $\%C_n$ is the %C in the source n soil (Gibbs, 2008). Corresponding soil proportions are presented in Box-and-Whisker-plots (Fig. 2.4). The relation between proportional soil sediment contributions (%) of the investigated land use types and the estimated corresponding land use areas (ha) was calculated using the combined estimated sediment contributing land use type areas (ha) (e.g., forest (PF + SF)) of all sub catchments. The resulting area values were divided by the average proportional soil contribution (%) of the respective land use types (Fig. 2.5) to obtain a relative impact factor for land use type specific soil erosion.

2.4 Results

2.4.1 Fatty acid analysis and comparison of soil sources

According to the main land use types, surface soil samples were grouped into 6 erosion sources: PF (protected forest), SF (secondary forest), M (maize) and C (cassava), T (teak) and FP (fruit plantation). SOC (%), $\delta^{13}C$ of bulk C and FAMEs are shown in Table 2.1.

Table 2.1. Mean topsoil (0-2 cm) SOC (%) and $\delta^{13}C$ (‰) values for soil bulk carbon and topsoil-derived compound specific $\delta^{13}C$ (‰) values for identified fatty acids for each soil source, i.e. land use type. Mean (M), standard error (SE) and number of samples (No.) analyzed are included.

	Protected Forest			Secondary Forest			Maize			Cassava			Teak			Fruit tree plantation		
Fatty Acid (‰)	M	SE	No.	M	SE	No.	M	SE	No.	M	SE	No.	M	SE	No.	M	SE	No.
SOC (%)	2.90	0.25	8	1.60	0.13	18	0.84	0.05	31	0.66	0.05	18	1.15	0.09	20	0.92	0.09	11
Bulk $\delta^{13}C$	-26.76	0.14	8	-27.56	0.16	18	-23.98	0.25	31	-24.82	0.25	18	-26.28	0.21	20	-26.07	0.34	11
Lauric Acid (C12:0)	-30.21	0.38	9	-29.10	0.12	3	-28.14	0.35	10	-27.19	0.45	6	-27.95	0.29	9	-28.31	0.11	10
Tridecanoic Acid (C13:0)	-27.55	0.54	9	-27.85	0.47	6	-27.38	0.61	8	-24.27	0.13	6	-25.33	0.61	9	-27.30	0.76	4
Myristic Acid (C14:0)	-31.89	0.57	9	-31.00	0.31	6	-28.27	0.28	15	-28.38	0.42	10	-29.42	0.42	9	-28.97	0.26	10
Myristoleic Acid (C14:1)	-27.90	0.32	9	-28.37	0.59	3	-24.70	0.60	15	-24.47	0.49	4	-26.89	0.44	9	-26.37	0.30	10
Pentadecanoic Acid (C15:0)	-30.17	1.07	3	-29.40	0.32	3	-27.56	0.52	17	-27.53	0.84	3	-28.98	0.91	9	-28.16	0.28	10
cis-10-Pentadecenoic Acid (C15:1)	-29.25	0.79	3	-29.99	0.04	2	-28.70	0.40	15	-26.20	0.87	4	-31.18	1.39	9	-27.95	0.31	10
Palmitic Acid (C16:0)	-31.32	0.41	9	-32.77	0.84	9	-27.49	0.41	18	-26.87	0.37	12	-29.73	0.99	12	-27.29	0.15	10
Palmitoleic Acid (C16:1)	-28.41	0.25	6	-30.13	1.04	9	-25.76	0.62	15	-30.82	1.12	6	-28.68	0.40	12	-28.70	1.15	10
Heptadecanoic Acid (C17:0)	-28.07	0.11	4	-28.96	0.16	3	-24.83	0.99	7	-26.53	2.07	3	-27.88	0.64	9	-29.07	0.72	10
Stearic Acid (C18:0)	-29.71	0.27	5	-32.90	1.00	9	-27.14	0.31	18	-26.82	0.30	3	-28.90	0.46	12	-27.53	0.23	10
C18 comb	-29.56	0.19	18	-29.84	0.53	12	-27.38	0.46	30	-30.22	0.48	5	-29.10	0.21	21	-28.11	0.39	15
Arachidic Acid (C20:0	-34.12	0.77	6	-33.01	1.03	9	-28.49	0.57	15	-28.41	0.37	5	-32.41	0.68	12	-30.73	0.36	10
Behenic Acid (C22:0)	-34.19	0.43	9	-33.09	0.92	6	-29.50	0.38	15	-29.67	0.56	4	-33.06	0.75	12	-32.27	0.31	10
Lignoceric Acid (C24:0)	-34.69	0.76	3	-33.36	0.96	6	-29.15	0.71	6	-29.73	0.57	4	-33.43	0.66	9	-31.76	0.40	9

*C18 comb' comprises of C18:1 (Oleic acid) and C18:2 (Linoleic acid) whose individual $\delta^{13}C$ signatures could not be completely resolved for every sample.

The highest SOC values were found in PF soil (2.9%). SF (1.6%) and T (1.15%) soils contained less SOC which was attributed to anthropogenic activities such as former deforestation promoting SOC loss. Due to burning and removal of leaf litter, SOC in heavily managed soils was expectedly low, i.e. FP (0.92%), M (0.84%) and C (0.66%).

The relationship between topsoil-derived compound specific $\delta^{13}C$ (‰) values (mean values of all FAMEs) for identified FAMEs and for soil bulk C $\delta^{13}C$ (‰) was characterized by more depleted (3-4‰) compound specific $\delta^{13}C$ (‰) values. However, the general isotopic differences between the various land use types remained similar between both isotopic values (Fig. 2.2).

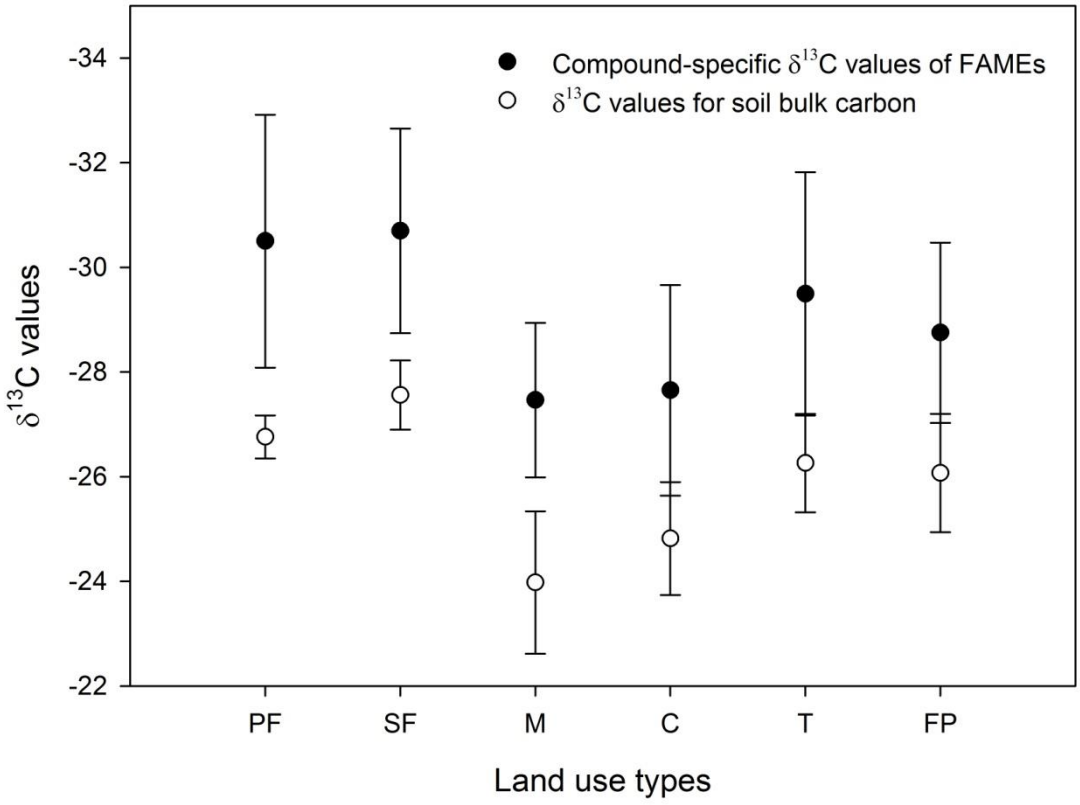

Fig. 2.2. Scatterplot showing the relationship between topsoil-derived average compound specific $\delta^{13}C$ (‰) values for identified fatty acidsand for soil bulk carbon $\delta^{13}C$ (‰) values under different land uses. Abbreviations: cassava (C), fruit tree plantation (FP), maize (M), protected Forest (PF), secondary forest (SF), teak (T).

To check for significant differences of $\delta^{13}C$ values of bulk C and FAMEs between soils from all investigated source plots, we used the Tukey HSD test (Table 2.3). For $\delta^{13}C$ values of bulk soils, significant differences were found for 10 out of 15 possible land use pairs. The largest

differences were determined for SF vs. M, SF vs. C, PF vs. M, M vs. FP and M vs. T (p <0.0001), as well as PF vs. C and T vs. C (p <0.001). No significant differences were found for SF vs. PF, PF vs. FP, PF vs. T, M vs. C and FP vs. T (p >0.05).

The selection of suitable FAMEs for SIAR-based land use source identification was done on basis of their discriminatory power of their individual $\delta^{13}C$ values and occurrence in all sediments. This step was performed regardless of the commonness or concentration of FAMEs. Sixty-eight out of 210 pair wise land use comparisons revealed a difference in their $\delta^{13}C$ signature for individual FAMEs (p <0.05) (Table 2.2). As expected, the majority of FAMEs showed a clear distinction between the $\delta^{13}C$ signatures of C_3 and C_4 plants. Greatest distinction was found for PF vs. M (C14:0, C16:0, C18:0, C20:0, C22:0, C24:0 (p <0.0001) and C12:0, C14:1, C18 comb (p <0.001)). A sound separation was also found between $\delta^{13}C$ signatures of FAMEs for some land use pairs with only C_3 vegetation (e.g., PF vs. FP: C14:0, C16:0 (p <0.0001), C12:0, C18:0 (p <0.001) and C24:0 (p <0.01); PF vs. T: C12:0 (p <0.0001) and C14:0 (p <0.001); SF vs. FP: C16:0, C18:0 (p <0.0001) and C14:0 (p <0.05); SF vs. T: C18:0 (p <0.0001) and C16:0 (p <0.01); FP vs. T: C15:1 and C16:0 (p <0.05)). No discrimination between $\delta^{13}C$ signatures of FAMEs were found for PF vs. SF and C vs. FP (p > 0.05).

Table 2.2. Significance levels derived from an Anova/Tukey-HSD Test of δ ^{13}C values of bulk carbon and different FAMEs for pair wise combinations of land use soil samples.

	Significant levels of δ ^{13}C values														
Land use pairs	bulk δ^{13}C	C12:0	C13:0	C14:0	C14:1	C15:0	C15:1	C16:0	C16:1	C17:0	C18:0	C18 comb	C20:0	C22:0	C24:0
SF-PF	n.s.	n.s.	n.s.	n.s.	n.s.	n.s.	n.s.	n.s.	n.s.	n.s.	n.s.	n.s.	n.s.	n.s.	n.s.
SF-M	****	n.s.	n.s.	***	*	n.s.	n.s.	****	**	*	****	***	**	**	***
SF-FP	**	n.s.	n.s.	*	n.s.	n.s.	n.s.	****	n.s.	n.s.	****	n.s.	n.s.	n.s.	n.s.
SF-T	**	n.s.	*	n.s.	n.s.	n.s.	n.s.	**	n.s.	n.s.	****	n.s.	n.s.	n.s.	n.s.
SF-C	****	n.s.	**	***	n.s.	n.s.	n.s.	****	n.s.	n.s.	****	n.s.	n.s.	n.s.	*
PF-M	****	***	n.s.	****	***	n.s.	n.s.	****	n.s.	n.s.	****	***	****	****	****
PF-FP	n.s	***	n.s.	****	n.s.	n.s.	n.s.	****	n.s.	n.s.	***	n.s.	n.s.	n.s.	**
PF-T	n.s	****	*	***	n.s.	n.s.	n.s.	n.s.	n.s.	n.s.	*	n.s.	n.s.	n.s.	n.s.
PF-C	***	****	**	****	*	n.s.	n.s.	****	n.s.	n.s.	**	n.s.	*	**	***
M-FP	****	n.s.	n.s.	n.s.	n.s.	n.s.	n.s.	n.s.	n.s.	**	n.s.	n.s.	*	**	*
M-T	****	n.s.	n.s.	n.s.	n.s.	n.s.	*	*	n.s.	*	*	**	***	****	****
M-C	n.s.	n.s.	*	n.s.	n.s.	n.s.	n.s.	n.s.	**	n.s.	n.s.	*	n.s.	n.s.	n.s.
FP-T	n.s.	n.s.	n.s.	n.s.	n.s.	n.s.	*	*	n.s.	n.s.	n.s.	n.s.	n.s.	n.s.	n.s.
FP-C	*	n.s.	n.s.	n.s.	n.s.	n.s.	n.s.	n.s.	n.s.	n.s.	n.s.	n.s.	n.s.	n.s.	n.s.
T-C	***	n.s.	n.s.	n.s.	n.s.	n.s.	*	**	n.s.	n.s.	n.s.	n.s.	n.s.	n.s.	*

Abbreviations: cassava (C), fruit tree plantation (FP), maize (M), protected Forest (PF), secondary forest (SF), teak (T). Significance codes: non-significant ($p > 0.05$) ‘ns’; $p < 0.05$ ‘*; $p < 0.01$ ‘**’; $p < 0.001$ ’***’; $p < 0.0001$ ‘****’.

Based on these results and their frequency of occurrence, especially in sediment samples (Table 2.3), mean values and standard deviations of $\delta^{13}C$ signatures of the 2 FAMEs Myristic Acid (C14:0) and Lignoceric Acid (C24:0) were used for further processing in SIAR.

Table 2.3. Compound specific $\delta^{13}C$ (‰) values for identified fatty acids for each sedimentation area. Mean (M), standard error (SE) and the number of samples (No.) analyzed are included.

	Area A			Area B			Area C1			Area C2			Area D			Area E		
Fatty Acid (‰)	M	SE	No.	M	SE	No.	M	SE	No.	M	SE	No.	M	SE	No.	M	SE	No.
Lauric Acid (C12:0)	-32.31	0.26	3	-30.78	0.19	3	-29.94	0.31	6	n.a.	n.a.	n.a.	-30.01	1.62	2	n.a.	n.a.	n.a.
Tridecanoic Acid (C13:0)	-29.20	0.93	3	-27.95	0.25	3	-28.77	0.73	8	-25.91	0.63	3	-27.22	0.32	3	-27.23	0.43	5
Myristic Acid (C14:0)	-28.32	1.22	5	-28.8	0.68	4	-26.95	0.74	9	-26.79	1.23	4	-28.62	0.68	5	-29.97	0.45	6
Myristoleic Acid (C14:1)	-30.15	0.80	4	n.a.	n.a.	n.a.	-30.1	0.78	8	-30.02	0.57	4	-30.72	0.38	3	n.a.	n.a.	n.a.
Pentadecanoic Acid (C15:0)	-27.97	0.99	3	n.a.	n.a.	n.a.	-26.71	0.51	7	-23.49	0.90	4	-27.93	2.19	4	n.a.	n.a.	n.a.
cis-10-Pentadecenoic Acid (C15:1)	-25.80	2.09	3	n.a.	n.a.	n.a.	-29.3	0.63	8	-29.93	1.04	3	-30.64	1.38	2	n.a.	n.a.	n.a.
Palmitic Acid (C16:0)	-28.65	3.50	5	n.a.	n.a.	n.a.	-24.33	1.35	7	-27.29	2.48	3	-27.05	1.13	6	-31.03	2.30	6
Palmitoleic Acid (C16:1)	n.a.	n.a.	n.a.	n.a.	n.a.	n.a.	-24.42	1.17	4	-25.8	1.84	2	-28.37	1.73	3	n.a.	n.a.	n.a.
Heptadecanoic Acid (C17:0)	-28.69	1.15	2	n.a.	n.a.	n.a.	-30.41	1.95	5	n.a.	n.a.	n.a.	n.a.	n.a.	n.a.	n.a.	n.a.	n.a.
Stearic Acid (C18:0)	-29.30	1.01	5	n.a.	n.a.	n.a.	-28.73	0.95	9	-25.36	0.61	4	-28.81	0.73	5	-20.10	1.03	6
C18 comb	-26.56	2.39	4	n.a.	n.a.	n.a.	-28.19	1.11	7	-27.73	3.04	4	-28.26	0.23	2	-27.18	1.73	4
Arachidic Acid (C20:0	-31.54	0.55	5	n.a.	n.a.	n.a.	-30.94	0.55	7	n.a.	n.a.	n.a.	-27.13	5.25	2	-30.58	0.66	3
Behenic Acid (C22:0)	-33.13	0.76	5	-25.66	2.39	3	-31.63	1.38	7	-29.13	0.48	3	-26	4.38	3	-32.39	0.55	6
Lignoceric Acid (C24:0)	-34.07	0.90	4	-28.54	1.38	4	-31.44	1.88	6	-29.28	2.53	3	-29.7	2.22	5	-32.49	0.67	6

*C18 comb' comprises of C18:1 (Oleic acid) and C18:2 (Linoleic acid) whose individual $\delta^{13}C$ signatures could not be completely resolved for every sample. n.a. – not available.

2.4.2 Point-in-polygon test

SIAR uses distributions instead of average values of $\delta^{13}C$ signatures of FAMEs in sources and hence will calculate source contributions even when a model is unlikely to meet the point-in-polygon assumption for every mixture. To increase the reliability of the SIAR output, we used a Monte Carlo simulation of mixing polygons for the point-in-polygon test (Smith et al., 2013).

Sediment samples, even when located close to each other, showed generally high variances in their FAME $\delta^{13}C$ signatures (Table 2.2). To obtain an approximate proportional contribution of the selected soil sources to the sediments of different sedimentation areas, we used mean values of the FAME $\delta^{13}C$ signatures of all individual sediment samples in each sedimentation area. The mean $\delta^{13}C$ values of the selected 2 FAMEs (C14:0 and C24:0) of 6 out of 7 sedimentation areas complied with the point-in-polygon assumption, i.e., the isotopic signature of the sediment was located within a polygon enclosing the signatures of the potential sources to provide a likely solution (Fig. 2.3). These mean values were then used for sediment source apportionment calculations in SIAR.

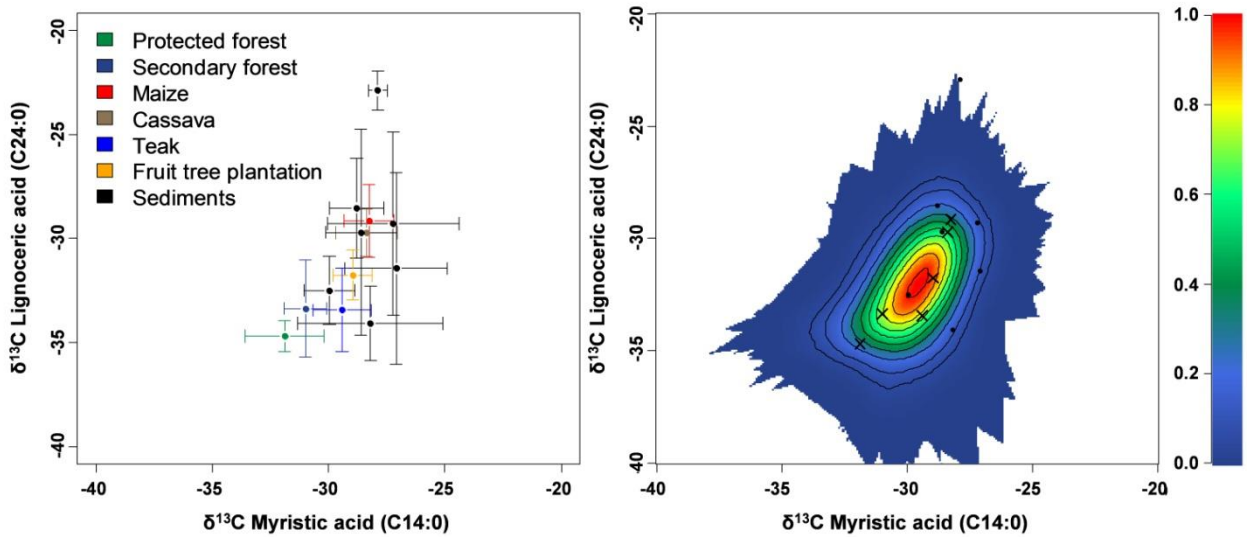

Fig. 2.3. Scatter plot and mixing polygon showing the intersect position based on the isotopic value coordinates of two fatty acids of sediment and source samples from Chieng Khoi catchment. Left side: Scatter plot of compound specific stable isotopic signatures of C14:0 and C24:0 for topsoil sources (protected forest, secondary forest, maize, cassava, teak, fruit tree plantations) and sediment samples including error bars. Right side: The mixing polygon for C14.0 and C24.0 showing the mean source signatures (black crosses) and mean sediments signatures (black dots). The different levels of confidence are indicated by different colors (for

grading see side bar). Sediment samples within the 95% level (outermost contour), i.e. A, B, C1, C2, D and E were used for further analysis.

2.4.3 Sediment source apportioning

SIAR produces true probability density functions which can be displayed as histograms or Box-and-Whisker Plots (Fig. 2.4). These show the distribution of possible solutions for all sources in the model. However, for a descriptive presentation of the sediment source contributions, we used median (Mdn.) values (Table 2.4). Matrix plots of estimates of each source proportion displayed correlation values between sources (Fig. 2.4). Well separated sources were characterized by low correlation values (e.g. -0.15 for PF and M in Area A). Sources close to each other resulted in higher correlations (e.g. -0.81 for M and C in Area C2). It should be noted that increased correlations among sources will increase the level of uncertainty in the model output.

In Area A, the sediment material was predominantly composed of soil originating from T (30%) followed by inputs from C (18%), FP (15%) and M (13%) (Fig. 2.4, Table 2.4). SF (8%) and PF (5%) contributed only to a minor extent. The highest contribution of sediment material of Area B originated from M (44%) and C (28%), while contributions of FP (9%), T (5%), SF (4%) and PF (1%) were negligible (Fig. 2.4). In Area C1, the contribution of C (45%) and M (22%) was highest followed by T (11%) and FP (11%) (Fig. 2.4). SF (3%) and PF (2%) contributed only minimal. Ranking of potential sources to sediments in Area C2 was similar to that in Area C1, but the combined share of C (44%) and M (36%) was distinctively higher (Fig. 2.4). For Area D, the majority of eroded soil material originated from C (33%) and M (33%) (Fig. 2.4). In Area D, FP (15%) was responsible for the second highest proportion of eroded soil for all investigated FPs, while T (8%), SF (5%) and PF (1%) contributed the lowest amounts. Soil contribution in Area E showed the highest values for C (24%), FP (20%), M (18%) and T (16%) (Fig. 2.4). Lower contributions originated from SF (13%) and PF (8%) (Fig. 2.4). In most cases, the possible solutions of proportional soil contributions were widely distributed. This was especially true for M, C, T and FP (A, B, C1, C2 and D), whereas the possible solutions of PF and SF were in a narrow range (e.g. C1 and C2). In Area E, the possible solutions of all proportional soil contributions were, except for PF, rather evenly distributed.

Table 2.4. Soil proportions of the 6 potential sources for the 6 investigated sedimentation areas in percent (%).

Area	Prop. Contributions (%)	Sources					
		PF	SF	M	C	T	FP
A	Min	1.2×10^{-4}	6×10^{-5}	4×10^{-5}	2.5×10^{-4}	1.3×10^{-8}	2.8×10^{-4}
	Q1	1.7	3.4	5.6	8.0	22.0	6.7
	Mdn	4.5	8.0	13.0	17.7	30.0	15.1
	M	6.4	9.5	16.1	20.0	30.6	17.5
	Q3	9.4	14.3	24.3	30.2	39.0	26.0
	Max	58.2	50.5	84.3	79.7	90.2	88.6
B	Min	2×10^{-6}	1.6×10^{-4}	2.1×10^{-3}	5.5×10^{-4}	6.3×10^{-4}	7.2×10^{-4}
	Q1	0.5	1.8	33.8	15.1	2.3	4.0
	Mdn	1.2	4.2	43.7	28.2	5.4	9.1
	M	1.6	6.3	44.1	28.7	7.9	11.5
	Q3	2.2	8.9	54.5	40.5	10.9	16.8
	Max	14.1	78.1	96.6	94.4	69.3	66.5
C1	Min	2.8×10^{-4}	1.0×10^{-4}	3.7×10^{-3}	1.7×10^{-2}	1.5×10^{-3}	2.4×10^{-3}
	Q1	0.6	1.1	10.6	32.5	4.8	4.8
	Mdn	1.5	2.5	22.0	44.9	11.0	10.9
	M	2.5	3.4	23.7	43.7	13.4	13.3
	Q3	3.2	4.8	33.8	56.7	19.9	19.7
	Max	22.8	26.2	93.7	94.3	84.3	84.1
C2	Min	3.8×10^{-5}	2.6×10^{-4}	3.5×10^{-3}	8.8×10^{-4}	4.3×10^{-4}	6.0×10^{-4}
	Q1	0.4	0.9	22.6	25.8	1.9	3.3
	Mdn	0.9	2.1	36.0	43.5	4.5	7.3
	M	1.3	2.9	37.1	42.2	6.9	9.7
	Q3	1.8	4.0	51.1	58.2	9.1	13.7
	Max	14.9	28.3	95.0	95.5	76.4	72.3
D	Min	2.7×10^{-5}	1.3×10^{-4}	6.1×10^{-3}	5×10^{-5}	5.4×10^{-4}	7.0×10^{-5}
	Q1	0.6	2.1	24.8	22.6	3.5	7.1
	Mdn	1.4	4.9	32.5	33.4	8.1	14.9
	M	1.9	6.3	32.9	32.7	10.2	16.0
	Q3	2.7	9.3	40.6	42.7	15.2	23.3
	Max	15.8	46.9	89.0	91.8	72.5	73.0
E	Min	1.1×10^{-4}	2.1×10^{-3}	6.4×10^{-4}	2.1×10^{-3}	1.2×10^{-3}	3.5×10^{-4}
	Q1	4.9	7.7	9.9	13.6	9.4	11.2
	Mdn	7.5	12.6	18.3	24.4	16.3	19.9
	M	7.6	12.7	18.9	24.3	16.4	20.1
	Q3	10.0	17.1	26.8	34.0	2.5	27.8
	Max	32.4	67.5	75.1	73.9	4.3	83.7

Abbreviations: cassava (C), fruit tree plantation (FP), maize (M), protected Forest (PF), secondary forest (SF), teak (T). Min: minimum value; Q1: 1st quartile; Mdn: median; M: mean; Q3: 3rd quartile; Max: maximum value

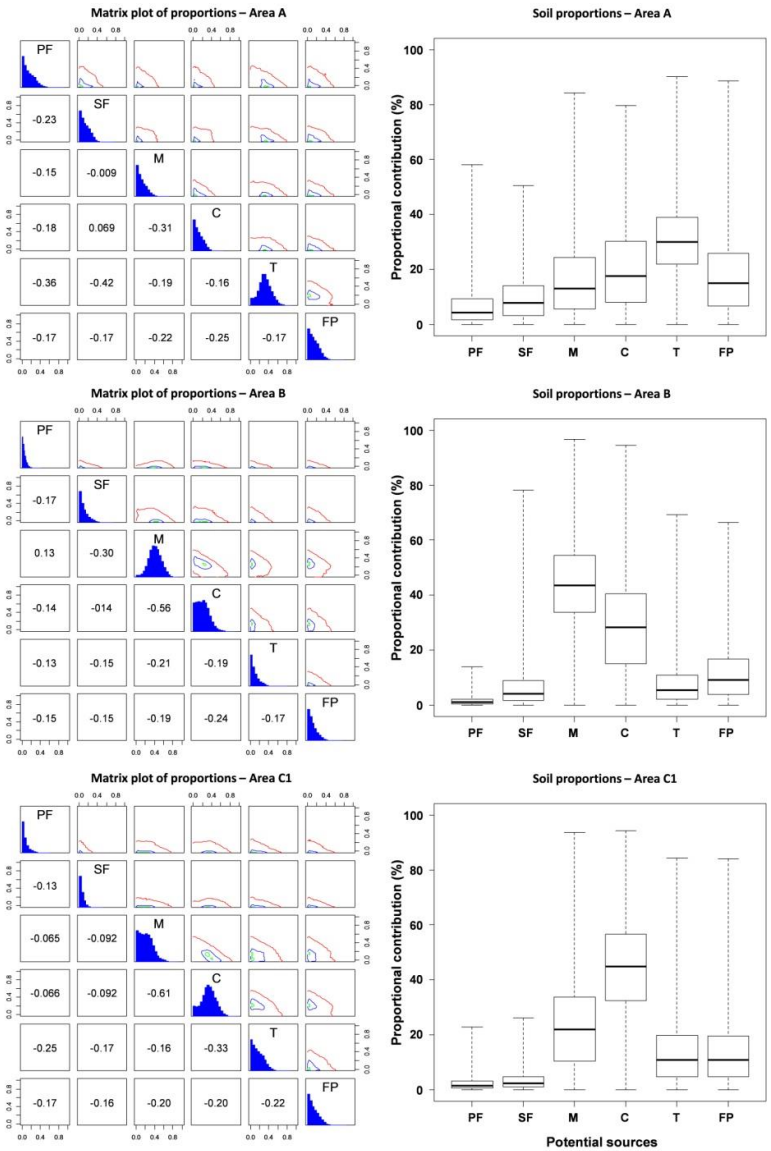
Matrix plot of proportions – Area A
PF
SF
M
C
T
FP
-0.23
-0.15
-0.009
-0.18
0.069
-0.31
-0.36
-0.42
-0.19
-0.16
-0.17
-0.17
-0.22
-0.25
-0.17
Soil proportions – Area A
Proportional contribution (%)
0
20
40
60
80
100
PF
SF
M
C
T
FP
Matrix plot of proportions – Area B
PF
SF
M
C
T
FP
-0.17
0.13
-0.30
-0.14
-014
-0.56
-0.13
-0.15
-0.21
-0.19
-0.15
-0.15
-0.19
-0.24
-0.17
Soil proportions – Area B
Proportional contribution (%)
0
20
40
60
80
100
PF
SF
M
C
T
FP
Matrix plot of proportions – Area C1
PF
SF
M
C
T
FP
-0.13
-0.065
-0.092
-0.066
-0.092
-0.61
-0.25
-0.17
-0.16
-0.33
-0.17
-0.16
-0.20
-0.20
-0.22
Soil proportions – Area C1
Proportional contribution (%)
0
20
40
60
80
100
PF
SF
M
C
T
FP
Potential sources

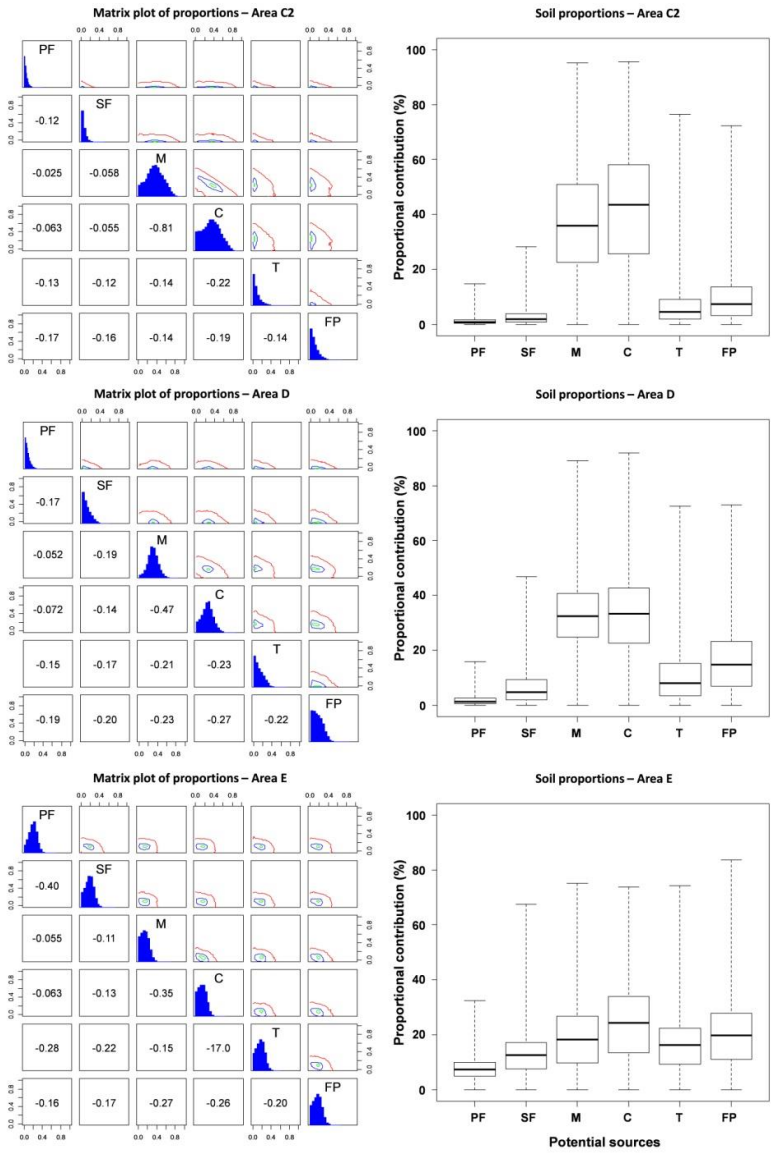

Fig. 2.4. Left side: Matrix plots of estimates of each source proportion calculated in the mixing models from the SIAR package output, represented by simulated values of the source proportions in the histograms. Correlation values between sources are inside the boxes to the left of histograms. Well separated sources are characterized by weak correlation values (e.g. protected forest vs. maize). Sources close to each other resulted in strong correlation (e.g. maize vs. cassava). Increased correlation among sources will increase the level of uncertainty in the model output. Right side: The actual soil proportions of all potential sediment sources for every tested sedimentation area were calculated using a linear correction equation (Eq. 2) based on the carbon content of each source soil. Abbreviations: cassava (C), fruit tree plantation (FP), maize (M), protected Forest (PF), secondary forest (SF), teak (T).

The comparison between proportional soil contributions (%) of the investigated land use types and the estimated corresponding land use areas (ha) is shown in Fig. 2.5. The proportional soil contribution as a function of the corresponding land use areas led to the following relative impact factors: forest (PF and SF) 0.4 ± 0.3, crops (M and C) 3.1 ± 0.9 and tree plantations (T and FP) 3.4 ± 1.4. Even though the standard deviation of these impact factor values were relatively high, a clear trend towards crops and various forms of tree plantation representing erosion prone land use types was derived.

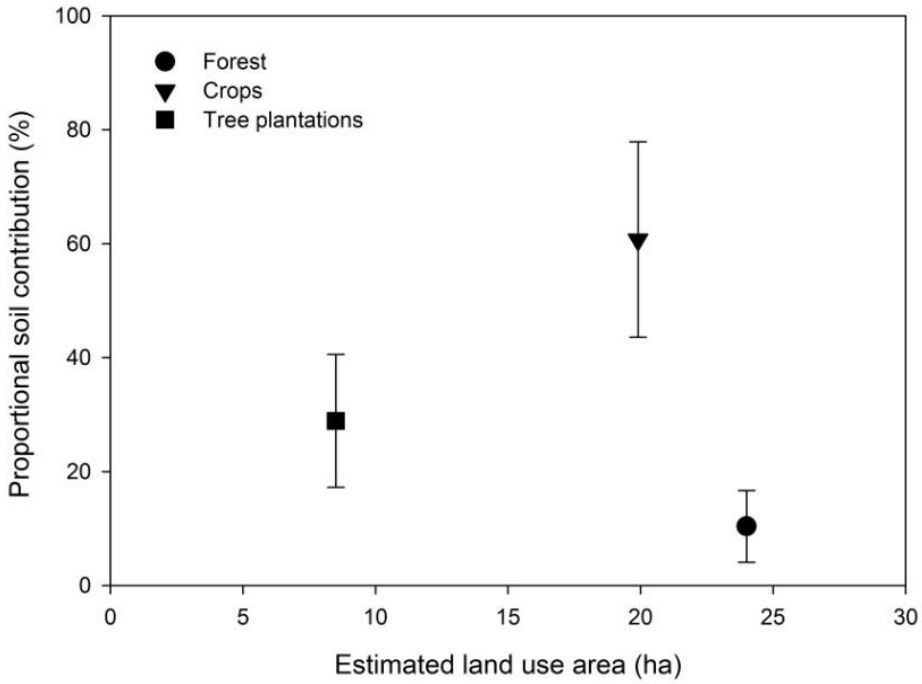

Fig. 2.5. Scatter plot showing the comparison between proportional soil contributions (%) of the investigated land use types and the estimated corresponding land areas (ha) covered by the different land use types. Land use types are summarized as forest (protected forest, secondary forest), crops (maize, cassava) and tree plantations (teak, fruit tree plantations).

2.5 Discussion

Our results corroborated the suitability of CSSI analysis in conjunction with the improved consecutive statistical procedures to study source-sink relationships of SOC in a small tropical catchment characterized by heterogeneous agricultural land use types. In a first step, Tukey's HSD test was used to distinguish various types of cultivated and forested soils based on $\delta^{13}C$ values of individual FAMEs. Secondly, the Bayesian point-in-polygon test was employed to identify whether a proposed mixing model could generate a reliable mass balance for all potential erosion sources. In the final step, the software package SIAR was applied to estimate the proportional source contributions.

2.5.1 Distinction of cultivated and forested land use types via $\delta^{13}C$ values of bulk topsoil C and FAMEs

In the context of estimating proportional source contributions with SIAR, Tukey's HSD test (Gaouzi et al., 2013; Xue et al., 2012) was successful in comparing to compare the isotopic signatures of 14 FAMEs of topsoil samples from 15 distinct land use pairs. The majority of these results were attributed to the different carbon (C) fixation pathways of C_3 and C_4 plants, where C_4 plants show generally less isotopic fractionation of C than C_3 plants. A small number of maize field soil derived FAMEs (e.g. C12:0, C15:1, C16:0) were more depleted than others corresponding to FAMEs of C_3. That might have been either attributed to recently converted C_3 vegetation to maize fields or to spatial variation of isotopic values in the field. In general, the average $\delta^{13}C$ value of all identified FAMEs of a specific land use type correlated well with the corresponding bulk $\delta^{13}C$ value (Fig. 2.2). Basically, the transmission of the $\delta^{13}C$ signal from vegetation to sediments requires three critical steps. Firstly, C atoms with $\delta^{13}C$ values typical for C_3 or C_4 plants are incorporated into FAs. Secondly, through leakage, decay of plant material and root exudation, FAs reach the soil, where they form associations with clay minerals. Thirdly, FA and clay mineral associations are conveyed to sediment deposition areas by water erosion.

The observation that the majority of isotopic differences were attributed to the different C fixation pathways was supported by obtained multi comparisons of soil bulk $\delta^{13}C$ values, where each land use pair which included maize (C_4 plant) showed very high significance levels (i.e., p <0.0001) (Table 2.3). Moreover, significant differences of soil bulk $\delta^{13}C$ values were also found between soils under different C_3 plants (e.g., SF vs. FP, SF vs. T). This supported the

application of C isotopes as suitable markers for the distinction of contrasting land use types in erosion studies (Häring et al., 2014).

An important advancement of our study over other reported approaches on source-sink relationships in catchments was the application of the point-in-polygon test in conjunction with SIAR (Smith et al., 2013). This test was a necessary addition to the quality evaluation of the isotopic mixing model outputs, hence reliability of obtained results by avoiding overinterpretation. This is due to two reasons: (1) the source data are distributions rather than average values, and (2) no discrete mixing polygons are used to assess for point-in-polygon situations (e.g., IsoSource) (Phillips and Gregg, 2003). Instead, SIAR always calculates source contributions even when a model is very unlikely to comply with the point-in-polygon assumption for every sediment sample (Parnell et al., 2010). Therefore, a prior examination of the data is crucial.

Most sediment samples, which lay outside the 95% confidence level of the point-in-polygon test, revealed less depleted $\delta^{13}C$ values than those derived from reference maize fields. A probable explanation for these relatively high $\delta^{13}C$ values was the trophic state of the specific sedimentation area in the Chieng Khoi Lake before sediment samples were obtained. This assumption was supported by Torres et al. (2009) who determined less depleted bulk $\delta^{13}C$ values (-26‰ and -18‰) in the surface sediments of an eutrophic and hypertrophic lake than in an oligo-mesotrophic lake (-30‰). In our study, sediment collection was performed at the end of the dry seasons when the Chieng Khoi Lake was almost drained completely. It needs to be emphasized that the lake did not drain equally fast leaving water puddles as accumulation sites for nutrients. This may have led to the eutrophication status prior to collection of sediment samples.

2.5.2 Separating erosion sources and determining source-sink relationships by CSSI analysis

The CSSI analysis was applicable to discriminate erosion sources based on land use types and to determine source-sink relationships in a small, agriculturally diverse catchment. Our CSSI-based observations suggested that fields under maize and cassava cultivation were predominantly prone to soil erosion. This was further corroborated as they covered less area than the surrounding forest (Fig. 2.5). This result fits earlier studies investigating erosion rates under maize cultivation in mountainous areas in Vietnam (Häring et al., 2014; Tuan et al., 2014) and Thailand (Kongkaew, 2000; Pansak et al., 2008) with erosion rates from maize on steep

slopes (59%) up to 174 Mg ha^{-1} (Tuan et al., 2014). In addition, Valentin et al. (2008) reported considerable soil loss (8.9 Mg ha^{-1} $year^{-1}$) under cassava in the Dong Cao catchment in Vietnam with a mean slope of 28 to 38%. Furthermore, in a small catchment of Hoa Binh province in Vietnam, Dung et al. (2008) found erosion rates under cassava to be generally higher than under secondary forest. Similar trends were measured in Sri Racha, Thailand, where erosion induced soil loss amounted to 311 Mg ha^{-1} on a 7% slope during a period of 40 months (Putthacharoen et al., 1998).

Interestingly, the sediment composition of Area A revealed teak as the main contributor to sediment material deposition in the respective lake border although only 20% of the surrounding land use was attributed to teak. In general, reforestation is a valuable strategy to restore degraded soils (Brauman et al., 2007; van Dijk and Keenan, 2007). It increases the infiltration capacity and porosity of soils; therefore attenuating surface run-off and soil erosion (e.g., Bonell et al., 2010; Ilstedt et al., 2007). On the other hand, soil erosion under teak plantation has aroused certain controversy as it has been regarded as unsuitable to provide the hydraulic benefits commonly associated with forests (Carle et al., 2009; Pandey and Brown, 2000). A recent study by Fernández-Moya et al. (2014) concluded that high rates of soil loss under teak plantation occurred mainly because of inappropriate forest management. This included planting of teak on steep slopes (>60%) or reduction of understory vegetation depleting SOC levels (Boley et al., 2009). These conclusions may also be reflected in the Chieng Khoi catchment, where teak has been cultivated on low fertility soils since the late 1990s as part of a governmental soil erosion control program. However, it needs to be noted that the success of erosion control is generally hampered by the deciduous nature, having often a bare canopy at the beginning of the rainy season and continuous removal of teak litter by farmers accelerating water erosion (O. Zemek, personal communication).

2.5.3 Important considerations when applying the CSSI approach

The $\delta^{13}C$ values and respective standard deviations of C14:0 and C24:0 obtained from the six potential soil sources revealed relatively wide ranges and overlaps between different sources. This might have induced considerable effects on the source apportionment via SIAR. Similar observations were made by Xue et al. (2012) when contributions of multiple nitrate sources in surface water were estimated. Consequently, the selection of FAMEs for source apportionment may result – even when they fulfill all prior criteria (e.g., significant different FAME $\delta^{13}C$ values between land use types, meeting the point-in-polygon assumption) – in dissenting soil

contributions of potential sources. We have noticed that source discrimination of not averaged sediment FAME $\delta^{13}C$ values resulted in very inconsistent soil contribution patterns. This was particular evident for adjacent sediment samples suggesting a high spatial variability of FAME $\delta^{13}C$ values in sediments. Collecting spatially-integrated mixtures allowed us to obtain representative soil samples of each land use type but the degree of variability in the source samples might still be under-estimated in most cases. Analyzing all individual sub-samples would have provided better insight on the variability of each CSSI value from that explicit land use type and improved most likely the interpretation and statistics using SIAR. However, these advantages stand in contrast to the analytical costs which would have been soared. Using spatially-integrated mixtures is therefore a trade-off between the determination of the degree of spatial variability of CSSI values and analytical costs which are necessary to meet the research objectives.

For the prospective application of the CSSI technique, several uncertainties of the spatial and temporal (i.e. stability of the isotopic signal with time) behavior of FAs in water bodies need to be solved. For example, fine sediments such as clay particles may have considerable implications on the statistical outputs of source-sink relationships via CSSI analysis. Clays form associations with FAs and may migrate a greater distance and hence distribute in a larger area, where they may get in contact with sediments from other erosion sites. This might be further interfered if soil types of comparable land use types are distinct across the study area. In such case, it is recommended to group the data by soil type to determine soil property dependent differences of CSSI concentrations or signatures.

It could be further speculated that the abundance of FAs from erosion sites may be superimposed by other FAs derived from phytoplankton and algae (Kluijver et al., 2015; Treignier et al., 2009) skewing the SIAR output. Another uncertainty might be caused by unpaved rural roads inducing undefined of sediment material. Several studies have shown that although unpaved rural roads occupy only a small area in a catchment, they deliver a disproportionately large percentage of annual sediment loads to water bodies (Nagle, 2002; Sidle et al., 2012; Ziegler et al., 2004). These sources have to be considered in prospective studies allowing a more concrete understanding of source-sink relationships in small rural catchments characterized by diverse and scattered land use types.

2.6 Conclusion

Our study showed that the FA-based CSSI approach in conjunction with the developed improved consecutive statistical procedure discriminated erosion sources based on land use type and therefore to determine source-sink relationships in rural, tropical catchments with diverse land use types. The SIAR output, however, revealed a large variability in contribution of the six potential soil sources. The resolution was largely hampered by the uncertainty of the isotopic composition of the different soil sources and the spatial variability of the sediment samples. To overcome this obvious limitation, we used for the first time a Bayesian point-in-polygon test which increased the reliability of the SIAR output.

We have evidenced that the CSSI analysis combined with Bayesian statistical methods is a promising approach to identify and apportion major land use soil sources in a small catchment by linking particular biomarkers (i.e., FAs) of distinct land use types to the sediment in deposition zones. However, we have also noted considerable overlaps of FAME $\delta^{13}C$ values between sources (e.g., diverse C_3 plants) which may obscure an accurate source apportionment. This fact was traced back to the high diversity of vegetation types (forest and crops) that may be – in contrast to aforementioned studies – regarded as a likely applicability threshold of the CSSI analysis. In prospective studies, the application potential of the CSSI approach with respect to different spatial scales (e.g., tropical heterogeneous small scale to temperate homogenous large scales and temporal scales) and also different agro-ecological zones (e.g., temperate versus tropical climates) should be defined to corroborate its robustness for tackling SOC-based source-sink relationships at catchment level**.**

Chapter III Towards global applicability? Erosion source discrimination across catchments using compound-specific $\delta^{13}C$ isotopes[2]

Christian Brandt[1], Gerd Dercon[2], Georg Cadisch[1], Lam T. Nguyen[3], Paulina Schuller[4], Claudio Bravo Linares[4], Alejandra Castillo Santana[4], Valentin Golosov[5], Moncef Benmansour[6], Nourredine Amenzou[6], Zhang Xinbao[7], Frank Rasche[1]

[1]Institute of Agricultural Sciences in the Tropics (Hans-Ruthenberg-Institute), University of Hohenheim, Stuttgart, Germany

[2]Soil and Water Management & Crop Nutrition Laboratory, Joint FAO/IAEA Division of Nuclear Techniques in Food and Agriculture, Department of Nuclear Sciences and Applications, International Atomic Energy Agency, Vienna, Austria

[3]Department of Environmental Management, Vietnam National University of Agriculture, Hanoi, Vietnam

[4]Universidad Austral de Chile, Facultad de Ciencias, Instituto de Ciencas Químicas, Valdivia, Chile

[5]Laboratory for Soil Erosion and Fluvial Processes, Faculty of Geography, Lomonosov Moscow State University, Moscow, and Kazan Federal University, Kazan, Russia

[6]Centre National de l'Energie des Sciences et des Techniques Nucléaires, Rabat, Morocco

[7]Chinese Academy of Sciences, Institute of Mountain Hazards and Environment, Chengdu, Sichuan, China

[2]A version of this chapter was published as:

Brandt, C., Dercon, G., Cadisch, G., Nguyen, L.T., Schuller, P., Bravo, C., Castillo, A., Golosov, V., Benmansour, M., 2018. Towards global applicability? Erosion source discrimination across catchments using compound-specific $\delta^{13}C$ isotopes. Agriculture , Ecosystems and Environment 256, 114–122.

3.1 Abstract

Accurate identification of soil erosion hot spots across catchments of different sizes and agro-ecologies through the use of conventional tracing techniques has proven challenging. Since this problem hinders implementation of precise soil conservation measures by land managers and decision-making bodies, novel evidence-based techniques are needed. To meet this need, the International Atomic Energy Agency (IAEA, Vienna, Austria) initiated the Coordinated Research Project entitled "Integrated Isotopic Approaches for an Area-wide Precision Conservation to Control the Impacts of Agricultural Practices on Land Degradation and Soil Erosion - D1.20.11" in 2008. This project emphasized the application of isotopic approaches to identify hot spots of land degradation in agricultural catchments to develop effective soil conservation measures. As one key outcome of this project, we present here an aligned protocol to explore the potential of compound-specific stable isotope (CSSI) analysis of individual fatty acids (FA) combined with Bayesian statistics to discriminate sediment sources across six catchments of different sizes and agro-ecologies. The global applicability of the CSSI approach was first tested on the basis of major land use categories (i.e., forest, cultivated and non-cultivated land) as potential sediment sources in the studied catchments. These land use categories were then further resolved into specific land use types (e.g., cassava and maize fields, orchards) to assess the potential resolution threshold of the CSSI technique. In a final step, the influence of miscellaneous sources (e.g., roads, channel banks) that had the potential to distort proportional contributions to sediment deposition was assessed. The introduced aligned protocol of the CSSI technique was applied to discriminate individual erosion sources based on land use types of tested catchments. Merging catchment-specific land use types with broader land use categories made it possible to determine inter-catchment comparisons of isotopic signatures due to significant differences in $\delta^{13}C$ values of fatty acids when cultivated land was present. Notably, no correlations were found between different catchment sizes, agro-ecologies, number and type of land use types, or soil organic carbon concentrations and the number of significant $\delta^{13}C$ fatty acid values of the various land use types. Thus, we propose that the presented CSSI technique has the potential to identify soil erosion hot spots in contrasting catchments of different sizes and agro-ecologies.

3.2 Introduction

Increased population growth generally leads to intensified agricultural land use, resulting in an inexorable depletion of soil productivity. This dilemma is aggravated when agricultural activities are extended to shallow and more vulnerable soils. Consequently, as regions develop economically and become wealthier, land degradation seems inevitable. Soil erosion is one of the main drivers of soil degradation in developing countries (Pimentel, 2006; Scherr, 1999). Erosion leads not only to on-site effects resulting in a loss of fertile topsoil, threatening crop productivity, but also induces off-site effects (e.g., sedimentation into streams and rivers accompanied by silting-up of water reservoirs and contamination of drinking water). More than three quarters of the total agricultural land area affected by erosion is situated in Africa, Asia and Latin America. Global estimates of the monetary value of resource reduction due to soil erosion are approximately $400 billion in financial losses per year (Pimentel et al., 1995; Lal, 2006).

Scientists, practitioners and political decision makers pursue a common goal of increasing and sustaining higher crop production through coordinated and joint research efforts to meet the demands of an increasing human population, while maximizing soil and water conservation (Scherr and McNeely, 2008; Hobbs, 2008; Soil and Water Conservation Society, 2003). The design and implementation of conservation measures to reduce impacts of soil erosion at the catchment level requires comprehensive studies that include: i) historical records of major changes in land use/management, ii) soil erosion risk assessment, iii) soil redistribution (loss/deposition) rates and patterns over spatial and temporal scales, iv) connection of field (farm) with off-site impacts, v) identification of hot spot areas, and vi) integration of the information gained to define site-specific soil conservation measures (Berry et al., 2003, 2005; Knight, 2005; Delgado and Berry, 2008). Efforts to identify sediment sources have considered a variety of soil attributes, including geochemical, mineralogic and mineral magnetic properties, sediment color (Grimshaw and Lewin, 1980), plant pollen (Brown, 1985) and the isotope geochemistry of lead (Pb), neodymium (Nd) and strontium (Sr) (Douglas et al., 1995, 2003).

Fallout radionuclides (FRNs), including caesium-137 (^{137}Cs), excess lead-210 ($^{210}Pb_{ex}$) and beryllium-7 (^{7}Be) have been determined as very suitable for distinguishing surface and subsurface materials as well as establishing soil redistribution patterns and rates across spatial scales (Walling and Woodward, 1992; He and Owens, 1995; Wallbrink et al., 1999). Though FRNs are valuable for estimating quantitative sediment budgets for a specific location, they are

not appropriate for assigning a denudation rate to a specific land use (Hancock and Revill, 2013).

Due to their origination in above-ground plant biomass and microorganisms (Wiesenberg et al., 2010; Badri and Vivanco, 2009; Ibekwe and Kennedy, 1995) and ability to form associations with clay minerals (Williams et al., 2006), lipid biomarkers (e.g., fatty acids (FAs)) have been used as indicators for tracking land use types (i.e., sources) into sediment materials (Mead et al., 2005; Ratnayake et al., 2011) An important criterion for use of long-chain FAs (i.e., C12:0 to C24:0) as erosion biotracers is their individual $\delta^{13}C$ isotopic signature, which is influenced by the vegetation cover, among other factors. Hence, an FA-based compound-specific stable istope (CSSI) approach is a major advance in determining source-sink relationships at the catchment level (e.g., Gibbs, 2008; Chikaraishi and Naraoka, 2003).

Although a growing number of studies demonstrated the applicability of the FA-based CSSI approach on individual catchment basis (Gibbs, 2008; Blake et al., 2012; Hancock and Revill; 2013), its global applicability with the application of an aligned protocol has not been explored with respect todistinct agriculturally used catchments of various sizes and agro-ecologies. The need to evaluate such broad-scale application is justified since earlier studies relied on different laboratory and statistical routines (e.g. Alewell et al., 2016; Hancock and Revill, 2013; Blake et al.,2012; Gibbs, 2008). A major step forward was recently taken by Brandt et al. (2016) who introduced the combination of the CSSI technique with Bayesian statistics. This innovative approach made it possible to reliably indentify and apportion potential erosion sources to sediment deposition in an agriculturally heterogenous catchment (207 ha, Chieng Khoi, Vietnam).

The IAEA Coordinated Research Project (CRP) entitled “Integrated Isotopic Approaches for an Area-wide Precision Conservation to Control the Impacts of Agricultural Practices on Land Degradation and Soil Erosion - D1.20.11” (2008 -2013) provided the overall framework of this paper. The main goal of the CRP was to develop integrated isotopic approaches to identify hot spots or critical areas of land degradation in agricultural catchments for effective soil conservation measures (i.e., precision conservation). The research objectives, with a focus on CSSIs, were to: (i) develop and validate protocols for application of the CSSI technique to identify and apportion the amount of source soils (land-degraded areas) from main land uses/management regimes (cropland, grassland and forestland) in the catchment; and (ii) create a basis for developing decision support tools to implement precision soil conservation, thus contributing to sustainable land management.

The primary objective of our study was thus to evaluate the global applicability of the FA-based CSSI technique, using an aligned protocol, to detect hot spots of soil erosion across catchments. The generic approach by Brandt et al. (2016) was used first to distinguish major land use categories (i.e., forest, cultivated, non-cultivated land) in six differently sized catchments of contrasting agro-ecologies. These land use categories were then further resolved into specific land use types to assess the potential resolution threshold of the CSSI technique. In a final step, the influence of miscellaneous sources (e.g., roads, channel banks) that could distort the proportional contributions of sources to sediment deposition was assessed. This 3-step approach made it possible to draw conclusions about and make recommendations on the global applicability of the FA-based CSSI technique to agriculturally used catchments of various sizes and agro-ecologies.

3.3 Materials and methods

3.3.1 Case study areas

To meet the study objective, six contrasting catchments were considered. The selection criteria were differences in size and contrasts in agro-ecologies. Catchment characteristics are given in Tables 3.1 and 3.2. Location maps of all studied catchments are depicted in Fig. 3.1. The *Chieng Khoi (CHK)* catchment (21°7´N, 105°40´E, 207 ha) was located in the Chieng Khoi commune, Son La province in mountainous Northwest Vietnam. Characteristic land use types (LUT) included areas of protected natural forest (NF), secondary forest (SF), teak plantations (TE), fruit tree plantations or orchards (OR), as well as intensively managed maize (MA) and cassava (CA) fields. Data on the CHK catchment were retrieved from Brandt et al. (2016). The *Nacimiento (NAC)* catchment (37°29´S, 72°44´W, 12.4 ha) was located in the Bio-Bio region of south-central Chile, while the *Los Ulmos (LOS)* catchment (40°02´S, 73°05´W, 19.8 ha) was located 400 km south of NAC. Both of these catchments were predominantly pine plantations (PI) and native forest (NF). Additionally, eucalyptus plantations (EU) were present in LOS. Other potential erosion sources involved the forest road (RO) and sediments present in the forest stream channel, bed and bank (SC). The *Popovskiy pond (POP)* catchment (51°78´N, 36°14´E, 198 ha) was located about 1 km north-north-west of the regional centre Kursk, Russia. In POP, possible sediment sources included apple gardens (orchard) (OR), broadleaf natural forests (NF), planted forests (PL), abandoned arable fields (AB), cereal fields (CE) and active gullies (GU). The *My Bouchta (MYB)* catchment (35°22´N, 5°22´W, 766 ha) was located in the region of Tanger – Têtouan in the North of Morocco. Agriculture was the dominant land use type

(60%) in the catchment. Typical crops included cereals (CE) such as barley, maize, and wheat but also beans, olives and almonds. Forest (NF) and shrubs (SL), consisting mainly of pines and oaks, amounted to 40% of the vegetation cover. The *Xinzheng (XIN)* catchment (30°25´N, 108°09´E, total 11.42 ha) belonged to the Three Gorge Reservoir Area and was located in Zhongxian County, Chongqing Municipality, China. Three small sub-catchments in XIN covered an area of 3.02 ha (T1) 3.45 ha (T2) 4.95 ha (T3). LUT included cypress (CF) and bamboo forests (BF), orange orchards (OR), mixed cultivation including bamboo, sorghum and peanut (MX), young bamboo (YB) and cypress tree plantations (YC), as well as paddy rice fields (RP) on the lower slopes.

Table 3.1. Catchment characteristics

	Study sites					
	Chieng Khoi	Los Ulmos	My Bouchta	Nacimiento	Popovskiy	Xinzheng
Abbreviation	CHK	LOS	MYB	NAC	POP	XIN
Country	Vietnam	Chile	Morocco	Chile	Russia	China
Latitude	21°01´N	40°02´S	35°22´N	37°29´S	51°78´N	30°25´N
Longitude	104°31´E	73°06´W	5°22´W	72°44´W	36°14´E	108°09´E
Elevation (m)	429 - 493	192	321 - 1,821	328	200-250	210 - 290
Precipitation (mm)	1,110	2,500	850	1,200	550	1,150
Temperature (°C)	21	13	17	13	6	19
Soil type	Ferralsols, Leptosols	Fine textured clay soils	Vertisols, Alfisols, Inceptisols, Entisols	Fine textured clay soils	Chernozem	Purple soils
Area (ha)	207	19.8	7660	12.7	198	12

In each catchment, major LUT were further grouped into land use categories (LUC). At the level of LUC, all natural, secondary, planted forests were summarized under the LUC “Forest” (FO). Not included in this category were TE (CHK) due to the management practice of removing the litter layer for fuel purposes by farmers, as well as YB and YC plantations (XIN) due both to their very small areas and young age of < 10 yrs at the time of sampling. All intensively managed LUT were merged under LUC “Cultivated Land” (CL), e.g. RP, MA and OR. A third LUC, “Non-Cultivated” (NC), encompassed SL (MYB), AB (POP) and RO (NAC and LOS).

Table 3.2. Vegetation cover related characteristics, including abbreviations.

Catchment (CAT)	Land use category (LUC)		Land use type (LUT)		No. LUT	Main vegetation types
CHK	cultivation	CL	cassava field	CA	10	*Manihot esculenta*
	cultivation	CL	maize field	MA	15	*Zea mays*
	forest	FO	native forest	NF	9	broad-leaved trees and bamboo
	cultivation	CL	orchard	OR	10	mango, jackfruit, tamarind, longan
	forest	FO	secondary forest	SF	9	broad-leaved trees, bamboo
	cultivation	CL	teak plantation	TE	9	*Tectona grandis*
LOS	forest	FO	eucalyptus	EU	2	*Eucalyptus nitens*
	no cultivation	NC	forest road	RO	2	forest road
	no cultivation	NC	stream sediment	SC	2	forest stream sediments
	forest	FO	native forest	NF	2	native forest
	forest	FO	pine forest	PI	2	*Pinus radiate*
MYB	cultivation	CL	cereal field	CE	9	Wheat
	forest	FO	native forest	NF	4	aleppo pine, radiata pine, cork oak
	no cultivation	NC	shrub land	SL	6	
NAC	forest	FO	eucalyptus	EU	3	*Eucalyptus nitens*
	no cultivation	NC	forest road	RO	3	forest road
	no cultivation	NC	stream sediment	SC	3	forest stream sediments
	forest	FO	native forest	NF	3	native forest
	forest	FO	pine forest	PI	4	*Pinus radiate*
POP	no cultivation	NC	abandoned arable land	AB	3	
	no cultivation	NC	active gully	GU	6	
	cultivation	CL	cereal field	CE	3	wheat
	cultivation	CL	orchard	OR	3	apple trees
	forest	FO	native forest	NF	3	broad-leaved trees
	forest	FO	planted forest	PF	3	
XIN	forest	FO	bamboo forest	BF	3	Bamboo
	forest	FO	cypress forest	CF	3	Cypress
	cultivation	CL	mixed cultivation	MX	3	bamboo, sorghum, peanut
	cultivation	CL	orchard	OR	6	Oranges
	cultivation	CL	rice paddy	RP	6	Rice
	cultivation	CL	young bamboo	YB	3	Bamboo
	cultivation	CL	young cypress	YC	3	Cypress

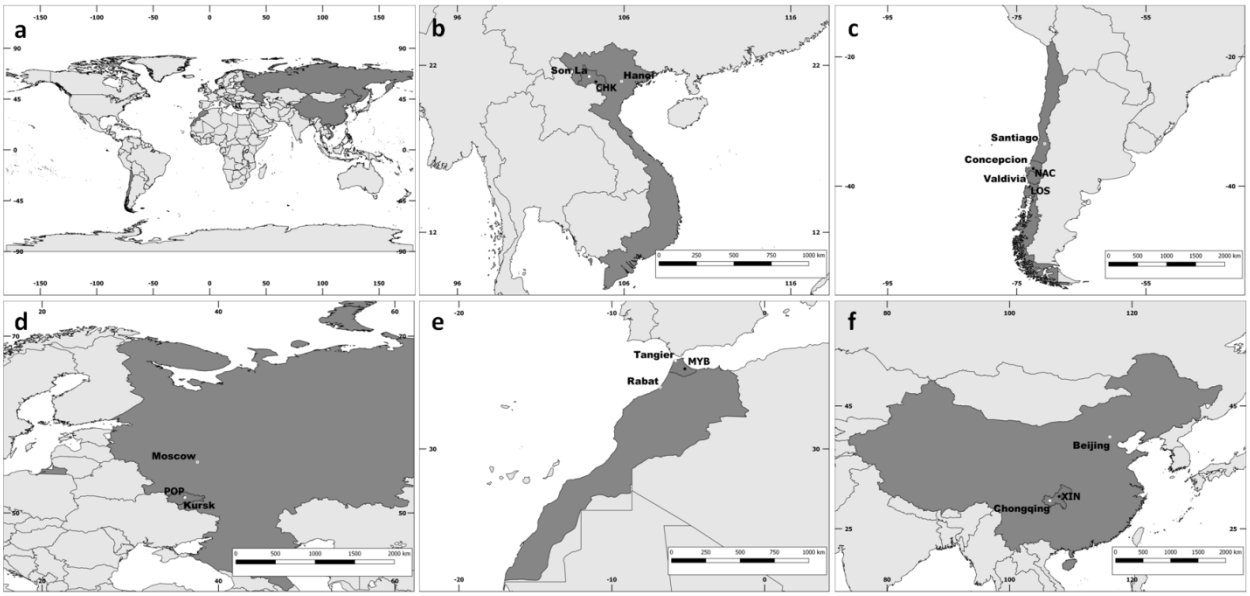

Fig. 3.1. Location maps of study catchments. From top left: a) World map depicting study countries; b) Chieng Khoi (CHK), Son La,Vietnam; c) Nacimiento, Bío Bío, and Los Ulmos, Los Ríos, Chile; d) Popovskyi Pond (POP), Kursk, Russia; e) My Bouchta, Tanger Tetouan, Morocco; f) Xinzheng, Chongqing; China.

3.3.2 Sample collection

An aligned sampling procedure, based on Gibbs (2014) was developed for this CRP and applied at all study sites. Generally, topsoil (0-2 cm) samples of each individual land use type were collected from at least 3 discrete plots of each LUT within the catchment areas. In each plot, soil samples were obtained from 3 different positions; within each of the 3 positions, 20 sub-samples from an area of 20 m^2 were combined to a composite sample of each LUT. Bulked soil samples were dried at 50°C directly after sampling, sieved (2 mm) and maintained under dry and dark conditions. Top sediment layers (0-2 cm) were obtained by combining 20 sub-samples from an area of 20 m^2 to ensure a representative sample. In some cases, soil and sediment sampling deviated slightly from the harmonized sampling procedure. In NAC, sediment samples at the outlet of the forest catchment were obtained within the weir bed at 7 different times between August 2009 and August 2012. The same procedure was used in LOS, where sources and sediments were collected in August 2010. In POP, sediment samples were taken from the section excavated in the centre part of the former pond bottom which had been drained 5 years prior to sampling. Two types of sediment were collected; (1) two depth-integrated samples (10-50 cm and 100-140 cm), and (2) three samples collected from specific sediment layers representing event-driven erosion deposits.

3.3.3 EA-IRMS analysis

At the University of Hohenheim, bulk carbon (C) isotopic compositions ($\delta^{13}C/^{12}C$) and organic C content of soil and sediment samples were determined using a Euro EA 3000 elemental analyzer (Hekatech, Wegberg, Germany) connected to a Delta plus XP mass spectrometer via a Conflo III Interface (Thermo Finnigan MAT, Bremen, Germany). Inorganic carbonates were first removed with 1 N hydrochloric acid so that only the $\delta^{13}C$ values of organic C components in soil and sediment samples were detected. Samples were then oven-dried at 70°C to constant weight, ball-milled and analyzed.

Calibration of $\delta^{13}C$ to VPDB was achieved using glutamic acid USGS-40 (-26.39 ± 0.04‰). Acetanilide (Merck, Darmstadt) (-26.6 ± 0.27‰) was used as a secondary laboratory reference material for internal calibration and determination of C. The average $\delta^{13}C$ of an internal wheat flour standard was -25.93 ± 0.11‰ across all sessions. At the Isotope Bioscience Laboratory ISOFYS at Ghent University, total C was determined using an elemental analyzer (ANCA, SerCon, Crew, UK) interfaced with a isotope ratio mass spectrometer (20-22, SerCon, Crew, UK). Calibration of $\delta^{13}C$ toward VPDB was achieved using a secondary sediment standard (-26.00 ± 0.13‰, uncertainty on VPDB scale) traceable to IAEA-CH-6 (accepted value = -10.43) along with an internal soil reference sample (-22.69 ± 0.17‰) used as quality control. $\delta^{13}C$ was calculated by expressing the measured ratios (R_{sample}) against the international Vienna-Pee Dee Belemnite (VPDB) standard (R_{VPDB}) (Equation 3.1):

$$\delta^{13}C_{sample}(‰) = \left\{\left(\frac{R_{sample}}{R_{VPDB}}\right) - 1\right\} x10^3 \quad (3.1)$$

3.3.4 Extraction, fractionation and derivatization of fatty acids

Extraction and analysis of fatty acids (FAs) was performed according to Blake et al. (2012) with slight modifications. Total lipid extraction procedure was based on a dichloromethane (DCM)/methanol (9:1, v/v) mixture. This was followed by solid phase extraction (SPE; aminopropyl bonded silica gel cartridges (Bond Elute), Agilent Technologies, Santa Clara, USA) to segregate the total lipids into acid and neutral fractions. After methylation according to Ichihara and Fukubayashi (2010), the methylated FA fraction was re-dissolved, and sampled on a gas chromatograph coupled to to a mass spectrometer via a combustion interface (GC-C-IRMS).

GC-C-IRMS analysis was done at the University of Hohenheim (samples obtained from CHK, MOR, and XIN) and Ghent University (LOS, NAC, POP). At the University of Hohenheim, a gas chromatograph (Agilent 6890, Agilent Technologies) coupled to a Delta plus XP mass spectrometer via a Conflo III Interface (Thermo Finnigan MAT) was used to measure $\delta^{13}C$ signatures of methylated FAs (FAMEs). Samples were injected into a splitless injector at 250°C and separated using a Varian Factor Four VF23-MS fused silica capillary column (high cyanopropyl modified methyl polysiloxane; 30 m, 0.25 mm internal diameter, 0.25 μm film thickness; Varian Inc., Santa Clara, CA, USA). Hydrogen was used as carrier gas. FAMEs were identified based on their retention times using the Supelco® 37 Component FAME Mix and the Supelco® C8 – C24 FAME Mix (Sigma-Aldrich, St. Louis, USA). At the Isotope Bioscience Laboratory ISOFYS at Ghent University stable isotope ratios of FAME were analyzed by capillary gas chromatography-combustion-isotope ratio mass spectrometry (GC-C-IRMS; Delta Plus XP, Thermo Scientific). Samples were injected into a PTV injector at 250°C and separated using a VF-5MS (60 m, 0.32 mm internal diameter, 0.2 μm film thickness). Helium was used as carrier gas. Pulses of standard CO_2 gas were injected at the start and end of each sample run to correct for intra-sample drift. A mixture of standardized FAMEs was analyzed every 6 samples and used to correct for instrumental drift during batch analysis and to standardize FAMEs to the VPDB scale. Samples were injected at least in duplicate (SE < 0.3 ‰), eight consecutive samples were bracketed with 2 external laboratory reference mixtures of different concentration covering the concentration range of the samples. The laboratory reference mixtures were composed of a mixture of saturated FAME (C14 till C22), calibrated on the VPDB scale using certified reference mixture (F8-3, Indiana University, US), traceable to NBS 19 and LSVEC (accepted values = +1.95 and -46.6 ‰, respectively). FAME were identified based on retention time and confirmed using a parallel GC-MS measurement on selected samples.

3.3.5 Data processing and analysis

GC-C-IRMS measurement of FAs required the addition of an extra methyl group to each FA. The C atom of the methyl group added to the FA to form a methylated FA (FAME), typically has a different $\delta^{13}C$ value than that of the original, non-methylated FA. To account for this, the $\delta^{13}C$ value of the methanol was determined in this study and used as correction factor (-35 ‰, VPDB) prior to sediment source ascription (Equation 3.2).

$$\delta^{13}C_{FA} = \frac{\delta^{13}C_{FAME} - (1 - X)\delta^{13}C_{Methanol}}{X} \quad (3.2)$$

Where $\delta^{13}C_{FAME}$ is the value measured, $\delta^{13}C_{Methanol}$ is the $\delta^{13}C$ of the methanol used in the derivatisation and X is the number of carbon atoms in the FA divided by the number of carbon atoms in the FAME derived from the FA.

Soil erosion tracing using CSSIs (e.g., FAMEs) requires that naturally abundant $\delta^{13}C$ values of FAMEs differed significantly between the source soils representing distinct LUT. Tukey's HSD test was applied to determine significant differences between $\delta^{13}C$ values of identical FAMEs among different source soils.

3.3.6 Determination of proportional land use specific soil contributions

The proportional contribution of each source soil to respective sediments was estimated by use of the mixing model SIAR (Stable Isotope Analysis in R) software package (Parnell et al., 2010a). SIAR uses a Bayesian model with a Markov chain Monte Carlo (MCMC) model fitting, which produces simulations of plausible values. The estimated values of the parameters are known as posterior distributions, representing a true probability density for the parameters of interest. A detailed description of SIAR can be found in Parnell et al. (2010a). True isotopic probability density functions showing the distribution of possible solutions for all sources in the model after correcting the isotopic proportions to soil proportions are displayed as Box-Whisker plots (Fig. 3.3). Respective numeric data of the quartiles are displayed in Table B1. Matrix plots of estimates of each source proportion are given to display correlation values between sources indicating the quality of source discrimination (Fig. A1). A strong negative correlation between two posterior values strengthens the possibility of a close relationship of two sources. Strong positive correlations indicate that one source alone is not adequate to provide a reasonable modeling result; another source is required (Inger et al., 2010; Parnell et al., 2010a, b).

Prior to each model run, we assessed the likelihood of every source contributing to the sediment mixtures in the SIAR model. When this assumption was violated, it was attributed to an unknown soil source. Linear mixing models (e.g., IsoSource; Phillips and Gregg, 2003) use a discrete mixing polygon to assess for point-in-polygon conditions. Consequently, the isotopic signature of the mixture must be located within a polygon enclosing the signatures of sources (Phillips and Gregg, 2003). SIAR, however, will always attempt to fit a model, even if the sources lie outside of the isotopic mixing polygon (Parnell et al., 2010). Thus, to enhance the

plausibility of results, we examined the data prior to the SIAR runs using a Monte Carlo simulation of mixing polygons for the point-in-polygon test (Smith et al., 2013). Convex hulls ('mixing polygons') were iterated using the distributions of the CSSI values of FAMEs of the intended source soils. The proportion of polygons which provide a solution (i.e., meet the point-in-polygon assumption) was then calculated. This provided a quantitative basis for model rejection and exclusion of sediments which were within less than 5% of the iterated mixing polygons.

Finally, the isotopic proportions of FAMEs were corrected to soil proportions (Equation 3). Since the isotopic values are related to the different carbon contents of the source soils, the SIAR data needed to be corrected by the SOC content of each source. This conversion uses a linear correction equation based on the bulk C content of each source soil:

$$\%source_n = \frac{I_n / \%C_n}{\sum_n^1 (I_n / \%C_n)} x10 \qquad (3.3)$$

where I_n is the mean proportion of source n in the mixture as estimated from isotopic values of C by SIAR, and $\%C_n$ is the %C in the source n soil (Gibbs, 2008). Corresponding soil proportions are presented in Box-and-Whisker plots (Fig. 3.2).

3.4 Results

3.4.1 Effects of different land use categories and catchments on $\delta^{13}C$ values of FAMEs

A two-way analysis of variance with a post hoc Tukey test of $\delta^{13}C$ values of methanol corrected FAMEs was conducted to examine the effect of different LUC on $\delta^{13}C$ values of FAMEs. Six frequently occurring FAMEs, i.e., lauric acid (Me C12:0), myristic acid (Me C14:0), palmitic acid (Me C16:0), stearic acid (Me C18:0), behenic acid (Me C22:0) and lignoceric acid (Me C24:0) were considered, making possible to group LUT into LUC (Table 3.3).

Table 3.3. Methanol corrected $\delta^{13}C$ –FAME (‰, VPDB) values of six frequently occurring fatty acids to enable intra-catchment comparisons. Fatty acids were extracted from topsoil (0-2 cm).

CAT	LUC	LUT	$\delta^{13}C$ - FAME values (‰, VPDB) of land uses											
			Me C12:0		Me C14:0		Me C16:0		Me C18:0		Me C22:0		Me C24:0	
			M	SE	M	SE	M	SE	M	SE	M	SE	M	SE
NAC	FO	PI	-32.1	0.3	-33.7	0.1	-30.6	0.1	-28.6	0.2	-30.5	0.1	-31.0	0.1
	NC	RO	-32.0	0.5	-33.3	0.2	-30.5	0.3	-29.3	0.2	-31.0	0.7	-31.1	0.8
	FO	NF	-33.9	0.5	-33.3	0.2	-30.3	0.2	-28.6	0.2	-32.0	0.2	-32.4	0.3
	NC	SC	-34.0	0.4	-34.2	0.3	-30.3	0.1	-30.6	0.2	-33.0	0.1	-32.8	0.2
LOS	FO	PI	-33.9	0.1	-35.3	0.1	-30.7	0.3	-29.2	0.0	-30.8	0.2	-32.8	0.1
	FO	EU	-32.8	1.2	-36.3	1.0	-30.5	0.0	-29.5	1.0	-29.7	0.1	-30.9	0.1
	NC	RO	-32.1	1.3	-34.3	0.4	-30.2	0.1	-29.4	0.5	-31.6	0.0	-30.7	0.1
	FO	NF	-35.4	0.2	-32.9	0.2	-29.2	0.1	-28.9	0.5	-30.9	0.1	-32.1	0.4
	NC	SC	-30.4	1.5	-33.8	0.3	-30.1	0.1	-30.3	0.2	-29.9	0.2	-30.6	0.6
POP	NC	AB	-34.4	1.1	-31.2	0.1	-28.4	0.5	-30.3	0.1	-34.8	0.3	-34.3	0.3
	NC	GU	-34.6	1.2	-30.7	0.2	-30.5	0.3	-31.7	0.3	-35.0	0.5	-33.2	0.2
	CL	CE	-35.6	1.0	-30.8	0.4	-27.5	0.6	-28.3	0.8	-32.5	0.5	-31.4	0.5
	CL	OR	-33.8	1.5	-31.4	0.3	-29.7	0.2	-29.7	0.6	-35.1	0.2	-34.9	0.6
	FO	NF	-32.8	2.1	-31.2	0.5	-29.2	0.4	-31.2	0.5	-34.6	0.3	-33.1	0.4
	FO	PF	-29.5	2.1	-32.7	0.5	-29.2	0.1	-30.5	0.2	-33.9	0.4	-32.7	0.3
CHK	FO	NF	-30.2	0.4	-31.9	0.6	-31.3	0.4	-29.7	0.3	-34.2	0.4	-34.7	0.8
	FO	SF	-29.1	0.1	-31.0	0.3	-32.8	0.8	-32.9	1.0	-33.1	0.9	-33.4	1.0
	CL	MA	-28.1	0.4	-28.3	0.3	-27.5	0.4	-27.1	0.3	-29.5	0.4	-29.2	0.7
	CL	CA	-27.2	0.5	-28.4	0.4	-26.9	0.4	-26.8	0.3	-29.7	0.6	-29.7	0.6
	CL	TE	-28.0	0.3	-29.4	0.4	-29.7	1.0	-28.9	0.5	-33.1	0.8	-33.4	0.7
	CL	OR	-28.3	0.1	-29.0	0.3	-27.3	0.2	-27.5	0.2	-32.3	0.3	-31.8	0.4
XIN	CL	OR	-33.4	0.3	-33.0	0.9	-31.1	0.9	-30.3	1.0	-34.5	1.3	-34.3	0.7
	CL	RP	-28.3	0.4	-31.3	0.7	-31.3	1.9	-28.7	0.7	-34.7	0.8	-32.7	0.5
	CL	MX	-28.8	0.6	-28.1	0.6	-26.9	0.4	-24.3	0.5	-31.8	0.4	-32.0	0.4
	CL	YB	n.a.	n.a.	-30.7	0.7	-29.9	1.1	-27.4	1.4	-33.3	1.2	-36.6	0.6
	CL	YC	-26.8	0.7	-28.8	1.1	-20.8	0.6	n.a.	n.a.	-31.0	2.8	-29.8	2.3
	FO	CF	-31.4	0.2	-33.2	0.4	-32.3	0.6	n.a.	n.a.	-35.5	0.2	-35.4	0.7
	FO	BF	n.a.	n.a.	-30.0	0.7	-32.6	0.2	-32.0	0.2	-33.2	0.7	-34.6	0.8
MYB	CL	CE	-31.0	0.6	-30.6	0.9	-30.1	0.7	-29.2	0.4	-32.3	0.4	-33.3	0.4
	FO	NF	-30.7	0.5	-32.9	0.7	-29.3	0.7	n.a.	n.a.	-32.6	1.0	-32.7	0.9
	NC	SL	-30.9	0.9	-31.3	0.6	-30.0	0.8	-29.9	0.5	-31.7	1.3	-34.1	1.1

Abbreviations: M: mean value, SE: standard error

Overall, the LUC with the median value for the highest isotopic fractionation was found for NC with a $\delta^{13}C$-FAME value of -31.8 ‰, VPDB, closely followed by FO (-31.6 ‰, VPDB) and CL (-29.5 ‰, VPDB) (Fig. 3.2). The $\delta^{13}C$ values of FAMEs were significantly affected by LUC ($p < 0.05$) and CAT ($p < 0.05$). For both factors, a significant interaction was determined ($p < 0.05$). Moreover, CL differed significantly from FO and NC ($p < 0.05$). No significant difference was found for FO and NC ($p > 0.05$).

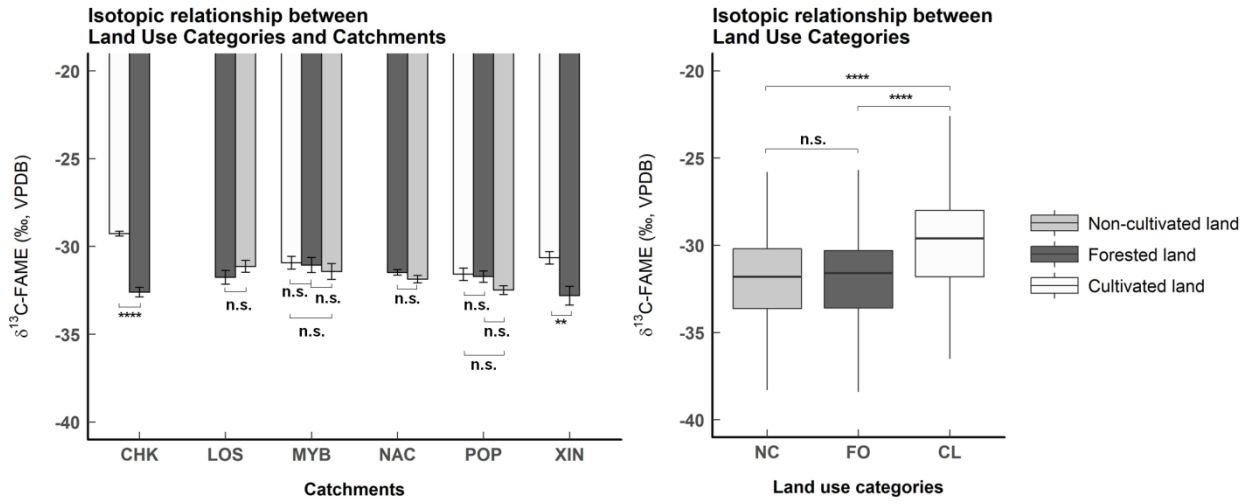

Fig. 3.2. Relationship of δ^{13}C-FAME values between individual land use categories and catchments (bar chart), and between total land use categories only (box-and-whisker plot). Significance codes: non-significant ($p > 0.05$) 'ns'; ($p < 0.05$) '*'; ($p < 0.01$) '**'; ($p < 0.001$) '***'; ($p < 0.0001$) '****'.

3.4.2 Selection of sediment samples via point-in-polygon testing

SIAR uses distributions instead of average values of δ^{13}C signatures of FAMEs in sources and hence will calculate source contributions even when a model is unlikely to meet the point-in-polygon assumption for every mixture. To increase the reliability of the SIAR output, a Monte Carlo simulation of mixing polygons for the point-in-polygon test was used (Smith et al., 2013). The results of the point-in-polygon test for the six catchments are shown in Fig. 3.3. The distance of selected δ^{13}C – FAME values revealed a clear distinction of LUC, specifically when CL was absent (e.g., in NAC and LOS). In more detail, the δ^{13}C – FAME values of the single sediment sample of LOS complied with the point-in-polygon assumption. Two sediment samples of NAC, which did not meet the point-in-polygon assumption, were rejected from further data analysis. Conversely, all sediment samples of POP were included in the analysis. In MYB, all sediment samples, except riverbank sediments, complied with the point-in-polygon assumption. In XIN, δ^{13}C – FAME values of two out of three sedimentation areas complied with the point-in-polygon assumption. Most sediment samples collected in CHK and which did not meet the point-in-polygon assumption showed δ^{13}C – FAME values of approximately -27‰, VPDB, suggesting an unknown sediment source.

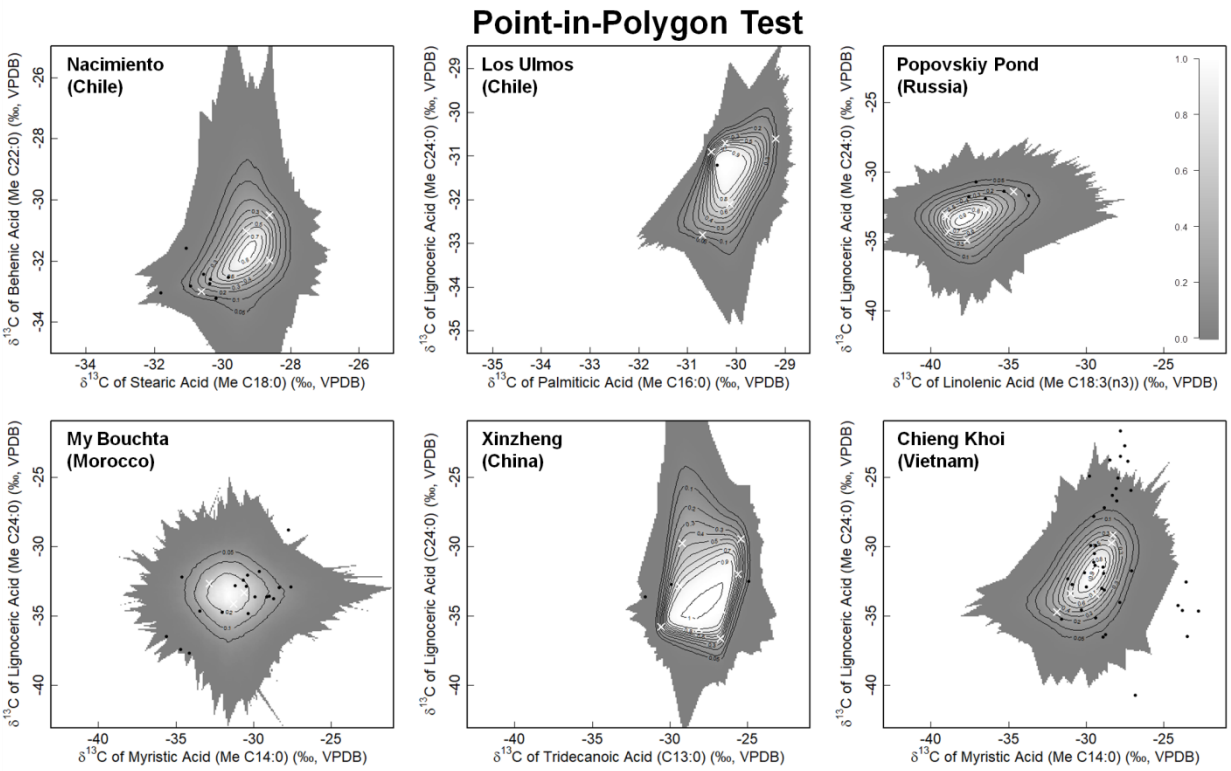

Fig. 3.3. The simulated mixing region showing the source signatures (white crosses) and sediments signatures (black dots). The proportion of iterations for which the sediment signature was within a mixing polygon is indicated by probability contours (5% level (outermost contour) and at every 10% level; for grading see side bar). If a sediment sample is within less than 5% of polygons, the proposed mixing model is considered unsuitable.

3.4.3 Proportional soil contributions in individual catchments

For this step, the selection of FAMEs was based on their occurrence in all soil and sediment samples in each individual catchment as well as significant differences in their $\delta^{13}C$ values. Compared to all other catchments, LUT of both Chilean catchments revealed very high SOC content, ranging from 3.0% (RO) to 9.0% (SC) in NAC and 2.8% (RO) to 19.2% (PI) in LOS (Tables C1 and C2). Highly significant $\delta^{13}C$ – FAME values were found for NAC when SC was included. In this case, the greatest distinction was found for PI vs. SC (i-C15:0, C18:0, C22:0 ($p < 0.05$)). Sediment material of NAC was composed mainly of soil originating from two non-cultivated LUT, SC (62%) and RO (12%) (Fig. 3.4, Table C1). Significances of $\delta^{13}C$ – FAMEs in LOS were generally lower than in NAC, where the greatest distinction was found for RO vs. EU (C22:0 ($p < 0.05$)). The highest contribution of sediment material of LOS originated from a non-cultivated source, RO (61%) (Fig. 3.4, Table C2).

SOC values of POP ranged from 1.3% (CE) to 4.2% (NF). Significant FAME differences were predominantly found among those LUT including CE (9 FAMEs, p <0.05). The soil contribution of CE (58%) was distinctly higher than any other LUT (Fig. 3.4, Table C3).

SOC values of MYB ranged from 0.4% (CE) to 4.6% (NF). Unlike all other catchments included in this study, $\delta^{13}C$ signatures of individual FAMEs of MYB did not show any LUT effect (p > 0.05). However, the majority of eroded soil material in MYB originated from CE (71%) (Fig. 3.4, Table C4). SOC values of XIN ranged from 1.0% (RP) to 4.2% (CF). A significant LUT effect on $\delta^{13}C$ signatures of individual FAMEs was found for MX vs. OR (C13:0, C14:0 (p < 0.05)). Highest proportional soil erosion rates in XIN were calculated for RP (23%) and YC (22%) (Fig. 3.4, Table C6).

SOC values in CHK were the lowest among all catchments, ranging from 0.7% (CA) to 2.9% (NF). The majority of FAMEs showed a clear distinction between the $\delta^{13}C$ signatures of C_3 and C_4 plants. Greatest distinction was found for NF vs. MA (C14:0, C16:0, C18:0, C20:0, C22:0, C24:0 (p < 0.05) and C12:0, C14:1, C18 comb (p < 0.05)). Highest soil contributions to sediment deposition in CHK were observed for CA (32%) and MA (27%) (Fig. 3.4, Table C6).

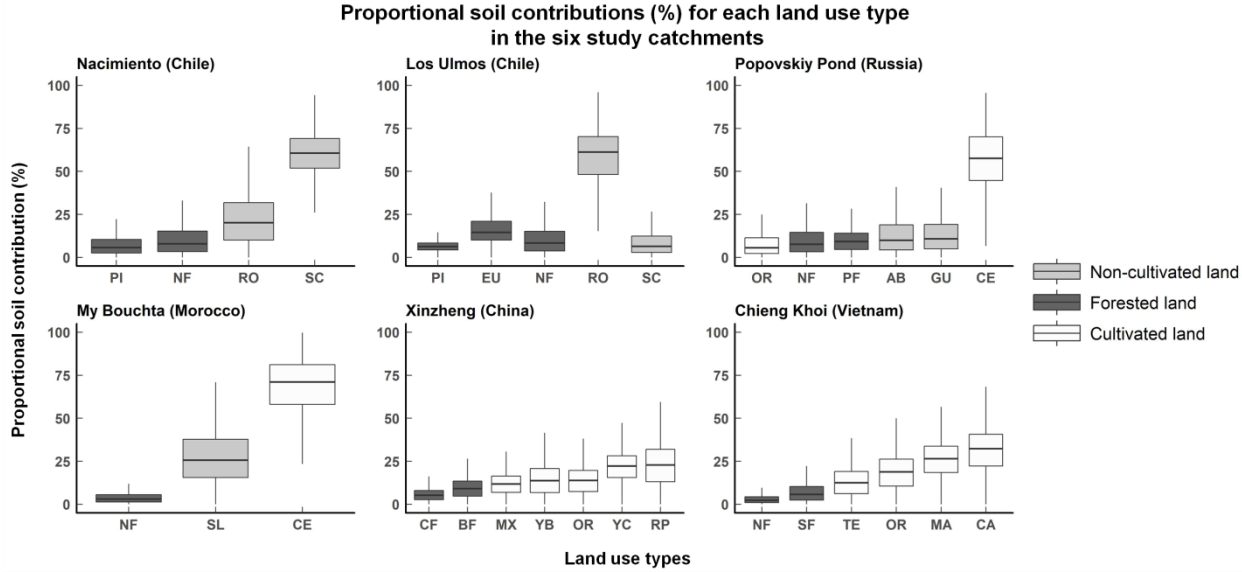

Fig. 3.4. Estimates of soil proportions for all catchments source proportion were calculated using a linear correction equation (Eq. 1) based on the carbon content of each source soil. The underlying isotopic proportions were calculated using the mixing models from the SIAR package for R.

3.5 Discussion

The benefits applying the FA-based CSSI technique to an individual catchment basis are well documented, but not yet validated at a global scale, which emphasizes distinct agriculturally used catchments of various sizes and agro-ecologies. Such validation is needed for broad-scale application at the global scale since earlier studies (e.g., Gibbs, 2008; Blake et al., 2012; Hancock and Revill, 2013, Alewell et al., 2016) relied on different laboratory and statistical routines.

3.5.1 Land use categories as a uniform dimension for catchment comparisons

Irrespective of agro-ecology and catchment size, the CSSI technique demonstrated its potential for global applicability in detecting relevant hotspots of soil erosion. Across most catchments, we have shown that the grouping of individual land use types (LUT) into major land use categories (LUC) is critical for reliable detection of hotspot sources into sediments. In our study, sediments originated, to a great extent, from LUC "Cultivated land (CL)" which was mainly characterized by crops (e.g., cereals) and tree plantations (e.g., teak, orchards). In the case of both Chilean catchments (NAC, 12.4 ha; LOS, 19.8 ha), the soil erosion hotspots belonged predominantly to "Non-cultivated land (NL)" (e.g., roads, river bank erosion). The major contribution by NL relative to that of CL is likely due to the physical stability of mature, erosion resistant volcanic soils typically found in the Chilean catchments (Shoji et al. 1993).

The use of LUT to characterize various vegetation types as sediment sources was specifically applicable when all LUC were represented in each catchment (i.e., Morocoo, 766 ha; Russia, 198 ha) or when both C_3 and C_4 (e.g., maize) vegetation types were found (Vietnam, 207 ha). However, significant differences were also found for LUT when no C_4 plants were present (e.g., Russia). Moreover, the resolution limit of the CSSI technique to distinguish LUT was reached in the case of the Chinese (XIN, 11.42 ha) catchment. This may have been due to the very small catchment size of XIN characterized by highly heterogeneous LUT with a long history of frequent land use transformation, interfering with the explicit localization of erosion hotspots. Hence, the combination of larger sized (>1 ha) fields with less diverse LUT are preferred for reliable application of the CSSI technique. A possible solution for such a limitation of the CSSI technique was recently demonstrated by Cooper et al. (2015) combining molecular as well as $\delta^{13}C$ and $\delta^{2}H$ CSSI analysis of *n*-alkane plant lipid extracts. With this approach, the resolution limit of the CSSI technique was reduced, making it possible to discriminate among trees, herbaceous perennials, and C_3 and C_4 graminoids.

3.5.2 Potential restriction of erosion source discrimination by compound-specific $\delta^{13}C$ isotopes

In a broader sense, the output of the CSSI technique, which requires the solving of a mixing model (e.g., Isosource, SIAR, MixSIAR), depends both on different isotopic values and a conversion factor (i.e., SOC and FAME content) (Gibbs et al., 2008; Alewell et al., 2016). Generally, the smaller the difference of isotopic values of sources and/or the higher the variability of isotopic values of sediments, the more uniform the isotopic proportions of the sources become. In the case of complete isotopic uniformity, the conversion factor exclusively controls the resulting soil proportions of sediment sources (e.g., Morocco). Inevitably, this leads to a preference of LUT with low SOC content as the major source of sediments, which is often the case for agricultural LUT. Accordingly, the output of the CSSI technique may be most reliable when three prerequisites are met. First, significant differences in $\delta^{13}C$-FAME values between the various sources must exist. Second, the correction factors (i.e., SOC and FAME contents) for each source must not differ greatly from each other. Third, $\delta^{13}C$-FAME values of the sediment samples from a given deposition area must not scatter strongly (i.e., no coverage of the entire isotopic range of the potential sources). Therefore, prior significance testing of $\delta^{13}C$-FAME values along with point-in-polygon tests with significant FAMEs is important to ensure both reliable discrimination of LUT and detection of unknown sources that might influence the sediment apportionment (Brandt et al., 2016; Blake et al., 2012; Torres et al., 2009).

3.5.3 Considerations for reproducibility

Generally, the significance test applied also allows for potential refinement of soil source sampling schemes. Although each catchment has its site-specific characteristics, it is recommended to use aligned and statistically sound soil sampling procedures that permit reproducible intra- (LUC, LUT) and inter-catchment comparisons. In this respect, the spatially stratified “Y-frame” sampling scheme (Vågen et al., 2013), recently used by Mirzaeitalarposhti et al. (2015) and Cobo et al. (2010) for regional soil quality studies across spatial scales, may serve as a baseline for prospective erosion studies using the CSSI technique. Furthermore, the adoption of geostatistics (Cobo et al., 2010; Wagner and Fortin, 2005; Davidson and Csillag, 2003) with the development of stable semivariograms using geo-referenced datasets in the CSSI framework may help to assess spatial variability of soil FAs and SOC, needed to ensure reliable CSSI results.

The decision on how to design a CSSI-based sediment source tracing study should be initially based on a precise characterization of the target catchment, emphasizing not only the identification of hotspots of agricultural LUT, but also those additional sources found in non-vegetated areas (e.g., roads, eroding channel banks). The importance of explicit consideration of non-vegetated areas was evidenced by our results in the Chilean catchments (e.g., NAC, LOS), where unpaved forest roads, as well as stream and channel bank erosion, have largely contributed to the sediment materials. Under such circumstances, the integration of complementary tracing techniques may enhance the precise identification of sediment sources. For example, Blake et al. (2012) as well as Hancock and Revill (2013) used geochemical properties (e.g., trace metals) to complement the separation of agricultural from non-vegetated sources, including channel banks.

3.6 Conclusions

Regardless of agro-ecology and catchment size, the aligned protocol of the CSSI technique confirmed its potential global applicability to detect relevant hotspots of soil erosion. Across most catchments, we showed that the grouping of individual land use types (LUT) in major land use categories (LUC) was critical for reliable detection of major hotspot sources into sediments. The use of LUT to characterize various vegetation types as sediment sources was specifically applicable when all LUC were represented in each catchment or when both C_3 and C_4 vegetation were present. The resolution limit of the CSSI technique to distinguish LUT was, however, reached when catchments were very small and characterized by highly heterogeneous LUT with a long history of frequent land use transformations. Hence, the combination of larger sized
(>1 ha) fields with less diverse LUT is preferable for reliable application of the CSSI technique. In this respect, the CSSI output may be most reliable when (i) significant differences in δ^{13}C-FAME values between the various sources exist, (ii) the correction factors of each source do not differ greatly from each other, and (iii) the δ^{13}C-FAME values of the sediment samples of a given deposition area are not scattered strongly. Moreover, progress in CSSI sediment tracing will be made through the combined use of saturated long chain FAs (> C20:0) to ensure the exclusive detection of plant-derived FAs and improved Bayesian mixing models that permit the incorporation of concentration dependency of biotracer elements, e.g. MixSIAR (Stock and Semmens, 2013).

One of the main objectives of the IAEA-coordinated research project (CRP), in which our presented study has been implemented, was to develop integrated isotopic approaches to identify hot spots or critical areas of land degradation in agricultural catchments. One major outcome of this project was the development of the presented aligned protocol of using the CSSI technique combined with Bayesian statistics to discriminate sediment sources across catchments of different sizes and agro-ecologies. As a further analytical development, we have recently integrated the CSSI technique with FRN analysis to successfully estimate past sediment budgets for specific LUT (Brandt et al., 2018). This integrated approach provided novel insights into the accelerating impact of land use change on soil retrogression and degradation, and overcame acknowledged limitations of using the CSSI and FRN techniques as stand-alone methods (Brandt et al., 2016; Hancock and Revill, 2013; Blake et al., 2012).

As a way forward, the integration of complementary proxies such as geochemicals and radionuclides (Blake et al. 2012; Hancock and Caitcheon, 2010; Hancock and Revill, 2013), ^{2}H isotopes, average chain lengths (ACL), and carbon preference indices (CPI) (Cooper et al. 2015), as well as spectral information via infrared diffuse reflectance Fourier transform spectroscopy (midDRIFTS) (Poulenard et al., 2012; 2009) along with the proposed CSSI and FRN rechniques will provide an in-depth knowledge of the investigated catchments and their most relevant sources, the locations of sediment deposition and the possible erosion pathways.

Chapter IV Integrating compound-specific $\delta^{13}C$ isotopes and fallout radionuclides to retrace land use type-specific net erosion rates in a small tropical catchment exposed to intense land use change[3]

Christian Brandt[1], Moncef Benmansour[2], Leander Walz[1], Lam T. Nguyen[3], Georg Cadisch[1], Frank Rasche[1]

[1]Institute of Agricultural Sciences in the Tropics (Hans-Ruthenberg-Institute), University of Hohenheim, Stuttgart, Germany

[2]Centre National de l'Energie, des Sciences et des Techniques Nucléaires, Rabat, Morocco

[3]Department of Environmental Management, Vietnam National University of Agriculture, Hanoi, Vietnam

4.1 Abstract

Retracing net erosion rates linked to land use change in tropical agricultural catchments dominated by small-holder farmers is challenging, due largely to catchment heterogeneity and uncontrolled farming practices. To tackle this problem and to complement a preceding study (Brandt et al., 2016), we introduce here an advanced approach that integrates compound-specific $\delta^{13}C$ isotopes (CSSI) and fallout radionuclides (FRN), Excess lead-210 ($^{210}Pb_{ex}$) and Cesium-137 (^{137}Cs) to estimate past net erosion rates of dominant land use types in the mountainous catchment Chieng Khoi (207 ha, Northwest Vietnam). Spatially-integrated topsoil (0 to 2 cm) samples of dominant land use types (e.g., protected and secondary forests, teak, fruit orchards, maize, cassava) were collected from at least three discrete plots of each land use type within the upland area (i.e., erosion sites) of the studied catchment. In the corresponding lowland area, a representative sediment profile was localized and divided into sections of 2 to 4 cm for CSSI and FRN analysis. Samples for FRN reference data were taken from undisturbed areas in close proximity.

[3]A version of this chapter was published as:

Brandt, C., Benmansour, M., Walz, L., Nguyen, L.T., Cadisch, G., Rasche, F., 2018. Integrating compound-specific $\delta^{13}C$ isotopes and fallout radionuclides to retrace land use type-specific net erosion rates in a small tropical catchment exposed to intense land use change. Geoderma 310, 53–64.

At a soil deposition site near a lakeshore, $^{210}Pb_{ex}$ data determined the age and sediment accumulation rates of 19 sediment layers to a depth of 38 cm. Based on $^{210}Pb_{ex}$ activity, maximum sediment accumulation rates of 127 t ha^{-1} y^{-1} were calculated, corresponding to erosion rates of about 16 t ha^{-1} y^{-1} for the total catchment area. CSSI data confirmed that maize and cassava were the most important erosion sources during a period of dramatic land use change (1987 to 2004), when forests were cleared, and high-yielding maize hybrids were introduced. Based on integrated FRN and CSSI data, net erosion rates of maize and cassava reached maximum rates of 4.8 t ha^{-1} y^{-1} (maize), 6.2 t ha^{-1} y^{-1} (cassava). This major finding verified the potential of integrating FRN and CSSI to accurately estimate land use type-specific net erosion rates. In conclusion, determining past sediment budgets for specific land use types provides insight into the accelerating impact of specific land use change on soil retrogression and degradation. Such knowledge is of prime importance for effective soil conservation through evidence-based land management and decision making.

4.2 Introduction

In mountainous areas of Southeast Asia, land use change is an acknowledged threat to ecosystem stability, putting rural livelihoods at serious risk (Valentin et al., 2008; Wezel et al., 2002). Accelerating urbanization, changing market forces, and loss of agricultural land in the lowlands has pushed farmers to migrate to upland regions. Typically, this migration has resulted in serious intensification of land use followed by soil retrogression and degradation (Yen et al., 2013). For example, in the Chieng Khoi catchment in the northwestern uplands of Vietnam, shifting cultivation has been increasingly abandoned in favor of hybrid cash crops, primarily maize (*Zea maize* L.) and cassava (*Manihot esculenta* Crantz) (Podwojewski et. al., 2008; MSEC, 2000). Consequently, severe erosion on steep slopes (up to 174 t $ha^{-1}yr^{-1}$) occurred (Dung et al., 2008; Lam et al., 2005; Pansak et al., 2008; Tuan et al., 2014), along with accelerated sedimentation of paddy fields, local reservoirs and rivers (Dung et al., 2009; Lippe et al., 2014; Schmitter et al., 2012).

Strategies to counteract further soil degradation and the extension of agricultural land into remaining forests require solid data so that evidence-based land management decisions and effective soil conservation measures can be made. In this respect, fallout radionuclides (FRN; e.g., Cesium-137 (^{137}Cs), excess lead-210 ($^{210}Pb_{ex}$) and Beryllium-7 (^{7}Be) have proven most suitable for generating soil redistribution patterns at the catchment scale (Dercon et al., 2012; Mabit et al., 2008; Zapata, 2003). Based on their different half-lives and origins, FRN make it

possible to date the layers of a sediment profile and provide quantitative estimates on the amount (kg m^{-2} y^{-1}) of relocated soil (Dercon et al., 2012; Mabit et al., 2008; Walling et al., 2003). ^{137}Cs (half-life 30.17 yr) is of anthropogenic origin and is produced during nuclear fission. From 1952 – 1980s, ^{137}Cs was globally disseminated by atmospheric testing of thermonuclear weapons (UNSCEAR, 2000). $^{210}Pb_{ex}$ (half-life 22.2 yr) is of geogenic origin and its atmospheric fallout is constant over time at a specific site (Appleby and Oldfield, 1978). For more detailed and up-to-date information of the specific FRN used for this study (i.e. ^{137}Cs, $^{210}Pb_{ex}$), we refer the reader to the following two major review articles: Mabit et al. (2013) and Mabit et al. (2014).

Although FRNs estimate the quantitative sediment budget for a specific location, they do not assign a denudation rate to a specific upland land use type (Blake et al., 2012; Hancock and Revill, 2013). To resolve this question, the compound specific stable isotope (CSSI) technique using lipid biomarkers has been recently introduced to trace the sources of sediments (Chikaraishi and Naraoka, 2003; Gibbs, 2008; Mead et al., 2005; Ratnayake et al., 2011). Principally, this technique uses land use cover- dependent differences in the $\delta^{13}C$ isotopic signatures of specific organic compounds (i.e., soil fatty acids (FA)). The CSSI technique has been successfully tested and validated to estimate the proportional contributions of different land use sources to sediment bodies (e.g. Alewell et al. 2016, Blake et al., 2012; Brandt et al., 2016; Hancock and Revill, 2013).

To reconstruct historical land use, Gibbs (2014) suggested a multi-isotopic investigation involving FRN and CSSI techniques. To complement a preceding study by Brandt et al. (2016), we present here an enhanced approach that integrates FRN and CSSI techniques to accurately estimate land use type-specific net erosion rates, making it possible to determine past sediment budgets for specific land use types. Thus, we hypothesized that integrating FRN-derived quantitative past sediment budgets with CSSI-calculated proportional soil contributions to the layers of a sediment profile would permit estimation of land use type-specific past net erosion rates. We further hypothesized that knowledge about past net erosion rates would provide critical insights into past soil redistribution, providing a way to evaluate the accelerating impact of specific land use change on soil degradation in heterogeneous agricultural catchments.

4.3 Materials and Methods

4.3.1 Study area and sample collection

4.3.1.1 Study site

The Chieng Khoi catchment is located in the Chieng Khoi commune (21°7´60´´N, 105°40´0´´E), Son La province in Northwest Vietnam (Brandt et al., 2016). In this catchment, an irrigation lake was constructed in 1974 to regulate the supply of water to downstream paddy rice fields. Originating from the dammed stream Doi Ban, the Chieng Khoi Lake, of about 26 ha, is situated in a karstic depression surrounded by a chain of calcareous mountains, with a catchment area of about 207 ha. Elevation of the area around the lake ranges from 429 to 493 m above sea level (a.s.l.) with a slope of up to 86%.

Characteristic land use types of the upland area surrounding the lake were identified as potential sediment sources. These land use types included crops such as maize (*Zea mays* L.) and cassava (*Manihot esculenta* Crantz), as well as commercial forests consisting of teak (*Tectona grandis* L.) or Chukrasia (*Chukrasia tabularis* A. JUSS.). Fruit orchards, including mango (*Mangifera indica* L.), jackfruit (*Artocarpus heterophyllus* LAM.), tamarind (*Tamarindus indica* L.), and longan (*Dimocarpus longan* LOUR.), were also identified. Additionally, protected and secondary forests surrounding the lake were considered as potential sediment sources.

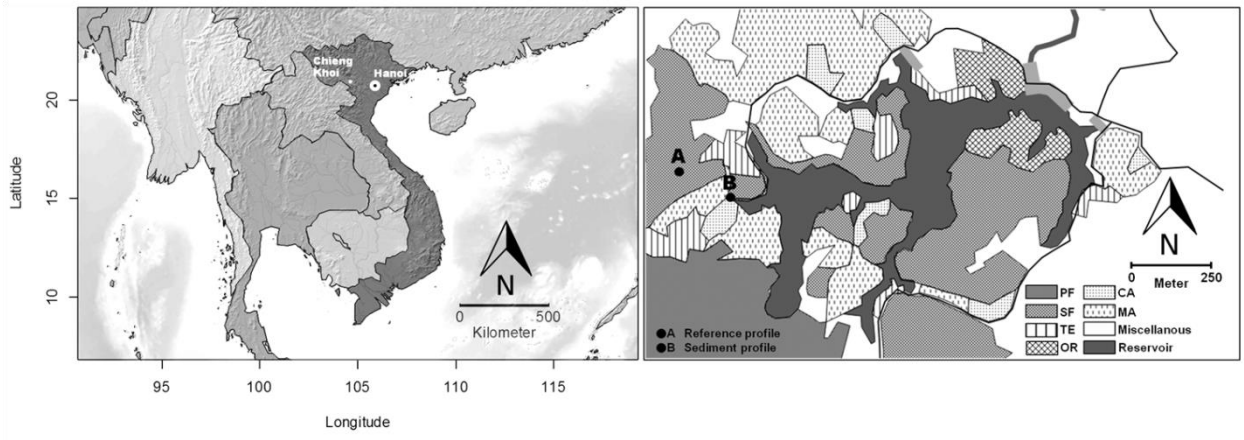

Fig. 4.1. Location map of the Chieng Khoi catchment in the Son-La Province, Northwest Vietnam. The locations of the reference (A) and sediment (B) profiles used in this study are shown at the west bank of the reservoir. Definition of abbreviations: PF = protected forest, SF = secondary forest, TE = teak, OR = fruit tree plantation, MA = maize, CA = cassava.

4.3.1.2 Land use history of the Chieng Khoi catchment

To quantify past sediment contributions from specific land use types, information on land cover history was obtained by interviewing local farmers of Ban Tum and Ban Me villages (Minh et al. 2011; Nguyen, personal communication). Considerable land use change started in the middle of the 20th century. Before 1973, almost the entire upland area of the catchment was covered in primary and secondary forest. Local varieties of upland rice and maize were cultivated only on small areas for shifting cultivation. During the early 1990s, deforestation intensified and the areas under cultivation increased. Cleared areas were cropped with fruit trees and increasingly with local varieties of bi- or tri-ennial cassava. Increasing land degradation and the loss of soil fertility led to the disappearance of upland rice (Oryza sativa L.) production after 1990. Cultivation of cotton (Gossypium spec.) was discontinued by the end of the 1980s, and white mulberry (Morus alba L.) for silkworms at the end of the 1990s (Lippe, personal communication). Near the end of the 1990s, teak, Chukrasia, and pine were introduced for reforestation and later extended to production forests. Cultivation of fruit orchards, including mango, jackfruit, tamarind, and longan, was also promoted. Since 1996, shrub- and tree-covered steep slope areas were successively replaced by high yielding hybrid maize and commercial 1-year cassava varieties. First, maize and cassava areas were intercropped with fruit trees. When demand and prices soared, intercropping was replaced by monoculture. This development was accompanied by increased use of chemical fertilizers, deep ploughing, and a transition from stick to furrow planting. After forest clearance, maize was cultivated as long as soil fertility was sufficient. When soil fertility declined on maize fields, 1-year cassava was introduced and cultivated for several years (Tuan et al., 2014). Fields are commonly left fallow when soil fertility declines below the requirement of cassava (Nguyen, personal communication).

4.3.1.3 Sample collection and preparation

Soil and sediment samples were collected from July to September 2010 and March to May 2012. Topsoil (0 to 2 cm) samples of individual land use types were collected from at least 3 discrete plots of each land use type within the upland area around the lake. In each plot, soil samples were obtained from 3 different positions (e.g., lower, middle, upper slope). At each position, 20 sub-samples from an area of 20 m^2 were combined to provide a composite sample of each land use type. Collecting composite samples made it possible to integrate spatial variability and therefore obtain a representative sample for each source. The alluvial fanlike site of the sediment core was located at the upper shore of a lake cove. This location was chosen

for the surrounding land use types, which were representative of the entire catchment area (Fig. 4.1b). The sediment core was divided into sections of 2 to 4 cm to a depth of 280 cm. The samples for CSSI and FRN analyses were taken every 2 cm. The generic feasibility test of integrating FRN and CSSI data to estimate land use type-specific net erosion rates was based on only one representative sediment profile. More profiles may have revealed in more detail the spatio-temporal variability of sediment deposition of the study area and refined information on the impact of specific land use types to past erosion processes. However, due to the need to limit the analytical expenditure for this exploratory approach, additional sediment profiles were not considered in this study. The first undisturbed reference site for ^{137}Cs and $^{210}Pb_{ex}$ was located in proximity to the sediment profile and the second site was located in the Ban Cang area neighboring the Chieng Khoi catchment. Reference sites were investigated for ^{137}Cs and for $^{210}Pb_{ex}$ to evaluate the reference inventory that would then be compared to the radioisotopic inventory in the sedimentation area where we expected higher ^{137}Cs and $^{210}Pb_{ex}$ levels.

4.3.2 FRN analysis

4.3.2.1 Gamma spectrometry analysis

Soil samples were dried, sieved (< 2 mm) and homogenized prior to measuring ^{137}Cs, ^{210}Pb and Radon-226 (^{226}Ra; from its daughter Bismut-224 [^{214}Bi]) after equilibrium) by gamma spectrometry. High resolution broad energy detectors (48% efficiencies) were used for the γ-analysis. Calibration of the detection systems was done using a certified multi-gamma source and was controlled using IAEA reference materials (IAEA 327, IAEA 375). Approximately 40 g of soil were placed in cylindrical containers (50 ml). ^{137}Cs, total ^{210}Pb and ^{214}Bi activities were determined from the net peak areas of gamma rays at 661.6, 46.5 and 609 keV, respectively. $^{210}Pb_{ex}$ was determined by subtracting ^{226}Ra from total ^{210}Pb activity. The counting time was around 24 hours, and resulted in precision of about 30, 12 and 5% for ^{137}Cs, ^{210}Pb and ^{214}Bi, respectively, at the 95% confidence level. Under these conditions, the uncertainty associated with $^{210}Pb_{ex}$ is about 20 to 25%. High uncertainties associated with ^{137}Cs concentrations are due to their very low activity values. The minimum detection activities under the experimental conditions, for ^{137}Cs and ^{210}Pb and ^{214}Bi, were around 0.4 and 5 and 1.8 Bq kg^{-1}, respectively. Quality control procedures were applied using control charts (i.e., efficiency, resolution, background), certified reference materials, and regular participation in inter-comparison exercises and proficiency tests organized by IAEA (Shakhashiro and Mabit 2009). In order to

assess sediment accumulation rates using FRN data, dry bulk density of soil and sediment samples was determined according to McKenzie et al. (2004).

4.3.2.2 Age determination of sediment layers using ^{137}Cs

The anthropogenic radionuclide ^{137}Cs was used as a tracer to identify the sediment layers of 1954 and 1964. These layers are expected to show spikes of ^{137}Cs concentrations since they represent the beginning of atmospheric nuclear testing in 1954 and the maximum ^{137}Cs deposition in 1964 (Ritchie and McHenry, 1990). The depth of these layers was used to review the age of layers as estimated from $^{210}Pb_{ex}$.

4.3.2.3 Estimation of sediment accumulation rates using $^{210}Pb_{ex}$

Estimation of sediment accumulation rates requires a model to calculate the depth-age relationship of the decrease in $^{210}Pb_{ex}$ with sediment depth. In this study, the Constant Flux and Constant Sedimentation rate (CFCS) and Constant Rate of Supply (CRS) dating models were used (Appleby and Oldfield, 1978; Krishnaswami and Kirkcochran, 1978). Subsequently, the age of the layers was determined by dividing the cumulative mass g cm^{-2} of each layer by the sediment accumulation rates, R in g cm^{-2} y^{-1}. The CRS model was developed to explain the interaction between the sedimentation rate R and the radioactive decay of $^{210}Pb_{ex}$ (Appleby and Oldfield, 1978).

4.3.3 CSSI analysis

The determination of bulk soil carbon (C) isotopic ratios ($\delta^{13}C$), organic C content of soil and sediment samples, as well as the extraction, fractionation, derivatization and $\delta^{13}C$ measurement of fatty acids (FAMEs) were performed according to Brandt et al. (2016). The report also contains a detailed description of the determination of proportional land use type-specific soil contributions. To limit the potential influence of fatty acids that are of non-vegetal origin, behenic acid (C22:0) and lignoceric acid (C24:0) were selected for further statistical analysis.

4.3.4 Estimation of land use type-specific net soil erosion rates by integrating FRN and CSSI

Land use type-specific net soil erosion rates were estimated using FRN-derived quantitative past sediment budgets and CSSI-derived proportional soil contributions from each land use type. Average net erosion rates were calculated by dividing the lake area (approximately 26 ha) by the entire catchment area (approximately 207 ha) to compensate for the absence of detailed data on which areas contributed most to sediment deposition. The resulting factor was then multiplied together with sediment accumulation rates estimated for a specific layer of the sediment profile. Net erosion rates were estimated using sediment accumulation rates calculated with the CRS model. The land use type-specific net erosion rates were then obtained by multiplication of net erosion rates with the proportional soil contributions (%):

$$\text{Net erosion rate} = \frac{\text{R x } A_{\text{lake}} \text{ ln}}{A_{\text{catchment}}} \quad \text{(Eq. 4.1)}$$

where:

Net erosion rates: annual net soil erosion rate (t ha^{-2} y^{-1})

R: sediment accumulation rates as estimated from CRS model (g cm^{-2} y^{-1})

In: mean feasible portion of source n in the mixture as estimated from SIAR (%)

A_{lake}: area of the lake (m^2)

$A_{catchment}$: area of the catchment (m^2)

4.4 Results

4.4.1 FRN analysis

4.4.1.1 Vertical distributions and inventories of ^{137}Cs and $^{210}Pb_{ex}$

Radionuclide vertical distributions and inventories were determined for both reference (Fig. 4.2a, b) and sediment (Fig. 4.2c, d) profiles. The layer-explicit data from two reference profiles were combined to obtain an average vertical distribution and concentration of ^{137}Cs (Fig. 4.2a). The mean concentration of ^{137}Cs decreased slightly within the top 3 cm followed by a broad peak between 5 cm and 9 cm and a sharp decline from 10 cm. A maximum of 1.05 Bq kg^{-1} was observed at 7 cm. Radioactivity below 16 cm was not detectable (<0.40 Bq kg^{-1}). $^{210}Pb_{ex}$ concentration was highest in the top layer with a value of 51.30 Bq kg^{-1} (Fig. 4.2b).

Concentrations of $^{210}Pb_{ex}$ were found in deeper layers, about 2 Bq kg^{-1} below 18 to 20 cm. The radionuclide inventories associated with the reference site were detected at about 220 and 3137 Bq m^{-2} for ^{137}Cs and $^{210}Pb_{ex}$, respectively. ^{137}Cs and $^{210}Pb_{ex}$ vertical distributions in the sediment profile are shown in Fig. 4.2c) and d). Generally, the concentrations of both ^{137}Cs and $^{210}Pb_{ex}$ varied greatly between layers. The mean concentration of ^{137}Cs was close to or below the detection limit of 0.40 Bq kg^{-1} (Fig. 4.2c). Highest activities were measured between 13 and 19 cm with a maximum at 15 cm (0.8 Bq kg^{-1}). ^{137}Cs concentrations below 20 cm were almost exclusively below the detection limit. The vertical distribution pattern of $^{210}Pb_{ex}$ concentration of the sediment profile (Fig. 4.2d) was distinctively different from the reference profile (Fig. 4.2b). Contrary to the exponential decrease observed from the top layer in $^{210}Pb_{ex}$ concentration in the reference profile, $^{210}Pb_{ex}$ activity in the sediment profile decreased linearly with the exception of an area of increased activity between 13 to 30 cm. Maximum concentration was found at 17 cm (34.6 Bq kg^{-1}).^{137}Cs and $^{210}Pb_{ex}$ inventories associated with the sediment accumulation site were about 258 and 9515 Bq m^{-2}, respectively.

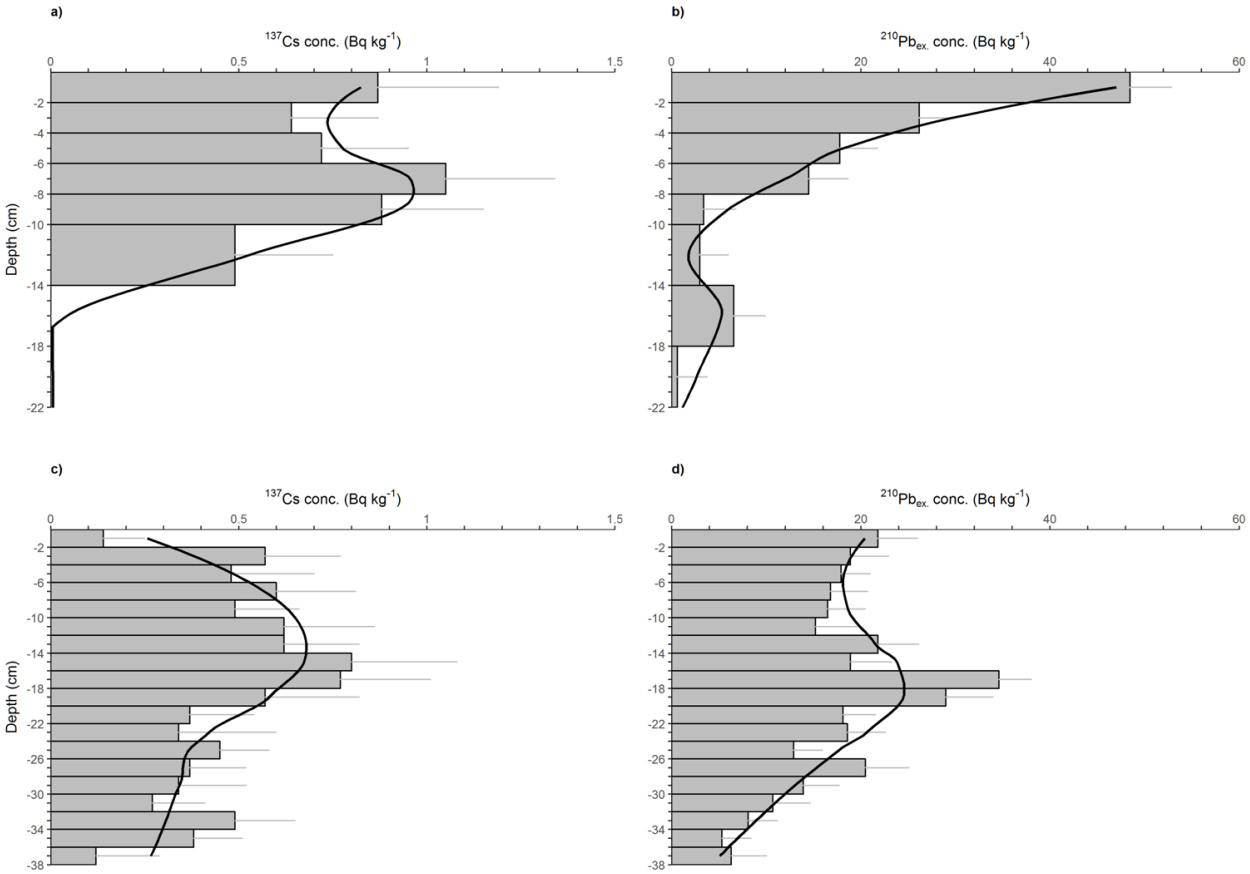

Fig. 4.2. The layer-explicit radionuclide data of two reference profiles were combined to obtain an average vertical distribution and concentration of a) ^{137}Cs and b) $^{210}Pb_{ex}$. The vertical

distribution and concentration of the mean values of the uncertainties associated with each radionuclide in the sediment profile are given for c) ^{137}Cs and d) $^{210}Pb_{ex}$. The uncertainty is expressed at 2σ. Included are locally weighted smoothing (LOESS) curves.

4.4.1.2 $^{210}Pb_{ex}$ chronology and sediment accumulation rates

Table 4.1 and Fig. 4.4 summarize the sediment accumulation rates and respective years of sedimentation based on $^{210}Pb_{ex}$ activity. Both dating models indicated a decrease in sediment accumulation rates with depth. This suggested an increase in sediment accumulation in the recent past (depth-age relationship). The sediment accumulation rates for 2010, the most recently documented year, amounted to 1.27 g cm^{-2} y^{-1} (CRS) and 1.32 g cm^{-2} y^{-1} (CFCS). Sediment accumulation rates before 1987 were minor (CRS), and increased at the beginning of the 1990s. A maximum was observed for the year 2004, with 1.39 g cm^{-2} y^{-1} (CRS) and 1.32 g cm^{-2} y^{-1} (CFCS). CFCS-derived sediment accumulation rates were constant for each section, while CRS-estimated rates differed for each sediment layer. The results of both dating models indicated that the individual soil layers of the upper 11 cm corresponded to the past decade (2000 to 2010). The estimated ages of older sediment layers deviated strongly between both models. The average relative uncertainty for each radionuclide (30-35% for ^{137}Cs and 20-25% for $^{210}Pb_{ex}$) was applied to all layers. As a reference, the year of maximum ^{137}Cs fallout (1964) is shown in Table 4.1. However, this reference value deviated from those of the dating models (Fig. 4.3). The estimated age of older sediment layers also differed between models. The variance in estimated sediment age increased with depth of the sediment (Fig. 4.3).

Table 4.1. Mean radionuclide inventories and uncertainties associated with each radionuclide in the reference and sediment profiles. The uncertainty is expressed at 2σ. The values of the reference profiles below the depth of 10 cm are based on layer thicknesses of 4 cm.

depth (cm)	Radionuclide inventories (Bq kg^{-1})							
	Reference				Sediment			
	^{137}Cs		^{210}Pb$_{ex}$		^{137}Cs		^{210}Pb$_{ex}$	
	M	uncertainty	M	Uncertainty	M	uncertainty	M	uncertainty
-2	0.87	0.32	48.47	4.37	0.14	0.11	21.8	4.17
-4	0.64	0.23	26.18	3.64	0.57	0.20	18.9	4.01
-6	0.72	0.23	17.76	3.95	0.48	0.22	17.9	3.08
-8	1.05	0.29	14.50	4.11	0.6	0.21	16.8	3.91
-10	0.88	0.27	3.37	3.40	0.49	0.17	16.5	3.99
-12					0.62	0.24	15.2	4.56
-14	0.49	0.26	2.96	2.99	0.62	0.20	21.8	4.35
-16					0.80	0.28	18.9	4.37
-18			6.58	3.27	0.77	0.24	34.6	3.42
-20					0.57	0.25	29.0	5.01
-22			0.59	3.14	0.37	0.17	18.1	3.47
-24					0.34	0.26	18.6	4.00
-26					0.45	0.13	12.9	3.04
-28					0.37	0.15	20.5	4.58
-30					0.34	0.18	13.9	3.82
-32					0.27	0.14	10.7	3.97
-34					0.49	0.16	8.10	3.08
-36					0.38	0.13	5.30	3.08
-38					0.12	0.17	6.30	3.74

Definition of abbreviations: M = mean.

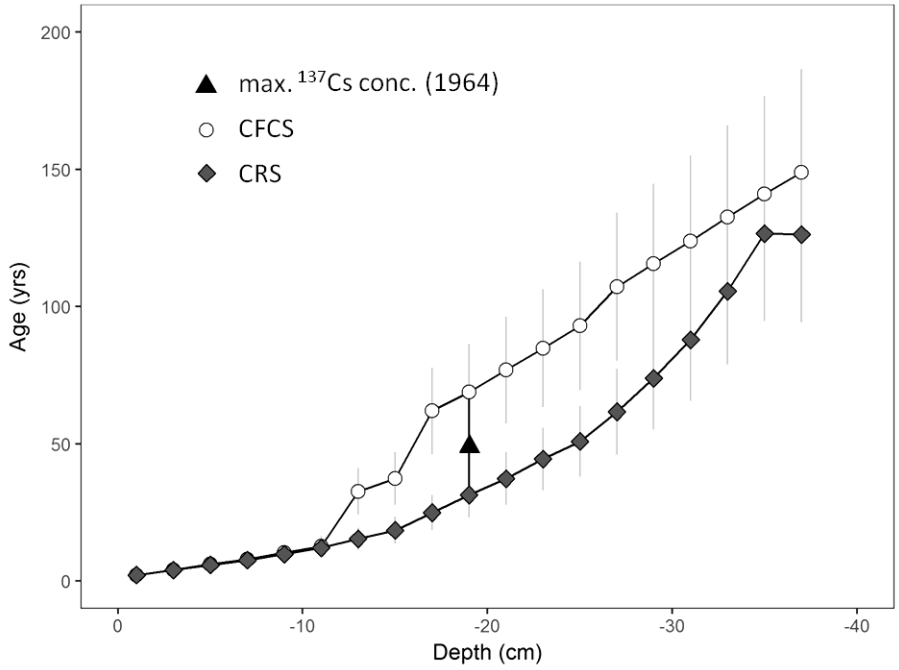

Fig. 4.3. Deviation of the Constant Flux and Constant Sedimentation rate (CFCS) and Constant rate of Supply (CRS) age determination models based on ^{210}Pb$_{ex}$ concentrations. Also, the depth location of maximum ^{137}Cs concentration (1964) is given.

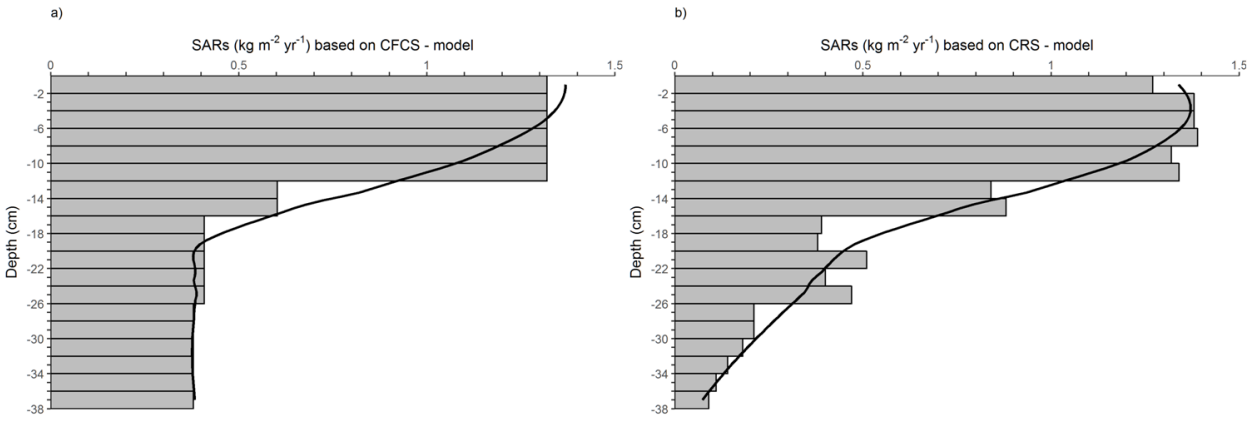

Fig. 4.4. Sediment accumulation rates based on $^{210}Pb_{ex}$ activity using the Constant Flux and Constant Sedimentation rate (CFCS) and Constant rate of Supply (CRS) age determination models.

4.4.2 CSSI analysis

4.4.2.1 Vertical $\delta^{13}C$ distribution

The vertical distribution of $\delta^{13}C$ (‰) values for soil bulk carbon and $\delta^{13}C$ values for C22:0, and C24:0 is shown for each sediment layer (2 cm) (Fig. 4.5). To better visualize main trends, locally weighted smoothing (LOESS) curves were added.

Bulk soil $\delta^{13}C$ values revealed a vertical distribution pattern similar to the vertical isotopic distribution of individual FAMEs. Across the profile, bulk soil $\delta^{13}C$ values ranged between -24 and -27‰ with a low level of uncertainty (SD max. ±0.5‰) (Fig. 4.5 a). The vertical distributions of $\delta^{13}C$ values for the different FAMEs ranged between -30 and -33‰. Isotopic values of FAMEs ranged between -32 to -33‰ in upper layers (0 to 5 cm). A peak at 11 cm displayed slightly less negative values, i.e., -30‰, while the layers between 13 cm and 17 cm ranged between -31 to -33‰. In deeper layers (19 to 37 cm), $\delta^{13}C$ values of C22:0 proceeded discontinuously with a trend towards less negative $\delta^{13}C$ values and with larger standard deviations (SD) (< ±1.7‰) (Fig. 4.5b). In contrast, $\delta^{13}C$ values of C24:0 varied only to a minor degree with depth and had similar SDs (< ±1.6‰) (Fig. 4.5c). Overall, SDs of FAME-specific $\delta^{13}C$ values did not change with depth (max. 3‰ between layers), while ME values deviated up to 3.5‰.

Analysis of variance (ANOVA) on bulk soil $\delta^{13}C$ values yielded significant variation among the layers of the sediment profile ($F(18, 19) = 17.73$, $p = 2.9 \times 10^{-8}$), ***P <0.001) (Fig. 4.5a). A significant effect of depth was observed for $\delta^{13}C$ values of C22:0 ($F(18, 31) = 2.06$, $p = 0.04$),

*P <0.05) (Fig. 4.5b), while none was determined for $\delta^{13}C$ values of C24:0 ($F(18, 32) = 1.70$, $p = 0.09$), P >0.05 (Fig. 4.5c).

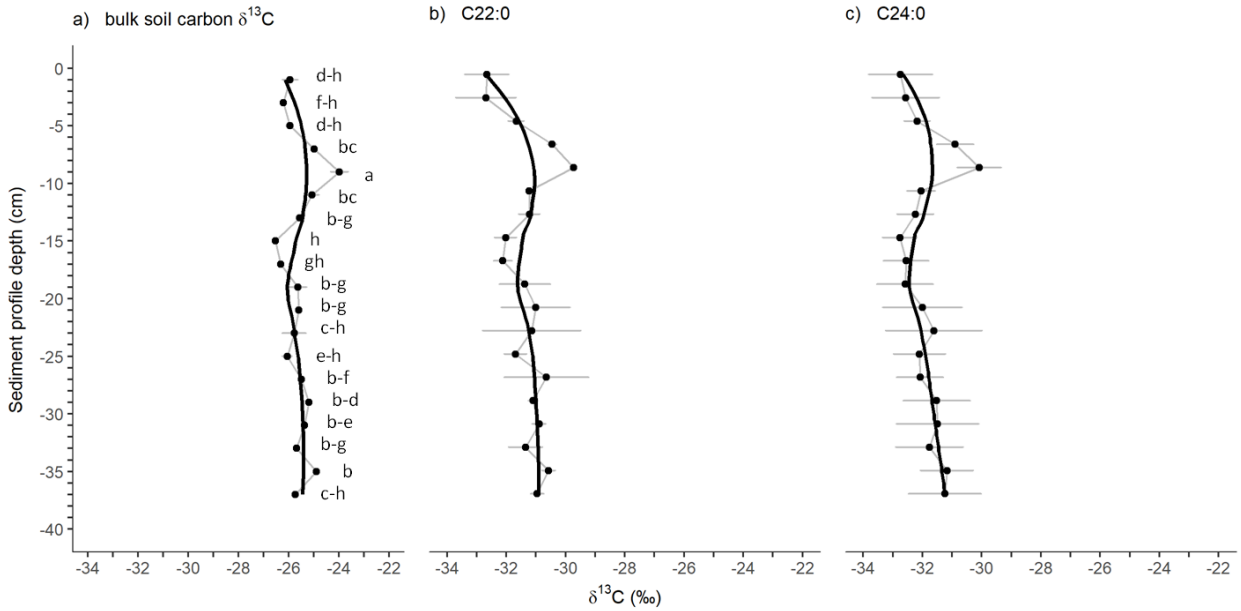

Fig. 4.5. Vertical distributions of $\delta^{13}C$ values of bulk soil carbon, C22:0 and C24:0 including locally weighted smoothing (LOESS) curves for the sediment core. Error bars represent the standard deviation of the mean.

4.4.2.2 Point-in-Polygon test

To increase the reliability of the SIAR output, a Monte Carlo simulation of mixing polygons for the point-in-polygon test was used (Smith et al., 2013). The mean $\delta^{13}C$ values of the selected two FAMEs (C22:0 and C24:0) from 19 sediment layers complied with the point-in-polygon assumption, i.e., the isotopic signature of the sediment was located within a polygon enclosing the signatures of the potential sources to provide a likely solution (Fig. 4.6). All layers were then used for sediment source apportionment calculations in SIAR.

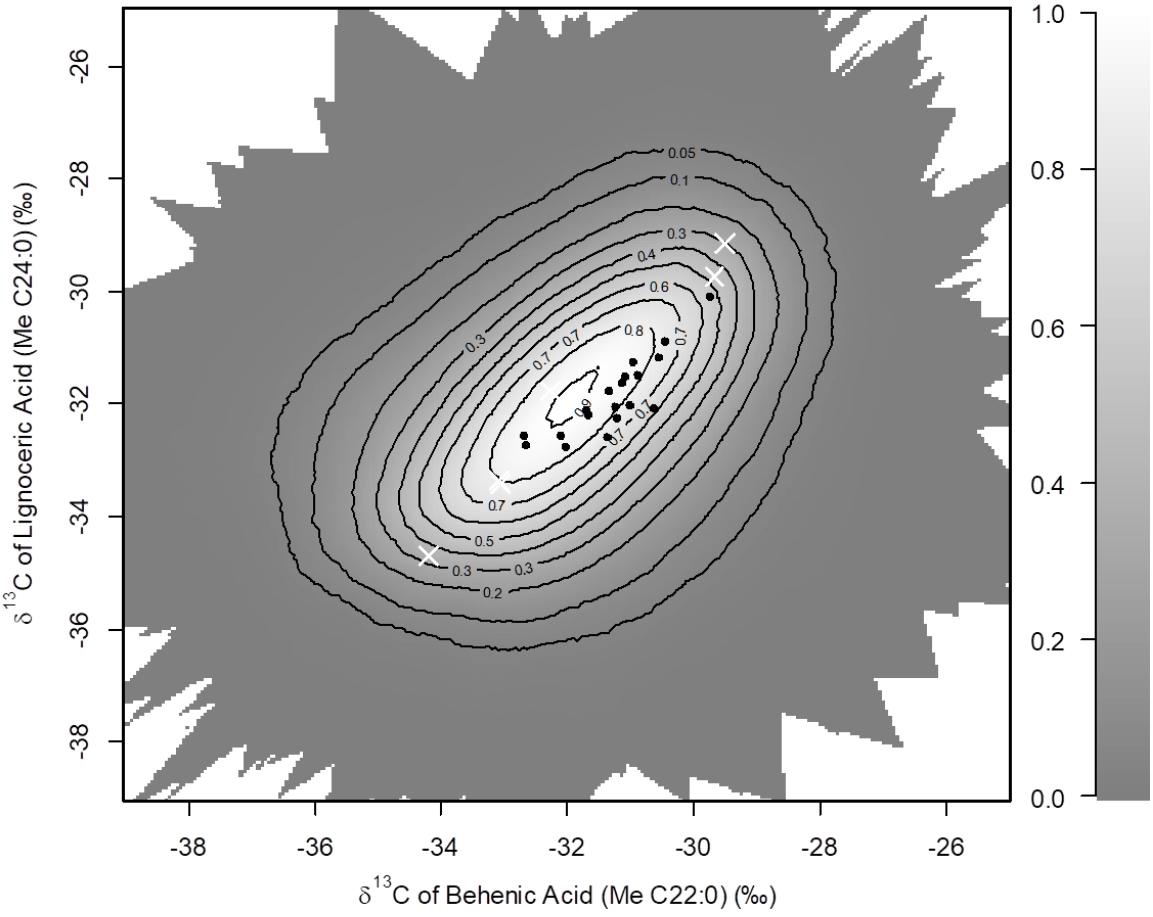

Fig. 4.6. The simulated mixing region for C22:0 and C24:0 showing the mean source signatures (white crosses) and mean sediments signatures (black dots). The proportion of iterations for which the sediment signature was within a mixing polygon is indicated by probability contours (5% level (outermost contour) and at every 10% level; for grading see side bar). If a sediment sample is within less than 5% of polygons, the proposed mixing model is considered unsuitable.

4.4.2.3 Separating erosion sources using SIAR

Box-and-Whisker plots displayed the vertical distribution of soil proportions for each sediment layer (2 cm) from 0 to 38 cm (Table 4.2, Fig. 4.7a). Soil proportions are displayed separately for each land use type to illustrate the change in individual contributions within the sediment profile. A general feature of the SIAR output is the sinuous character of each land use contribution within the profile. The most distinct variations in soil contributions were observed for the cropping areas (maize and cassava) and forested areas (protected forest and secondary forest). In most years, soil contributions from both forest types were lower than those of the other land use types (Table 4.2, Fig 4.7c). In contrast, in 1987 and 1994 their proportions were surpassed only by cassava (Table 4.2, Fig. 4.7c). Lowest soil contribution rates for both forests were observed for 2002 (Table 4.2, Fig. 4.7a). Soil contributions of cassava and maize increased during the 1990s and exhibited highest proportions in the year 2002, declining in the following years (Table 4.2, Fig. 4.7a). Compared to all land use types, soil proportions of cassava were greatest during the entire observation period, excluding 2002. With the exceptions of 1987, 1994 and 2002, maize and fruit orchards displayed second and third largest proportional shares of the investigated sediment layers (Table 4.2, Fig. 4.7c). Comparable to forests, soil proportions from teak were lowest in 2002 (Table 4.2, Fig. 4.7a).

4.4.3 Land use type-specific net erosion rates

The progression of net erosion rates (t ha^{-1} y^{-1}) for each land use type from 1987 to 2010 is shown in Fig. 4.7b. A comparison of net erosion rates between land use types for each individual year is shown in Fig. 4.7d. The sinuous character of net erosion rates within the profile was less clearly expressed than for soil proportions. Variation in net erosion rates was lowest for forested land use types, i.e., protected and secondary forests, and highest for intensively managed land uses, i.e. maize and cassava, with teak and fruit orchards ranging between the extremes (Table 4.2, Fig. 4.7b). Net erosion rates of protected and secondary forest were lower than those of the other land use types for each year of the observation period (Table 4.2, Fig. 4.7d). Net erosion rates of cassava and maize increased during the 1990s and highest rates were observed for the year 2002 (Table 4.2, Fig. 4.7b). Net erosion rates of cassava were not different in 2002 and 2004. Except for 2002, net erosion rates of cassava were higher than those of the other land use types. Ranking of net erosion rates for maize and orchards was similar to the ranking of soil proportions (Table 4.2, Fig. 4.7d).

In total, estimated sediment accumulation rates, determined with the CRS model, amounted to 39 t ha^{-1} y^{-1} (1987) and 127 t ha^{-1} y^{-1} (2009) for the upland areas of the Chieng Khoi catchment. Considering that sediment accumulation rates are functions of the basin (26 ha) and the entire catchment area (207 ha), net erosion rates amounted to 4.8 t ha^{-1} y^{-1} (1987) (39 x (26/207) and 16 t ha^{-1} y^{-1} (2009).

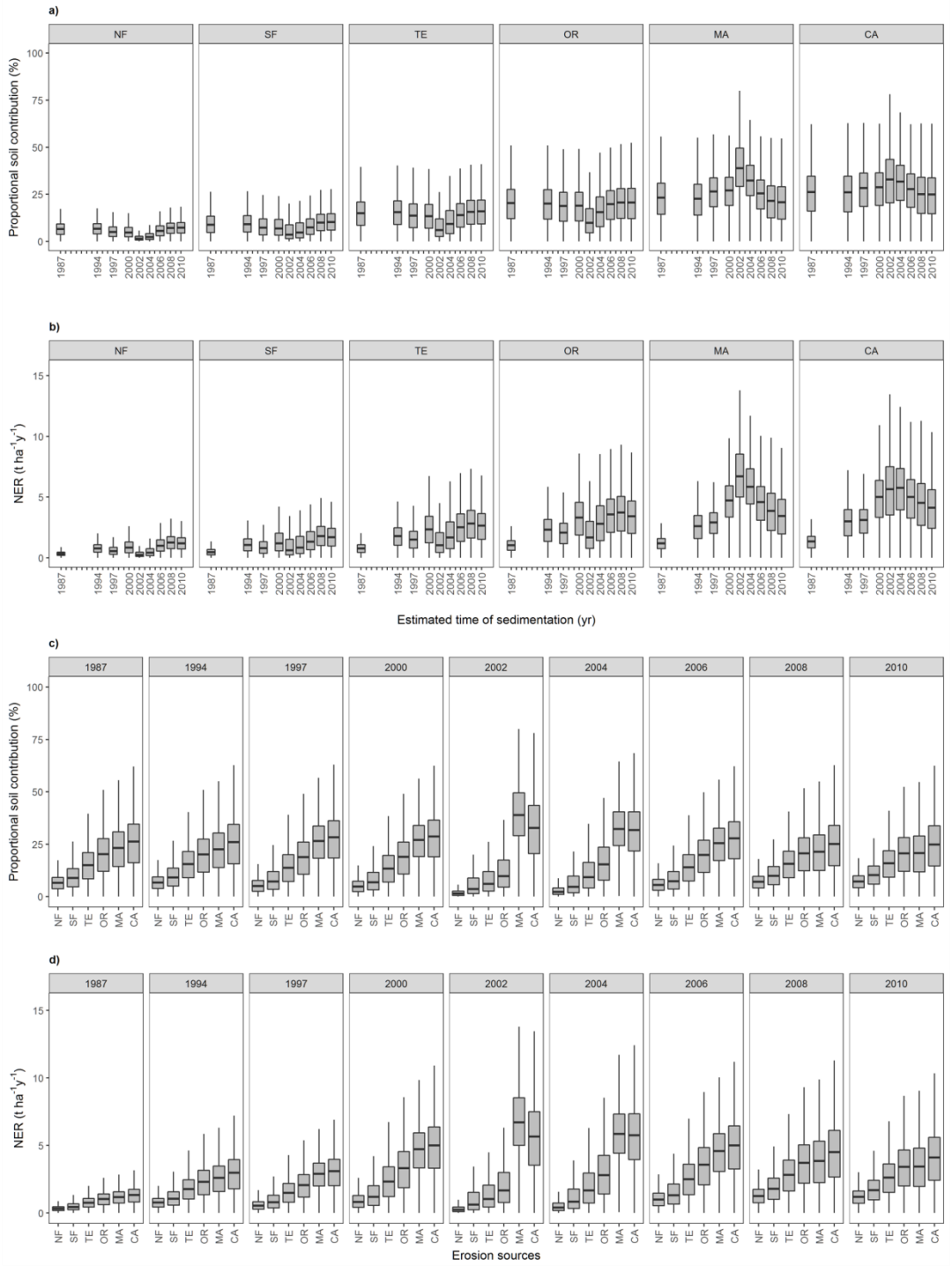

Fig. 4.7. Change in proportional soil contribution rates and net erosion rates for individual land use types (a, b). Change in proportional soil contribution rates and net erosion rates for individual years (c, d). Proportions (%) (a, c) and net erosion rates (t ha^{-1} y^{-1}) (b, d) of all potential erosion sources for each sediment layer (2 cm) from 0 to 18 cm were assigned to its corresponding year of sedimentation (1987 to 2010).

Table 4.2. Soil proportions (%) and net erosion rates (t $ha^{-1}y^{-1}$) of the six potential sediment sources from 1987 to 2010.

Land use type	year	Proportional soil contributions (%)						Net erosion rate (t $ha^{-1}y^{-1}$)					
		Min	Q1	Mdn	M	Q3	Max	Min	Q1	Mdn	M	Q3	Max
protected forest	1987	<0.1	3.7	6.5	6.7	9.2	28.1	<0.1	0.2	0.3	0.3	0.5	1.4
	1994	<0.1	3.9	6.7	6.8	9.3	29.9	<0.1	0.4	0.8	0.8	1.1	3.4
	1997	<0.1	2.5	5.0	5.4	7.7	30.4	<0.1	0.3	0.5	0.6	0.8	3.3
	2000	<0.1	2.4	4.7	5.1	7.4	27.9	<0.1	0.4	0.8	0.9	1.3	4.9
	2002	<0.1	0.6	1.4	1.9	2.6	18.9	<0.1	0.1	0.2	0.3	0.4	3.3
	2004	<0.1	1.0	2.2	2.9	4.1	21.6	<0.1	0.2	0.4	0.5	0.7	3.9
	2006	<0.1	3.0	5.5	5.8	8.2	30.4	<0.1	0.5	1.0	1.0	1.5	5.5
	2008	<0.1	4.2	7.0	7.2	9.7	33.5	<0.1	0.8	1.3	1.3	1.7	6.0
	2010	<0.1	4.3	7.2	7.3	9.9	45.7	<0.1	0.7	1.2	1.2	1.6	7.6
secondary forest	1987	<0.1	4.7	8.8	9.4	13.3	49.5	<0.1	0.2	0.4	0.5	0.7	2.5
	1994	<0.1	5.0	9.1	9.7	13.6	54.0	<0.1	0.6	1.0	1.1	1.6	6.2
	1997	<0.1	3.4	7.2	8.2	11.9	49.0	<0.1	0.4	0.8	0.9	1.3	5.4
	2000	<0.1	3.2	6.8	7.9	11.6	45.5	<0.1	0.6	1.2	1.4	2.0	8.0
	2002	<0.1	1.4	3.6	6.3	8.8	58.6	<0.1	0.2	0.6	1.1	1.5	10.1
	2004	<0.1	1.9	4.6	6.6	9.7	53.9	<0.1	0.3	0.8	1.2	1.8	9.8
	2006	<0.1	3.6	7.3	8.2	11.9	40.3	<0.1	0.7	1.3	1.5	2.1	7.3
	2008	<0.1	5.7	9.9	10.3	14.3	52.8	<0.1	1.0	1.8	1.9	2.6	9.5
	2010	<0.1	5.9	10.2	10.6	14.7	45.7	<0.1	1.0	1.7	1.8	2.4	7.6
teak	1987	<0.1	8.5	15.0	15.1	21.0	60.9	<0.1	0.7	1.2	1.2	1.6	3.5
	1994	<0.1	8.9	15.5	15.6	21.5	67.4	<0.1	1.6	2.6	2.6	3.5	8.2
	1997	<0.1	7.2	13.7	14.1	20.0	69.0	<0.1	2.0	2.9	2.9	3.7	8.8
	2000	<0.1	7.0	13.3	13.8	19.6	58.0	<0.1	3.3	4.7	4.6	5.9	13.6
	2002	<0.1	2.5	6.0	8.3	2.0	9.7	<0.1	5.0	6.7	6.8	8.5	16.0
	2004	<0.1	4.1	9.3	10.9	16.3	67.2	<0.1	4.4	5.9	5.9	7.3	15.2
	2006	<0.1	7.5	13.9	14.2	20.0	75.0	<0.1	3.1	4.6	4.5	5.9	13.3
	2008	<0.1	9.0	15.6	15.8	21.7	62.6	<0.1	2.2	3.9	3.9	5.3	13.2
	2010	<0.1	9.2	15.9	16.0	21.9	71.4	<0.1	2.0	3.4	3.5	4.8	12.1
fruit orchards	1987	<0.1	12.0	20.3	20.3	27.6	77.3	<0.1	0.8	1.3	1.3	1.8	4.2
	1994	<0.1	11.7	20.1	20.0	27.4	83.4	<0.1	1.8	3.0	2.9	4.0	9.4
	1997	<0.1	10.7	18.8	18.8	26.0	76.4	<0.1	2.0	3.1	3.0	4.0	9.1
	2000	<0.1	10.7	18.9	18.8	26.0	75.8	<0.1	3.3	5.0	4.9	6.4	14.8
	2002	<0.1	4.5	9.7	1.8	7.4	6.0	<0.1	3.5	5.6	5.6	7.5	16.1
	2004	<0.1	7.8	15.4	16.2	23.5	66.2	<0.1	3.9	5.7	5.6	7.3	15.6
	2006	<0.1	11.6	19.8	19.7	26.9	77.2	<0.1	3.3	5.0	4.9	6.4	13.8
	2008	<0.1	12.2	20.7	20.6	28.0	76.3	<0.1	2.7	4.5	4.4	6.1	13.3
	2010	<0.1	12.1	20.6	20.6	28.2	79.3	<0.1	2.4	4.1	4.1	5.6	12.7
maize	1987	<0.1	14.4	23.2	23.0	30.9	69.7	<0.1	0.4	0.8	0.8	1.1	3.1
	1994	<0.1	13.9	22.6	22.5	30.3	71.6	<0.1	1.0	1.8	1.8	2.5	7.7
	1997	<0.1	18.3	26.5	26.1	33.7	80.5	<0.1	0.8	1.5	1.5	2.2	7.6
	2000	<0.1	19.1	27.0	26.5	34.0	77.5	<0.1	1.2	2.3	2.4	3.4	10.1
	2002	<0.1	9.1	8.9	9.3	9.5	2.8	<0.1	0.4	1.0	1.4	2.1	13.7
	2004	<0.1	24.4	32.3	32.4	40.4	84.0	<0.1	0.7	1.7	2.0	3.0	12.2
	2006	<0.1	17.1	25.5	25.0	32.6	74.0	<0.1	1.3	2.5	2.6	3.6	13.5
	2008	<0.1	12.5	21.4	21.5	29.5	73.5	<0.1	1.6	2.8	2.8	3.9	11.3
	2010	<0.1	11.8	20.8	20.9	29.0	72.8	<0.1	1.5	2.6	2.6	3.6	11.8
cassava	1987	<0.1	16.1	26.2	25.6	34.5	82.3	<0.1	0.6	1.0	1.0	1.4	3.9
	1994	<0.1	15.6	26.0	25.4	34.5	82.1	<0.1	1.3	2.3	2.3	3.1	9.6
	1997	<0.1	18.5	28.3	27.5	36.3	82.6	<0.1	1.2	2.1	2.1	2.8	8.4
	2000	<0.1	19.0	28.7	27.8	36.5	84.9	<0.1	1.9	3.3	3.3	4.6	13.2
	2002	<0.1	0.5	2.8	2.4	3.5	3.3	<0.1	0.8	1.7	2.0	3.0	9.6
	2004	<0.1	21.8	31.7	31.1	40.5	86.2	<0.1	1.4	2.8	2.9	4.3	12.0
	2006	<0.1	18.1	27.8	27.0	35.8	76.5	<0.1	2.1	3.6	3.5	4.8	13.9
	2008	<0.1	14.8	25.1	24.7	33.9	74.1	<0.1	2.2	3.7	3.7	5.0	13.7
	2010	<0.1	14.6	24.8	24.5	33.8	76.6	<0.1	2.0	3.4	3.4	4.7	13.1

Definition of abbreviations: Min = minimum value, Q1 = 1st quartile, Mdn = median, M = mean, Q3 = 3rd quartile, Max = maximum value.

4. 5 Discussion

4.5.1 Age determination and sediment accumulation rates using ^{137}Cs and $^{210}Pb_{ex}$

In this study, ^{137}Cs was used as an anthropogenic radionuclide tracer to determine the depth locations of two sediment layers. Maximum ^{137}Cs activity was measured between 7 and 9 cm in the reference profile and between 15 and 19 cm in the sediment profile (Fig. 4.2a), and can be explained by the high global deposition of fallout ^{137}Cs during 1964. Although a decline in exponential shape was generally adopted by authors to interpret the reference profiles associated with undisturbed sites, a more realistic approach should consider the temporal variation of the depth profile resulting from the time-dependent fallout input and the post depositional redistribution of ^{137}Cs within the soil profile after deposition from the atmosphere. Redistribution of ^{137}Cs within the soil profile represents the result of a complex set of mechanisms including physical, physico-chemical and biological processes. In this case, the profile was characterized by a relatively broad peak, with the maximum concentration located a few centimeters below the soil surface (He and Walling, 1997; Zapata, 2003). For the sediment profile of lake, considering the low ^{137}Cs activity of maximum 0.8 Bq kg^{-1} across the entire profile, as well as the high uncertainty of 35 %, the exact position of the layer corresponding to the year with maximum ^{137}Cs deposition could not be identified accurately. This was attributed to the geographical location of the Chieng Khoi catchment in the Southern hemisphere, which meant that it was only slightly exposed to ^{137}Cs fallout (Walling et al., 1999). Indeed, the ^{137}Cs inventory was found to be low, about 220 Bq m^{-2}, in this area. At the border of the lake where the sediment profile was obtained, the ^{137}Cs inventory was found to be significantly higher than that of the reference site (about 258 Bq m^{-2}). This was due to sediment accumulation in this zone. In the undisturbed reference profile, $^{210}Pb_{ex}$ activity decreased exponentially with increasing depth of the soil body (Fig. 4.2b). In contrast to the shape of the ^{137}Cs profile commonly obtained for undisturbed soil, the continuous input of $^{210}Pb_{ex}$ resulted in maximum activity occurring at the surface rather than slightly below the surface (Mabit et al., 2008, 2014; Walling et al., 1995). For the sediment profile, the layer-explicit variation in $^{210}Pb_{ex}$ activity was the consequence of variations in sedimentation rates and initial concentrations. Similar depth distributions of $^{210}Pb_{ex}$ concentrations have been observed elsewhere (Benmansour et al., 2013; Du and Walling, 2012).

Since the exponential equation of the CFCS model did not fit to all soil layers taken together, it was used for each layer individually, leading to four constant sediment accumulation rates. As a result, the shift in constant sediment accumulation rates between sections was often abrupt,

with strong differences in sediment accumulation rates among two sections resulting in a gap in the estimated date (Table 4.3, Fig. 4.4). Since $^{210}Pb_{ex}$ activity did not decrease constantly with sediment depth, the CRS model proved to be more reliable for the assessment of sediment accumulation rates than the CFCS (Table 4.3, Fig. 4.4). However, the use of $^{210}Pb_{ex}$ with the CRS model also revealed a certain deviation from the result obtained by ^{137}Cs as a consequence of the uncertainties on activities, especially for ^{137}Cs with an average uncertainty of 35%. Therefore, taking account of the low ^{137}Cs activity across the whole sediment profile, as well as its high uncertainty, the exact position of the layer corresponding to the year with maximum ^{137}Cs deposition could not be accurately identified and the ^{137}Cs profile was not helpful for confirming the ages of layers derived from $^{210}Pb_{ex}$. Observed sediment accumulation rate data via the CRS model were comparable to earlier studies, which have demonstrated increased soil losses after land use change from forest to continuous maize and cassava cropping (Häring et al., 2014; Wezel et al., 2002; Van De et al., 2008). Likewise, the increase in sediment accumulation rates over time was a plausible consequence of increased land use change and the continuous expansion of crop production onto steep slopes. Subsequently, reduced soil coverage and exposure to high intensity rain events resulted in increased soil loss and long-term land degradation (Wezel et al., 2002; Van De et al., 2008).

Table 4.3. Sediment layer-specific sediment accumulation rates, age and respective year of sedimentation based on $^{210}Pb_{ex}$ activity using the CFCS and CRS age determination model.

	Sediment accumulation rates and age determination						
	Sediment accumulation rates (g cm^{-2} y^{-1})		Age (yrs)		Year of sedimentation		
depth (cm)	CFCS	CRS	CFCS	CRS	CFCS	CRS	^{137}CS
-2	1.32	1.27	2.2	2.2	2010	2010	
-4	1.32	1.38	4.1	4.0	2008	2008	
-6	1.32	1.38	6.1	5.9	2006	2006	
-8	1.32	1.39	8.0	7.6	2004	2004	
-10	1.32	1.32	10.3	9.8	2002	2002	
-12	1.32	1.34	12.7	12.1	1999	2000	
-14	0.6	0.84	32.7	15.4	1979	1997	
-16	0.6	0.88	37.4	18.5	1975	1994	
-18	0.41	0.39	62.0	24.9	1950	1987	
-20	0.41	0.38	68.8	31.4	1943	1981	1964
-22	0.41	0.51	76.9	37.3	1935	1975	
-24	0.41	0.40	84.8	44.5	1927	1968	
-26	0.41	0.47	93.0	50.9	1919	1961	
-28	0.38	0.21	107.2	61.7	1905	1950	
-30	0.38	0.21	115.6	73.9	1896	1938	
-32	0.38	0.18	123.9	87.9	1888	1924	
-34	0.38	0.14	132.6	105.6	1879	1906	
-36	0.38	0.11	141.1	126.6	1871	1885	
-38	0.38	0.09	149.0	126.6	1863	1885	

Definition of abbreviations: CFCS = Constant Flux and Constant Sedimentation rate model,
CRC = Constant Rate of Supply model.

4.5.2 Discrimination and allocation of soil sources over time using CSSI

Mean bulk SOC $\delta^{13}C$ values obtained from protected forest, secondary forest, teak and fruit orchards (all C_3 vegetation) ranged from -26.8 to -26.1‰ (Table 4.4). Similar bulk SOC $\delta^{13}C$ values (-27.6 to -26.5 ‰) obtained from forest soils were reported for the same geographical region (Häring et al., 2013) and for native forests in New Zealand (Gibbs, 2008). The identified $\delta^{13}C$ CSSI-FAME signatures of protected forest, secondary forest, teak and fruit orchards (Table 4.4) were also in line with other CSSI studies in which $\delta^{13}C$ CSSI-FAME values ranged from -28.9 (C 16:0) to -32.4 (C 24:0) in shrub and tree soils (Blake et al., 2012), and from -28.47 (C 18:0) to -32.29 (C 24:0) in natural forest soils (Hancock and Revill, 2013). CSSI and bulk SOC $\delta^{13}C$ signatures obtained from maize (C_4) soil were less depleted (-24‰ ±1.4) as compared to soil under C_3 plants. Bulk SOC $\delta^{13}C$ values of maize soils were consistent with other studies (Häring et al., 2013; Kramer and Gleixner, 2006; Wiesenberg et al., 2004). Häring et al. (2013) confirmed that, due to deforestation and subsequent mono-cropping of maize, bulk SOC $\delta^{13}C$ values increased marginally at 0-30 cm by +1.6‰ within 10 years at Alisol sites and

+1.4‰ within 16 years at Luvisol sites. The reported marginal increase was most likely a result of low maize SOC input rates, thus promoting increased SOC losses with time since forest conversion (Häring et al., 2013). Blake et al. (2012) observed more strongly discriminated $\delta^{13}C$ signatures from maize soils (-28‰). The authors suggested that the overall bulk SOC $\delta^{13}C$ signatures clearly highlight the dominance of C_3 plant material derived from past crop rotations. Cassava soils showed bulk SOC $\delta^{13}C$ and CSSI signatures similar to maize. In upland areas of the Chieng Khoi catchment, cassava is usually grown after several years of maize cultivation, when soil fertility is depleted (Tuan et al., 2014).

Our results showed that CSSI signatures extracted from 19 sediment layers corresponded to bulk SOC $\delta^{13}C$ values. Thus, a comparison of CSSI signatures of the different sediment layers with CSSI values of the land use types indicated certain soil provenances. Likewise, the vertical isotopic distribution patterns were strongly influenced by C_3 and C_4 vegetation, which covered soil sources at different times (i.e., years). This was exemplified by the $\delta^{13}C$ peak at the depth of 7 to 11 cm, suggesting an increased isotopic contribution of maize soils containing less depleted $\delta^{13}C$ values, which are typical for C_4 vegetation, e.g. maize. The presence of different C_3 plants could also have modified the overall bulk soil $\delta^{13}C$ signature. Depleted $\delta^{13}C$ values in upper (0 to 5 cm) and lower (13 to 17 cm) sediment layers were typical for C_3 vegetation. Hence, these results suggested an increased SOC contribution of C_3 vegetation-covered soil sources to sediment deposition.

The period from 1987 to 1994 was characterized by the gradual conversion of shifting cultivation to intensified agricultural production. Upland rice disappeared, while teak, pine and fruit trees were introduced as reforestation measures. Since then, deforested areas have been highly susceptible to water erosion, resulting in significant relocation of forest soil and associated SOC within the catchment. Results of the proportional soil contribution estimates showed that the proportions of forested soils (i.e., protected and secondary forests) to sediment deposition peaked during these years. The proportions of the remaining land use types were lowest during this period, especially maize and cassava.

After 1994, previously shrub- and tree-covered steep slopes were successively converted to crop land for high yielding hybrid maize and commercial 1-year cassava varieties, resulting in less soil cover and initiating high rates of soil erosion (Moench, 1991; Van De et al., 2008). This process was reflected in a decrease in proportional soil contributions from protected and secondary forests as well as teak and, to some degree, fruit orchards. At the same time, the proportion of soil contributed by maize and cassava increased and peaked during the years 2000 to 2004. Although crop areas were continuously extended after 2004, our results showed a

decline in proportional soil contributions of maize and cassava to levels that were typical for the years 1994 to 2000. After forest clearing, typical isotopic C_3 signals may have been dominant in these soils, even though production of C_4 crops had already begun in the same region. Häring et al. (2013) observed that in the surface soil (0 to 30 cm), forest-derived SOC decreased exponentially (0.08 (Alisol) to 0.24 (Luvisol) kg m^{-2} y^{-1}) with time after forest conversion, while maize derived SOC was low due to comparatively low SOC input rates (0.02 to 0.03 kg m^{-2} y^{-1}). This finding may explain the higher isotopic contribution of natural and secondary forests.

Table 4.4. Mean $\delta^{13}C$ values for soil bulk carbon and compound-specific $\delta^{13}C$ (‰) values for C22:0 and C24:0 for 2 cm depth layer. Mean (M) and standard error (SE) are included.

depth (cm)	$\delta^{13}C$ values (‰)								
	soil bulk C			C22:0			C24:0		
	M	SD	SE	M	SD	SE	M	SD	SE
-2	-25.9	0.31	0.22	-32.7	0.74	0.43	-32.7	1.08	0.63
-4	-26.2	0.03	0.02	-32.7	1.01	0.58	-32.6	1.13	0.66
-6	-26	0.13	0.09	-31.7	0.26	0.15	-32.2	0.43	0.25
-8	-25	0.03	0.02	-30.5	0.14	0.08	-30.9	0.62	0.36
-10	-24	0.34	0.24	-29.7	n.a.	n.a.	-30.1	0.74	0.43
-12	-25.1	0.28	0.2	-31.2	0.07	0.04	-32	0.48	0.24
-14	-25.6	0.11	0.08	-31.2	0.35	0.2	-32.2	0.61	0.35
-16	-26.5	0.05	0.04	-32	0.36	0.21	-32.8	0.57	0.33
-18	-26.3	0.01	0.01	-32.1	0.31	0.18	-32.5	0.76	0.44
-20	-25.6	0.35	0.25	-31.4	0.85	0.49	-32.6	0.94	0.54
-22	-25.6	0.07	0.05	-31	1.16	0.67	-32	1.34	0.78
-24	-25.8	0.47	0.34	-31.1	1.65	0.82	-31.6	1.62	0.81
-26	-26.1	0.18	0.12	-31.7	0.37	0.21	-32.1	0.87	0.5
-28	-25.5	0.06	0.04	-30.6	1.42	0.82	-32.1	0.78	0.45
-30	-25.2	0.10	0.07	-31.1	0.15	0.11	-31.5	1.12	0.64
-32	-25.4	0.03	0.02	-30.9	0.23	0.16	-31.5	1.39	0.98
-34	-25.7	0.03	0.02	-31.4	0.56	0.4	-31.8	1.13	0.65
-36	-24.9	0.10	0.07	-30.6	0.22	0.16	-31.2	0.88	0.51
-38	-25.7	0.12	0.09	-31	0.22	0.13	-31.2	1.22	0.71

Definition of abbreviations: M = mean, SD = standard deviation, SE = standard error.

4.5.3 Estimated land use type-specific net erosion rates

Our results clearly indicate that identifying sediment accumulation rates and proportional soil contributions makes it possible to allocate land use type-specific net erosion rates as a baseline for insights on the impact of land use change on soil erosion. The observed trend of dramatic increase in sediment accumulation rates during the past three decades, accompanied, crucially, by the proportional increase in sediments from C_4-dominated land use types (i.e., maize), was substantiated by the recorded land use history of the Chieng Khoi catchment (Minh et al., 2011; Nguyen and Lippe, personal communication).

Land use type-specific net erosion rates exhibited similar patterns in their chronological succession as land use type-specific proportional soil contribution rates (Fig. 4.7a). Therefore, the relevant explanations for these patterns given in section 4.2 are also valid for net erosion rates. Notably, estimated average net erosion rates and land use type-specific net erosion rates were, however, lower than erosion rates determined in other studies. On experimental erosion plots under maize in the same catchment, Tuan et al. (2014) observed average soil losses of 42 t ha^{-1} y^{-1} and 112 t ha^{-1} y^{-1} with maximum rates of 174 t ha^{-1} y^{-1} depending on farmers' practices and location. Maximum net erosion rates calculated in our study were found for maize in the year 2002, amounting to 5.3 t ha^{-1} y^{-1}, a rate similar to the lowest ones determined by Tuan et al. (2014). Similarly, Phien and Loan (2005) measured erosion rates of 43 t ha^{-1} y^{-1} on fields under cassava production, while Häring et al. (2014) determined soil erosion rates ranging from 12 to 89 t ha^{-1} y^{-1} under maize.

Unlike earlier studies, which used experimental erosion plots with minimum sediment losses to determine net erosion rates, the integrated FRN – CSSI approach made it possible to probe deposition sites distant from those land use types responsible for the sediment. This implied that portions of the total sediments may have been deposited before having reached the deposition sites of interest, e.g., at the bottom of the field or temporary water courses. A proportion of the sediments may also have been deposited further into the lake. This possibility may account for the divergence between the net erosion rates estimated in the present study and those determined by others. Therefore, assessing spatial variability of net erosion rates within catchments has to be considered in future (or ongoing) studies.

In addition, the selection of conversion models used to estimate erosion and deposition rates from FRN is always subject to uncertainties (Mabit et al., 2008). In this study, the average relative uncertainties were ~35% for ^{137}Cs and ~25% for $^{210}Pb_{ex}$ which were due to their low activities in the study region. As a possible alternative to ^{137}Cs in this case, anthropogenic

radioisotopes of plutonium ($^{239+240}$Pu) have been suggested as promising soil and sediment tracers to determine soil erosion rates with lower uncertainty (Schimmack et al., 2002). For two alpine valleys, Alewell et al. (2014) found lower coefficients of variance (CV) for reference $^{239+240}$Pu values (CV = 13 to 17 %) as compared to ^{137}Cs (CV = 32%). Having a similar temporal yet spatially more homogenous distribution to that of ^{137}Cs, $^{239+240}$Pu could be a suitable alternative to ^{137}Cs in prospective integrated FRN – CSSI studies.

4.6 Conclusions

This novel approach, integration of FRN and CSSI, was successful in assigning past erosion rates to specific land use types. Dominant net erosion rates between 1987 to 2010 were determined, a period characterized by dramatic land use change from mature forest to intense maize and cassava production on steep slopes. Even though remaining methodological limitations may hamper precise land use type-specific past net erosion rates, our results corresponded to a remarkable increase in sediment accumulation rates during the past 25 to 30 years. This was accompanied by a significant proportional increase in sedimentation due to a shift in land use to C_4 plants. Nonetheless, we observed relatively high uncertainties for FRN inventories of undisturbed reference and sediment deposition sites (~35% for ^{137}Cs, ~25% for $^{210}Pb_{ex}$). Hence, to further corroborate the integrated FRN – CSSI approach for calculating land use type-specific net erosion rates, anthropogenic radioisotopes of plutonium ($^{239+240}$Pu) with generally lower uncertainties (< 20%) should be tested in more detail as alternatives to ^{137}Cs (Alewell et al., 2014). Moreover, remaining uncertainties associated with the CSSI technique need be compensated for by emphasizing complementary techniques. For example, through the use of ^{2}H isotope analysis, average chain length (ACL), and carbon preference index (CPI) for long-chain hydrocarbons, Cooper et al. (2015) successfully distinguished between various plant sources, including plant functional types (e.g., C_3 graminoids versus trees). Moreover, by taking concentration dependence, covariate effects and uncertainty in the tracer data into account, advanced Bayesian mixing models such as MixSIAR (Stock and Semmens, 2013) will improve the geometric isotopic mixing space, resulting in more accurate proportion estimations.

In conjunction with these approaches, the novel approach of integrating of FRN and CSSI introduced here will verify its potential in estimating land use type-specific net erosion rates. Likewise, this will enable the determination of past sediment budgets for specific land use types, providing insights into the accelerating impact of specific land use change on soil retrogression

and degradation. Such knowledge is of prime importance for evidence-based land management and decision making for effective soil conservation.

Chapter V General Discussion

5.1 Isotopic discrimination of land use types in intensely cultivated and fragmented catchments

CSSI-fingerprinting based on $\delta^{13}C$ values of FAMEs and in conjunction with Bayesian statistical methods proved suitable to distinguish major sediment sources, which were attributable to specific land use types, thus allowing determining SOC source-sink relationships in intensely cultivated catchments with diverse land use types. This research suggests that maize and cassava cropping areas were the main sediment sources in the upland area surrounding the Chieng Khoi reservoir.

Bulk SOC $\delta^{13}C$ and CSSI values extracted from soils of the different land uses were mostly in line with previous studies. Similar bulk SOC $\delta^{13}C$ values for forest soils were reported by Häring et al. (2013) and Gibbs (2008). CSSI values for forests, teak and orchards were comparable to CSSI values for shrub and tree soils (Blake et al., 2012; Hancock and Revill, 2013). Bulk SOC $\delta^{13}C$ values of maize soils were naturally less depleted (-24‰ ±1.4) and consistent with other studies (Häring et al., 2013; Kramer and Gleixner, 2006; Wiesenberg et al., 2004). Blake et al. (2012), however, reported more strongly discriminated $\delta^{13}C$ signatures from maize soils (-28‰), suggesting an effect of C_3 plant material derived from past crop rotations. An influence of past crop rotation on CSSI and bulk SOC $\delta^{13}C$ values can also be assumed in this study since cassava is usually grown after several years of maize cultivation, when soil fertility is depleted (Tuan et al., 2014). Our results are supported by earlier studies investigating erosion rates under maize and cassava cultivation in mountainous areas in Vietnam (Häring et al., 2014; Tuan et al., 2014, Valentin et al., 2008) and Thailand (Kongkaew, 2000; Pansak et al., 2008). Teak plantations on steep slopes were another source of major sediment contribution. Regarding its suitability for reforestation teak cultivation has aroused certain controversy in the past (Carle et al., 2009). Fernández-Moya et al. (2014) concluded that increased soil loss occurs mainly because of inappropriate management, such as planting teak on steep slopes (>60%) or reducing the understory vegetation, which depletes SOC concentrations (Boley et al., 2009). These conclusions may also be reflected in the Chieng Khoi catchment were intended erosion control is often hampered by the deciduous nature of teak trees having often a bare canopy at the beginning of the rainy season. Especially the continuous removal of teak litter and branches for fuel is conflicting with the aim to prevent soil erosion.

In this study we used the commonly performed *a priori* classification of sediment sources to align sediment source apportionment estimates with specific land uses. This allows assigning sediment losses to actual land uses and effectively directing soil management strategies. Collins et al. (2017) pointed out that tracer concentrations in a land use-based source group are likely to be controlled by numerous factors that may increase within-source variability (see also Chapter 5.4.2), likely negatively effecting the use of CSSI-fingerprinting in complex catchments. By collecting spatially integrated mixtures we aimed at limiting within-source variability. The degree of variability in the source samples might nevertheless still be under-estimated. Increasing the number of samples would certainly provide a better insight on the spatial variability of the CSSI value and improved most likely the interpretation of the sediment sources. But these advantages stand in contrast to the significantly increased analytical costs. Therefore, using spatially integrated mixtures is a trade-off between the determination of the degree of spatial variability of CSSI values and analytical costs which are necessary to meet the research objectives. Alternative to land use-based source grouping and based on a study of Walling and Woodward (1993), Pulley et al. (2017) suggested objective sediment source grouping to minimize uncertainty associated with quantitative source apportionment estimates using PCA and cluster analysis to select the source grouping.

High standard deviations of δ^{13}C-FAME values that were common among sediment source and sink samples were often reflected by large variability in the proportional sediment contribution of the different sediment sources. The *a priori* use of a multi comparison test (e.g. Tukey's HSD test), to identify CSSI values that were significantly different from each other, proved useful to limit uncertainty and to improve the accuracy of sediment source apportionment using an stable isotope mixing model (e.g. SIAR). Furthermore, examining the isotopic values preceding the SIAR runs using a Monte Carlo simulation of mixing polygons for a point-in-polygon test provided a quantitative basis for model rejection and exclusion for sediments samples and enhanced the quality of the results.

The reason we were able to differentiate between different land use types based on variations in δ^{13}C values of soil lipids was attributed to the effects that physiological and environmental factors induced on isotopic discrimination in plants and the subsequent transference of these δ^{13}C values from plants into soil. Additionally, soil lipid δ^{13}C values are likely to be influenced by resident soil organic matter from weeds, past crop rotations or from natural vegetation when the land has been cleared only recently (Blake et al., 2012, Häring et al., 2014). The most

important physiological factor, differences in the way CO_2 is fixed in photosynthesis, has allowed us the fundamental and clear differentiation of land use types with C_3 or C_4 planting. In our study, this case was only found in Chieng Khoi catchment, where maize is currently cultivated extensively (Chapters 2 and 3). Variations in the $\delta^{13}C$ values of soil lipids we found between different land uses under cultivation with C_3 plants were likely attributed to a combination of environmental factors and the influence of past land use on the land. A comprehensive review of environmental factors that have a presumed influence on the isotope signature has been provided by Reiffarth et al. (2016). The influence of some of these factors on the use of CSSI-fingerprinting in different agro-ecological zones will be discussed in the next chapter.

5.2 CSSI-fingerprinting at different agro-ecological zones and spatial scales

The benefits of CSSI-fingerprinting are well documented (e.g., Gibbs, 2008; Blake et al., 2012; Hancock and Revill, 2013, Alewell et al., 2016). These studies have focused on determining sediment source contributions for individual catchments using different laboratory and statistical routines. In this study we aimed at testing the CSSI-fingerprinting approach under conditions of different agro-ecological zones. To allow comparability we used the protocol from the first case study to distinguish the main sediment sources of six catchments from the northern and southern hemisphere (i.e. Chile, China, Morocco, Russia, Vietnam). Grouping catchment-specific land use types into broader land use categories (i.e., forest, cultivated and non-cultivated land) allowed comparing CSSI values between the different catchments. The use of land use types to characterize various vegetation types as sediment sources was specifically applicable when all land use categories were represented in each catchment or when both C_3 and C_4 vegetation were present. No correlations were found between catchments of different sizes, agro-ecological zones, number and type of land use types, or SOC concentrations and the number of significant $\delta^{13}C$ FA values of the various land use types (data not shown).

Our results suggested that mostly, sediments originated from cultivated land, typically crops and tree plantations (e.g., teak, orchards). The sources of most sediment in both Chilean catchments (Nacimiento, 12.4 ha; Los Ulmos, 19.8 ha), derived from non-cultivated land (e.g., roads, riverbank erosion). A recent study by Bravo-Linares et al. (2018) that traced sediment transport in the same upland forest catchments of Chile demonstrated that unpaved forestry roads were the main source of sediment (30–75%). This is in accordance with our results of the Los Ulmos catchment were unpaved forestry roads amounted to about 61%. Contrastingly our

results for Nacimiento suggested channel bank erosion to be the main sediment source. Bravo-Linares et al. (2018) demonstrated that stream channel derived sediments were mainly comprised of sediment coming from the unpaved roads in the upper part of the catchments (74–98%). A possibly far-fetched explanation for our contrasting results might derived from settled sediments of unpaved forestry road, which mixed with soil material of stream channels, thus also obscuring its isotopic signal.

The size and fragmentation of the catchment under investigation will not only affect the spatial variability of the biomarker distribution and concentration, but also the effects that affect the ^{13}C concentration in plants and in the soil. The examined catchments (Chapter 3), whose soil lipids were the basis of this fingerprinting study, are attributed to very different agro-ecological zones, i.e. zones defined on the basis of combinations of temperature characteristics, moisture regimes, microbial activities, soil types and vegetation cover. Although all these factors may have a direct or indirect influence on the isotopic discrimination of the C atoms of the FAs, it is expected that the greatest influence will come from the C fixation process. None of the studied catchments is particularly extensive (12 -766 ha) (Chapter 3), which supports the assumption that within the catchments there were no significant and consistent large-scale differences in precipitation or temperature. Contrary, the aspect of a hill slope, i.e. compass direction that a slope faces, can have very significant influences on its local climate (microclimate). The sun-facing side of a hill slope is usually warmer and drier due to the higher evapotranspiration and therefore also exposed to an increased risk of water stress, possibly affecting the ^{13}C concentration in plants. Even though the relationship between higher altitude and ^{13}C content in plants is not yet clear, studies have shown an enrichment of ^{13}C at increasing altitude. A possible explanation might be lower levels of CO_2 and O_2 concentration and lower temperatures, resulting in greater evaporation and finally in stomata closing (e.g. Wang et al., 2010). Körner et al. (1991) reported increasing ^{13}C concentrations with height, ranging between −0.9‰ and +2.7‰ km^{-1} in humid regions. Van de Water et al. (2002) pointed out that in arid areas water stress may overtake other factors that determine $\delta^{13}C$ values with elevation, but due to the increase of precipitation with altitude may lead to a decreasing trend upward. Wang et al. (2010) reported no altitudinal $\delta^{13}C$ changes of C_3 plants in semi-humid zones. An increase in ^{13}C concentration for C_3 plants with altitude was also observed by Kloeppel et al. (1998) in cold-temperate boreal forests. Wang et al. (2010) found comparatively little variability in C_4 plants related to altitude. A study by Wei and Jia (2009) demonstrates that the altitude-induced environmental impact on leaf wax-derived *n*-alkanes ($\delta^{13}C_{wax}$) is also conveyed to bulk organic

matter ($\delta^{13}C_{SOM}$). This, however, happens only when a specific altitude-dependent precipitation threshold is reached. No correlation was found below that threshold.

Another factor that has influence on C isotope discrimination is soil strength or soil compaction, i.e. the physical resistance to root penetration. Masle and Farquar (1988) reported that C isotope discrimination decreases with increasing soil strength because of both an increase in photosynthetic capacity and a decrease in stomatal conductance. Increasing soil strength might occur as a result of reduced soil moisture levels and external pressure to the soil, both of which may have natural or anthropogenic reasons. Anthropogenic causes of soil compaction include the use of heavy machineries, the interaction of soil tillage and water impact as well as livestock trampling. A natural cause that could be observed especially in the Chieng Khoi catchment (Chapter 2) is of topographical origin. Hilltops are often characterized by shallow surface soil layers, low organic matter and subsoil layers with higher bulk density. This is a form of natural soil compaction due to the way soil material was formed by weathering of the parent material and the constant movement of soil from the hilltops to the lower slopes by natural soil erosion. Years of cultivation and poor soil management practices can increase this effect (McKenzie, 2010).

In conclusion, CSSI-fingerprinting may be most reliable when (i) significant differences in δ^{13}C-FAME values between the various sources exist, i.e. δ^{13}C values of plant derived soil lipids land use types are limited to a set of few and physiological contrasting vegetation types, e.g. respective representatives of the C_3, C_4 and CAM metabolisms, (ii) the correction factors of each source do not differ greatly from each other, i.e. spatial variation in soil properties is limited, especially in concentrations of SOC and of the chosen marker compounds, e.g. FAs, or *n*-alkanes, when the land use types of interest have no history of crop rotations or land use changes and would be of the same soil type, (iii) the spatial variability of the δ^{13}C-FAME values of the sediment samples of a given deposition area is limited.

5.3 Determing past land use specific net erosion rates using CSSI-fingerprinting and FRNs

Gibbs (2014) suggested a multi-isotopic investigation approach involving CSSI and FRN techniques to reconstruct historical land use. Yet, to our knowledge no work has been published in peer-reviewed-journals to date, determining past land use specific net erosion rates using CSSI-fingerprinting and FRNs. Even though, such knowledge can provide valuable insight into the impact of specific land use conversions in terms of soil degradation and soil erosion and could support the implementation of soil conservation measures by informed decision making. While CSSI-fingerprinting has been successfully tested and validated to estimate the proportional contributions of different land use sources (Chapter 2 and Chapter 3), FRNs allow dating the layers of a sediment profile and provide quantitative estimates on the amount of eroded soil. In this study the joint use of CSSI-fingerprinting and FRNs, was successful in assigning past erosion rates to specific land use types. Dominant net erosion rates between 1987 to 2010 were determined, a period characterized by dramatic land use change from mature forest to intense maize and cassava production on steep slopes.

To determine the age of the soil layers of the reference profile, we used ^{137}Cs as a radionuclide tracer. This, however, proved unsuitable. Very low values of ^{137}Cs activity (< 0.8 Bq kg^{-1}) accompanied with high uncertainties (35 %), which prohibited the exact identification of the layer, which represented the year (1964) of maximum global deposition of thermo-nuclear fallout. This was mainly attributed to the geographical location of the Chieng Khoi catchment in the Southern hemisphere, which was only slightly exposed to ^{137}Cs fallout (Walling et al., 1999).

Contrastingly, in the undisturbed reference profile, continuous input of $^{210}Pb_{ex}$ resulted in maximum activity occurring at the surface rather than slightly below the surface (Mabit et al., 2008, 2014; Walling et al., 1995). Layer-explicit variations in $^{210}Pb_{ex}$ activity, indicating different sedimentation rates, were observed for the sediment profile and complied with depth distributions of $^{210}Pb_{ex}$ concentrations of previous studies (Benmansour et al., 2013; Du and Walling, 2012). Observed sediment accumulation rates were determined using the CRS model and were comparable to earlier studies, which have demonstrated increased soil losses after land use change from forest to continuous maize and cassava cropping (Häring et al., 2014; Wezel et al., 2002; Van De et al., 2008). To further corroborate the integrated FRN – CSSI approach for calculating land use type-specific net erosion rates, anthropogenic radioisotopes

of plutonium ($^{239+240}$Pu) with generally lower uncertainties (< 20%) should be tested in more detail as alternatives to ^{137}Cs (Alewell et al., 2014).

The bulk SOC δ^{13}C and CSSI values extracted from the sediment layers revealed a vertical isotopic distribution pattern, which suggests that land uses with C_3 and C_4 vegetation have dominated sediment deposition at different times (i.e., years). Our results demonstrated that after the period of 1987 to 1994, which was defined by gradual conversion of shifting cultivation to intensified agricultural production, the proportion of soil contributed by maize and cassava increased and peaked during the years 2000 to 2004. This finding is in line with studies on land use history of this region. After 1994, previously shrub- and tree-covered steep slopes were successively converted to crop land for high yielding hybrid maize and commercial 1-year cassava varieties, resulting in less soil cover and initiating high rates of soil erosion (Moench, 1991; Van De et al., 2008). Although crop areas were continuously expanded after 2004, thus making an increased sediment contribution likely, this was not reflected in our results. A possible explanation might derive from the delay that occurs after forest clearing. Typical isotopic C_3 signals may be still dominant in these soils, even though production of C_4 crops had already begun (Häring et al., 2013).

Land use type-specific net erosion rates exhibited similar patterns in their chronological succession as land use type-specific proportional soil contribution rates but were lower than erosion rates determined in other studies. While in our study maximum net erosion rates for maize production areas amounted to 5.3 t ha^{-1} y^{-1}, Tuan et al. (2014) observed average soil losses of 42 t ha^{-1} y^{-1} and 112 t ha^{-1} y^{-1}. Similarly, Phien and Loan (2005) measured erosion rates of 43 t ha^{-1} y^{-1} on fields under cassava production, while Häring et al. (2014) determined soil erosion rates ranging from 12 to 89 t ha^{-1} y^{-1} under maize. The divergence between the net erosion rates estimated in the present study and those determined by others may be attributed to a deposition of portions of the total sediments before having reached the sites of the profile or having been deposited further into the lake.

When the research objective does not only include the investigation of current erosion events but also aims at looking back in time as in the deconstruction of a sediment core to identify changes in land use over time, one must also consider temporal effects in addition to the aforementioned factors of isotope discrimination. Boyd et al. (2006) demonstrated that once formed, the CSSI value of the individual organic compounds did not change significantly after formation. It has to be taken into account, however, that the degree of ^{13}C content of the

atmospheric CO_2 at the time of formation of the biomarker has an influence on its CSSI value. Since the beginning of the Industrial Revolution the concentration of ^{13}C in atmospheric CO_2 is decreasing. This can be attributed to the burning of fossil fuels (Farquhar et al., 1989; Savage et al., 2010). This change in atmospheric ^{13}C (and also ^{14}C) concentrations is known as the Suess effect. Given that pre-industrial atmospheric CO_2 values are about 2.0‰ more enriched than present day values (Gibbs, 2014) requires a $\delta^{13}C$ correction of all but the present days sediment samples (Verburg, 2007). For recent decades, a time-dependent correction of -0.022 ‰ per year applies (Chamberlain et al., 2005; Hopkins and Ferguson 2012). The deconstruction of our sediment core to identify changes in land use over time lacks the correction of the Suess effect. However, the standard deviation for the majority of CSSI values was greater than the correction factor for the corresponding year. Therefore, we expect that the trend of the results would not have changed if the Suess effect had been taken into account. Furthermore, Matsumoto et al. (2007) pointed out that soil microorganisms may also contribute to the shift of ^{13}C to ^{12}C in atmospheric CO_2.

5.4 Sources of uncertainty using CSSI-fingerprinting

5.4.1 Tracer selection

To minimize uncertainty, the selection of a suitable tracer must be based on the following preconditions. The tracer of choice must be: (i) transferable, i.e. continuously transferred from plants onto and into the soil during the vegetation phase; (ii) chemically conservative, i.e. resistant to chemical conversion between source and sink; (iii) recalcitrant, i.e. not readily susceptible to microbial degradation; (iv) mobile, i.e. easily attached and transported with surface soil from source to sink; (v) isolable, i.e. extraction, purification and analysis with a sufficiently high degree of certainty (Reiffarth et al., 2016).

In this study FAs were used as sediment transport tracers. FAs are constantly transferred from aerial or root parts of plants to soil, ubiquitous, chemically stable and persistent (Simoneit, 2005; Wiesenberg et al., 2010). Furthermore, they can form aggregates with fine soil particles, especially clay minerals, which makes them mobile and they are readily isolable. To date FAs have been most commonly used as CSSI sediment tracers. To distinguish sediment sources, most authors chose from medium-chain (6 to 12 C); long-chain (13-21 C) and very-long-chain (more than 22 C) those FAs that were either present in all sources and sediments (Gibbs, 2008) or that additionally provide the best overall distinction for all sediment sources (Blake et al.,

2012; Hancock and Revill, 2013; Brandt et al., 2016, 2018a, 2018b). Agreement exists within the scientific community that short and medium-length fatty acids should be avoided because of their predominantly non-vegetal origin. Blake et al. (2012) focused on long and very-long-chain fatty acids, i.e C16:0 – C32:0. Similarly Gibbs (2014) suggested the use of straight-chain saturated long and very-long-chain fatty acids (VLCFA), especially C14:0 – C24:0. Alewell et al. (2016) proposed restricting the investigation to VLCFAs to not introduce errors due to aquatic contributions from algae and microorganisms. VLCFAs are typical in the above ground biomass of plants (Reina-Pinto and Yephremov, 2009). Low amounts of VLCFAs were also reported for the degradation products of suberin in roots (Naafs et al., 2004; Otto and Simpson, 2006; Wiesenberg et al., 2012)

By using long and very-long-chain FAs to distinguish sediment sources we accepted that not all FAs are predominantly or even exclusively of plant origin for this study. We always based the selection of suitable FAs on their discriminatory power for all potential sources and presence in all soils and sediments. While there is no guarantee for exclusive plant origin, we strongly suggest to base future CSSI sediment tracing approaches solely on VLCFAs, to minimize inaccuracies caused by sources other than terrestrial plants. The endeavor to minimize the influence of other FA sources should take precedence over great discrimination of sediment sources that was obtained with shorter chain FAs, possibly leading to a false sense of security. To further avoid non-terrestrial plant sources of FAs, Cooper et al. (2015) used *n*-alkanes as sediment tracer. Being a component of plant cuticular waxes, long chain *n*-alkanes (C27−C33 (Chikaraishi and Naraoka, 2003)), have unique biological origins which allow them to be used as plant-specific biomarkers of organic matter contributions (Cooper et al., 2015). At the same time, they share the excellent properties, i.e. transferability, chemical conservancy, recalcitrance, mobility, of FAs that predestine them as suitable sediment tracer compounds (Bourbonniere and Meyers, 1996).

A promising extension of the CSSI method has been reported by Cooper et al. (2015) in which they not only analyzed $\delta^{13}C$ but also $\delta^{2}H$ isotopes of *n*-alkanes. This approach allowed discriminating among trees, herbaceous perennials, and C_3 and C_4 graminoids. Finally, to allow for more accurate distinction of sediment sources in a catchment, a composite fingerprint using different chemical and physical properties of the sediments is recommendable (Walling et al., 2008).

5.4.2 Within-source group variability

Accounting for the variability of tracers in the sources is a key issue to limit uncertainties associated with soil sampling strategies (Yu and Oldfield et al., 1989; Sutherland, 1991). At the field scale, the main reasons for spatial variability of SOC and related sediment tracer, i.e. FAs or *n*-alkanes, are patterns of plant community (Allen et al., 2010). Differences in plant size, plant functional type and spatial distribution of vegetation affects the location where C is incorporated into the soil (e.g. Hook and Burke, 2000). At catchment level, spatial variability is mainly determined by the soil type, e.g. differences in clay content and land use management. The ability of fatty acids or n-alkanes to bind to clay minerals can lead to different tracer concentrations in different soil types. While tracer concentrations of SOC, and thus of FAs or *n*-alkanes, are often higher in clay rich soils, they are often lower in coarser soils (Van den Bygaart and Kay, 2004, Don et al., 2007).

To account for these issues the general soil sampling strategy for this study included the sampling of multiple sub-samples of the top 2 cm soil layer within a predefined area and combining them into a composite sample representative for an individual sampling location. The rational for this approach is the assumption that the uppermost soil layer is mobilized during erosion processes and transported to sediment deposits or bodies of water. Several scholars have expressed concern that this type of sampling is suitable for reducing the potential impacts of within-source group variability and making the source samples more representative. Owens et al. (2016) have suggested that, instead of sampling spatially integrated mixtures of land use types, collecting already eroded soil and sediment or using Gerlach troughs for direct sampling during runoff events. Similarly, Wilkinson et al. (2015) and van der Waal et al. (2015) obtained sediment source samples from already eroded areas. Collins et al. (2017) states that for these approaches, a profound understanding of the connectivity between eroding areas and sediment deposition sites is required. The exclusive sampling of apparently eroded areas, such as gullies, however, presents other challenges. In general, the concentration of FAs is highest in the top 0-5 cm horizon and expected to decrease exponentially with increasing depth (e.g. Hancock and Revill, 2013, Gleixner, 2013). Therefore, care should be taken to ensure that the soil material is collected close to the humic horizon and not at deeper soil horizons of the gullies. There is no unique and rigid approach to soil and sediment collection to fit the specific characteristics of every catchment and research goal the design of the sampling scheme. To account for spatio-temporal-variability, it is advisable to optimize sampling schemes (Owens et al., 2016). In this respect, the spatially stratified “Y-frame” sampling scheme (Vågen et al.,

2013), recently used by Mirzaeitalarposhti et al. (2015) and Cobo et al. (2010) for regional soil quality studies across spatial scales, may serve as a baseline for prospective erosion studies using CSSI-fingerprinting.

5.4.3 Soil-particle size considerations

In this study we used the less than 2 mm particle size obtained by sieving after drying that was proposed by Gibbs (2008) and used by others (Blake et al., 2012; Hancock and Revill, 2013). The rationale behind this approach is that even if lipids may have a higher affinity for binding onto finer particles, water percolation permits all particles sizes an equal opportunity to adsorb the lipids. Gibbs (2014) argued that separating the sample into fine clay or colloidal material may be adverse for the detection of the CSSI values characteristic for a specific soil.

Considerations for analyzing certain soil-particle sizes may nevertheless be relevant bearing in mind that the particle size distribution of the eroding soil is often very different from that of the sediments. The transport of soil during soil erosion processes can lead to a separation of soil particles in terms of their size, especially due to the abrasion and disaggregation caused breakdown of aggregates (Droppo, 2001). Therefore, sediment can show particle size-dependent variability of SOC concentrations (Walling et al., 1998). Sediments deposited at the bottom of a slope often consist of coarser sand fractions. The fine-grained (<63 µm) and SOC enriched fraction is further translocatated and may subsequently be deposited in aquatic environments. The CSSI approach requires that sufficient quantities of tracer compounds are present to be detectable in the sediment, thus larger quantities of sediment for analysis should be considered (Reiffarth et al., 2016). Obtaining sufficient sample masses of restricted particle size ranges may be logistically challenging and cost prohibitive (Collins et al., 2017). A practical alternative to particle size separation was proposed by Alewell et al. (2016) in which they ball milled all soil and sediment samples after removing stones and root material.
Although we recommend that different soil-particle size fractions should be tested and compared in future CSSI-fingerprinting studies, we believe that the use of the less than 2 mm particle size for the purposes of our study was sufficient to identify the major sediment sources. Ultimately the choice of soil-particle size fraction depends on the characteristics of the sediment fraction responsible for any environmental issues in question (Upadhayay et al., 2017).

5.4.4 Sediment source apportioning modeling

A significant source of uncertainty is linked to the choice of the correction factor, which is used to convert the isotopic proportions that are provided by the selected mixing model into actual soil proportions. For this study we used % C_{org} as proxy (Gibbs, 2008, 2014; Blake et al., 2012; Hancock and Revill, 2013), assuming that the relative % C_{org} of each source is closely linked to the relative tracer concentration. On the other hand an error is introduced when the relative C distribution in each source is very different to the relative distribution of the specific tracer FAs. Alewell et al. (2016) have demonstrated that relative FA (C26:0, C28:0) concentrations were considerably different to % C_{org} at their source sites consisting of forest, pasture and arable land. Furthermore, Upadhayay et al. (2017) strongly recommend the use of concentration-dependent stable isotope mixing models (SIMMs). Both have argued that using concentration-independent SIMMs (Gibbs, 2008, Blake et al., 2012; Hancock and Revill, 2013, Alewell et al. 2016, Brandt et al. 2016) that ignore the difference in relative FAs between the sources are incorrect. Concentration-independence assumes an identical isotopic tracer composition for all sources that however is rather an exception than the rule. Although they prove that the differences between the models are significant, the trend of the proportional contribution of the different sediment sources remains similar (Upadhayay et al., 2017).

5.5 CSSI-fingerprinting as a basis to explore new paths and solutions for focused soil conservation strategies

The results of this work have shown that the types of land use most at risk of erosion are those whose soils are intensively cultivated and at least temporarily without soil cover. In particular, the main sediment sources are maize and cassava cultivation in the Vietnam, wheat cultivation in Morocco and Russia and unpaved forest roads and channel bank erosion in Chile. The results of the Xinzheng catchment in China do not allow a clear statement, which is probably due to the isotopic similarity of the land uses that occur there. Particularly high is the erosion risk in Vietnam, where monocropping of maize is practiced on steep slopes. The main annual loss of soil is caused by heavy rainfall at the beginning of the monsoon season, when the young maize has just been planted and the soil cover is minimal. To make matters worse, at the end of the season cropping residues are burned, which further depletes the soil of SOC and plant nutrients. The rapidly advancing erosion in the highlands of Northwest Vietnam and beyond not only endangers the continued existence of crop production in these areas but can also lead to increasing ethnic and socio-economic inequalities and tensions. Silting of irrigation reservoirs

already leads to decreased water storage capacity and thus potentially critical shortages of irrigation water for paddy rice cultivation during the dry season.

Generally, effective soil conservation techniques may include minimum and zero tillage, contour-based cropping systems (e.g. strip cultivation, grass barriers, natural vegetative strips, alley cropping), cover crops, relay cropping, mulching, riparian buffer strips (e.g. planting of trees or grasses), and contour terracing. Since monoculture maize cropping will not disappear from the fragile upland systems without comparable lucrative alternatives, effective soil protection measures should focus on improved soil cover during the critical weeks at the beginning of the rainy season. For example, minimum tillage combined with cover crops has the potential to provide improved soil conservation in without the significant disadvantages associated to contour hedgerow systems (Hobbs, 2007; Shafi et al., 2007; Pansak et al., 2008; Hilger et al., 2013). In this sense Tuan et al. (2014) have suggested to grow *Arachis pintoi* as cover crop.

Information on the type and proportional contribution of different sediment sources of a catchment is a key requirement for the design and implementation of targeted soil conservation strategies, sediment mitigation planning, and aquatic habitat management policies. In order to effectively reduce sediment flows in a catchment area, sediment management strategies need to focus on the most important sources. Usually, sediment source assessments are based on the determination of the intensity of different erosion processes and thus an assessment of the probable contributions from the sources involved. Catchment managers are often requested to perform sediment budget analyses to conceptualize sediment problems and estimating sediment loadings (USEPA, 1999). Sediment budgeting provides an inventory of the sources of sediment in a catchment and estimates sediment production and delivery rates from each source (Reid and Dunne, 1996). The adoption and use of the CSSI technique as catchment sediment management tool within a regulatory framework becomes relevant when the proportional contributions of anthropogenic erosion caused by various agricultural practices (e.g. cropping, pastures, plantations) or non-agricultural alterations (e.g. forest roads) are being compared with natural sediment fluxes from natural forest (Hancock et al., 2012). If the proportional contribution of sediments of particular land use activities on each process is known, the overall influence of a suite of existing or planned land use activities can be estimated, thus providing a solid information base for the implementation of soil conservation techniques and the adoption of conservation agriculture. The CSSI approach may be particularly effective when synced with in-stream monitoring of suspended sediment loads and automated, time integrated sampling of

sediment, which can allow determining sediment budgets of a catchment (Hancock et al., 2007; Rustomji et al., 2008).

There are also big uncertainties regarding the application of the CSSI-fingerprinting methodology as a regular management tool. The most serious arguments against a widespread practical application of CSSI fingerprinting are the work and cost-intensive analytical procedures (Reiffarth et al., 2016). Although it is difficult to predict exact cost development and contrary to the generally accepted opinion, the analytical costs may not necessarily decrease steadily. Increasing automation, declining gross profit margins, and increasing competition among commercial analysis laboratories may lead to decreasing prices for isotope analysis. This trend may be offset by volatile (e.g., MeOH) or steadily increasing commodity prices, particularly for helium. Between 1998 and 2017 the price of private industry's Grade-A gaseous increased from \$1.514/m³ (\$42/mcf) to about \$7.21/m³ (\$200/mcf) (USGS, 1999; 2018). Even without significantly increasing raw material costs, the analytical costs remain significant.
Wherever progressive soil erosion is to be halted and there are serious efforts and means to implement soil conservation measures, CSSI-fingerprinting, conjointly with other fingerprinting techniques, might nevertheless be the most valuable approach to gain insight into hot-spots of soil erosion when more cost-effective and direct methods for identifying erosion hotspots have not produced satisfactory results. It is conceivable that the application of this method will be most effective when on-the-spot checks, interviews with experts on local on soil conditions, i.e. farmer, or even the screening of photos or satellite imagery for signs of exposed soil, yields no satisfactory results.

Summary

The loss of fertile topsoil due to soil degradation and erosion not only threatens crop productivity, but also induces sedimentation of aquatic systems and leads to social-, economical-, and environmental problems in many regions of the world. The abandonment of shifting cultivation in favor of intensive mono-cultural cropping systems on sloping land accompanied by rainfall detachment and surface runoff induced soil erosion is one of the most pressing environmental and agricultural problems in the highlands of Southeast Asia. Informed soil management strategies require knowledge on the main sediment sources in a catchment.

Compound-specific stable isotope (CSSI) fingerprinting, based on $\delta^{13}C$ values of fatty acid methyl ester (FAME), allows identifying hot-spots of soil erosion, particularly with regard to assigning sediment sources to actual land uses. In this regard, we assessed the potential of the CSSI – fingerprinting approach to assign sediment sources to specific land use types in various intensely cultivated catchments. In a first step we improved the statistical procedure to identify sediment sources in a heterogeneous agricultural catchment in the mountainous northwestern region of Vietnam. In a next step we tested the CSSI-fingerprinting under different agro-ecological conditions to evaluate its global applicability, using an aligned protocol. Finally, we integrated CSSI-fingerprinting and fallout radio nuclide (FRN, $^{210}Pb_{ex}$, ^{137}Cs) analysis to estimate past net erosion rates linked to land use types.

Specifically, the first case study aimed at testing the applicability of the CSSI – fingerprinting approach on the basis of soil and sediment samples derived from the Chieng Khoi catchment in Northwest Vietnam. Following CSSI analysis we set up a statistical decision sequence to identify hot spots of soil erosion by i) testing for significant differences between $\delta^{13}C$ values of fatty acids of different contributing land use types and thereafter ii) examining the data using a Monte Carlo simulation of mixing polygons to provide a quantitative basis for model rejection and exclusion for sediment samples which violate the point-in-polygon assumption, as well as iii) applying a Bayesian model with a Markov chain Monte Carlo (MCMC) model fitting using "SIAR" (Stable Isotope Analysis in R), which produces simulations of plausible values and therefore representing a true probability density for the proportional contribution of sediment sources. Significant differences of $\delta^{13}C$ values for identical FAME were most often found between soils under C_3 (protected and secondary forest, teak and fruit plantations) and C_4 (maize) vegetation. We were also able to find significant different $\delta^{13}C$ values between land

uses with exclusive C_3 vegetation. The resulting soil proportions were plausible for the six investigated sedimentation areas and suggested that fields under crop production, such as maize and cassava, but also teak plantations were main sediment sources in the upland area surrounding the Chieng Khoi reservoir.

To test the CSSI-fingerprinting approach under conditions of different agro-ecological zones (i.e. Chile, China, Morocco, Russia, Vietnam) we used the protocol from the first case study to discriminate sediment sources of six catchments from the northern and southern hemisphere. The CSSI-fingerprinting approach was first tested based on major land use categories (i.e., forest, cultivated and non-cultivated land) as potential sediment sources in the studied catchments. These land use categories were then further resolved into specific land use types (e.g., cassava and maize fields, orchards) to assess the potential resolution threshold of the CSSI technique.

In a final step, the influence of miscellaneous sources (e.g., roads, channel banks) that had the potential to distort proportional contributions to sediment deposition was assessed. Merging catchment-specific land use types with broader land use categories allowed determining inter-catchment comparisons of isotopic signatures due to significant differences in $\delta^{13}C$ values of fatty acids when cultivated land was present. Notably, no correlations were found between catchments of different sizes, agro-ecological zones, number and type of land use types, or soil organic carbon concentrations and the number of significant $\delta^{13}C$ fatty acid values of the various land use types. A third case study aimed to estimate earlier net erosion rates that were likely to be impacted by land-use changes in the Chieng Khoi catchment area. To tackle this challenge and to complement our first case study, we integrated CSSI-fingerprinting, $^{210}Pb_{ex}$ and ^{137}Cs. Additionally to the spatially-integrated topsoil (0 to 2 cm) samples of land uses that were identified as potential sediment sources (e.g., protected and secondary forests, teak, fruit orchards, maize, cassava) in our first case study, sediment samples of a representative profile were used for CSSI and FRN analysis. Samples for FRN reference data were taken from undisturbed areas in proximity. At a sediment deposition site near the lakeshore of the Chieng Khoi reservoir, $^{210}Pb_{ex}$ data determined the age and sediment accumulation rates of 19 sediment layers to a depth of 38 cm. Based on $^{210}Pb_{ex}$ activity, maximum sediment accumulation rates of 127 t ha^{-1} y^{-1} were calculated, corresponding to average erosion rates of about 16 t ha^{-1} y^{-1} for the total catchment area. CSSI data confirmed that maize and cassava were the most important erosion sources during a period of dramatic land use change (1987 to 2004), when forests were cleared, and high-yielding maize hybrids were introduced. Based on integrated FRN and CSSI

data, net erosion rates of maize and cassava reached maximum rates of 4.8 t ha^{-1} y^{-1} (maize), 6.2 t ha^{-1} y^{-1} (cassava).

In conclusion, the integrated Bayesian SIAR-CSSI approach was an appropriate tool to identify and assign sediment sources to actual land uses in small and heterogeneous catchments. This methodology was also suitable to identify hot-spots of soil erosion in contrasting catchments of different sizes and agro-ecological zones. Integrating CSSI-fingerprinting and fallout radio nuclide analysis to determine past sediment budgets provided insight into the impact of specific land use changes on soil retrogression and degradation. Such knowledge is of great value for informed and effective soil conservation through evidence-based land management and decision making.

Zusammenfassung

Der Verlust von fruchtbarem Oberboden durch Bodendegradation und -erosion bedroht nicht nur die Pflanzenproduktivität, sondern führt auch zur Sedimentierung von aquatischen Systemen und führt in vielen Regionen der Welt zu sozialen, ökonomischen und ökologischen Problemen. Der Verzicht auf Wanderfeldbaus zugunsten intensiver monokultureller Anbausysteme auf Hangflächen, begleitet von durch Niederschlag verursachte, oberflächennaher Bodenerosion, ist eines der drängendsten Umwelt- und Agrarprobleme im Hochland Südostasiens. Fundierte Strategien für Bodenmanagement erfordern Kenntnisse über die wichtigsten Sedimentquellen in einem Einzugsgebiet.

Das substanzspezifische Stabilisotopen (CSSI) Fingerprinting-Verfahren, basierend auf den $\delta^{13}C$-Werten von Fettsäuremethylester (FAME), ermöglicht die Identifizierung von Hotspots der Bodenerosion, insbesondere im Hinblick auf die Zuordnung von Sedimentquellen zu tatsächlichen Landnutzungen. In diesem Zusammenhang haben wir das Potenzial des CSSI-Fingerprinting-Verfahrens untersucht, um Sedimente spezifischer Landnutzungsarten in verschiedenen, intensiv kultivierten Einzugsgebieten zuzuordnen. In einem ersten Schritt haben wir das statistische Verfahren zur Identifizierung von Sedimentquellen in einem heterogenen landwirtschaftlichen Einzugsgebiet im gebirgigen Nordwesten Vietnams verfeinert. Im nächsten Schritt testeten wir das CSSI-Fingerprinting-Verfahren unter verschiedenen agrarökologischen Bedingungen, um dessen globale Anwendbarkeit unter Verwendung eines einheitlichen Protokolls zu bewerten. Schließlich integrierten wir CSSI-Fingerprinting und Fallout-Radionuklidanalyse (FRN, $^{210}Pb_{ex}$, ^{137}Cs), um vergangene Nettoerosionsraten in Verbindung mit Landnutzungstypen zu schätzen.

Die erste Fallstudie zielte darauf ab, die Anwendbarkeit der CSSI-Fingerprint-Verfahren auf der Basis von Boden- und Sedimentproben aus dem Chieng Khoi-Wassereinzugsgebiet in Nordwest-Vietnam zu testen. Nach der CSSI-Analyse haben wir eine statistische Entscheidungssequenz erstellt, um Hot Spots der Bodenerosion zu identifizieren, indem wir i) auf signifikante Unterschiede zwischen den $\delta^{13}C$-Werten von Fettsäuren unterschiedlicher Landnutzungstypen testen und danach ii) die Daten mit einer Monte-Carlo-Simulation der Mischpolygone untersucht, um eine quantitative Grundlage für den Ausschluss von Sedimentproben zu schaffen, die die point-in-polygon-Annahme verletzen, sowie iii) mit "SIAR" (Stable Isotopenanalyse in R) ein Bayessches Modell angewendet haben, dass auf einer

Markov chain Monte Carlo (MCMC) Modellanpassung basiert und welches Simulationen plausibler Werte liefert und somit realistische Wahrscheinlichkeitsdichten für die proportionellen Beiträge von Sedimentquellen darstellt. Signifikante Unterschiede der $\delta^{13}C$-Werte für identische FAMEs wurden am häufigsten zwischen Böden unter C_3 (geschützter und sekundärer Wald, Teak- und Obstplantagen) und C_4 (Mais) Vegetation gefunden. Wir konnten auch signifikante $\delta^{13}C$-Werte zwischen Landnutzungen mit ausschließlicher C3-Vegetation finden. Die resultierenden Sedimentanteile waren für die sechs untersuchten Sedimentationsgebiete plausibel und legten nahe, dass in den Anhöhen um das Chieng Khoi-Reservoir Ackerflächen unter Mais- und Maniokanbau, aber auch Teakplantagen die Hauptsedimentquellen waren.

Um das CSSI-Fingerprinting-Verfahren unter verschiedenen agrarökologischen Bedingungen (Chile, China, Marokko, Russland, Vietnam) zu testen, haben wir das Protokoll der ersten Fallstudie verwendet, um Sedimentquellen von sechs Einzugsgebieten der nördlichen und südlichen Hemisphäre zu unterscheiden. Das CSSI-Fingerprinting-Verfahren wurde zuerst auf der Grundlage von wichtigsten Landnutzungskategorien (d. H. Wald, kultiviertes und nicht kultiviertes Land) als mögliche Sedimentquellen in den untersuchten Einzugsgebieten getestet. Diese Landnutzungskategorien wurden schließlich in spezifische Landnutzungsarten (z. B. Maniok- und Maisfelder, Obstgärten) aufgelöst, um die potenzielle Auflösungsschwelle des CSSI-Fingerprinting-Verfahrens zu bewerten. In einem letzten Schritt wurde der Einfluss verschiedener Quellen (z. B. Straßen, Kanalufer) bewertet, welche die proportionalen Beiträge zur Sedimentablagerung verzerren können. Die Zusammenführung von einzugsgebietsspezifischen Landnutzungstypen mit allgemeineren Landnutzungskategorien erlaubte die Bestimmung von Einzugsgebietsvergleichen von Isotopensignaturen aufgrund signifikanter Unterschiede der $\delta^{13}C$-Werte von Fettsäuren, wenn Ackerflächen vorhanden waren. Insbesondere wurden keine Korrelationen zwischen verschiedenen Einzugsgebietsgrößen, agrarökologischen Zonen, Anzahl und Art der Landnutzungstypen oder organischen Kohlenstoffkonzentrationen im Boden und der Anzahl der signifikanten $\delta^{13}C$-Fettsäurewerte der verschiedenen Landnutzungsarten gefunden.

Eine dritte Fallstudie hat darauf abgezielt frühere Nettoerosionsraten zu schätzen, die wahrscheinlich durch Landnutzungsänderungen im Chieng Khoi-Wassereinzugsgebiet beeinflusst wurden. Um diese Herausforderung anzugehen und unsere erste Fallstudie zu ergänzen, haben wir das CSSI-Fingerprinting-Verfahren und Fallout-Radionuklidanalyse (FRN, $^{210}Pb_{ex}$, ^{137}Cs), gemeinsam angewendet. Zusätzlich zu dem räumlich integrierten Oberbodenproben (0 bis 2 cm) von Landnutzungsarten, die in unserer ersten Fallstudie als

mögliche Sedimentquellen identifiziert wurden (z.B. geschützter und sekundärer Wald, Teak- und Obstplantagen, Mais- und Maniokfelder), wurden Sedimentproben eines repräsentativen Profils für die CSSI- und FRN-Analyse verwendet. Die Proben für die FRN-Referenzdaten wurden aus ungestörten Bereichen in unmittelbarer Nähe entnommen. An einer Sedimentablagerungsstelle, nahe am Ufer des Chieng Khoi Reservoirs, wurden mit Hilfe von $^{210}Pb_{ex}$-Daten das Alter und die Sedimentansammlungsraten von 19 Sedimentschichten bis zu einer Tiefe von 38 cm bestimmt. Basierend auf der Radionuklidaktivität von $^{210}Pb_{ex}$ wurden maximale Sedimentablagerungsraten von 127 t ha^{-1} y^{-1} berechnet, was durchschnittlichen Erosionsraten von etwa 16 t $ha^{-1}y^{-1}$ für das gesamte Einzugsgebiet entspricht. Die CSSI-Daten bestätigten, dass Mais- und Cassavafelder die wichtigsten Erosionsquellen während einer Zeit dramatischer Landnutzungsänderungen (1987 bis 2004) waren, als Walder abgeholzt und ertragreiche Maishybriden eingeführt wurden. Basierend auf integrierten FRN- und CSSI-Daten erreichten die Nettoerosionsraten für Maisfelder maximal 4,8 t ha^{-1} y^{-1} und für Cassavafelder maximal 6,2 t ha^{-1} y^{-1}.

Zusammenfassend lässt sich sagen, dass der integrierte Bayessche-SIAR-CSSI-Ansatz ein geeignetes Instrument zur Identifizierung und Zuordnung von Sedimentquellen zu tatsächlichen Landnutzungen in kleinen und heterogenen Einzugsgebieten war. Diese Methodik war auch geeignet, Hot Spots der Bodenerosion in kontrastierenden Einzugsgebieten unterschiedlicher Größe und agrarökologischer Zonen zu identifizieren. Die Integration von CSSI-Fingerprinting-Verfahrens und Fallout-Radionuklid-Analyse zur Bestimmung früherer Sedimentbudgets ermöglichte Einblicke in die Auswirkungen spezifischer Landnutzungsänderungen auf Bodenregression und -degradation. Dieses Wissen ist von großem Wert für einen fundierten und effektiven Bodenschutz durch evidenzbasiertes Landmanagement und Entscheidungsfindung.

References

Ainsworth, E.A., Long, S.P., 2004. What have we learned from 15 years of free-air CO2 enrichment (FACE)? A meta-analytic review of the responses of photosynthesis, canopy properties and plant production to rising CO2. New Phytol. 165, 351–372.

Alewell, C., Birkholz, A., Meusburger, K., Schindler Wildhaber, Y., Mabit, L., 2016. Quantitative sediment source attribution with compound-specific isotope analysis in a C3 plant dominated catchment (central Switzerland). Biogeosciences 13, 1587–1596.

Alewell, C., Meusburger, K., Juretzko, G., Mabit, L., Ketterer, M.E., 2014. Suitability of $^{239+240}$Pu and ^{137}Cs as tracers for soil erosion assessment in mountain grasslands. Chemosphere 103, 274–280.

Allen, D.E., Pringle, M.J., Page, K.L., Dalal, R.C., 2010. A review of sampling designs for the measurement of soil organic carbon in Australian grazing lands. Rangeland J. 32, 227–246

Appleby, P.G., Oldfield, F., 1978. The calculation of lead-210 dates assuming a constant rate of supply of unsupported ^{210}Pb to the sediment. Catena 5, 1–8.

Badri, D.V., Vivanco, J.M., 2009. Regulation and function of root exudates. Plant Cell Environ. 32, 666-681.

Bao, N.X.E., 2004. Geology and mineral resources map of Viet Nam, (F-48-XXVII), scale 1:200.000, Dep. of Geology and Mining, Viet Nam, Ha Noi, 145 pp.

Barthod, L.R.M., Liu, K., Lobb, D.A., Owens, P.N., Martinez-Carreras, N., Koiter, A.J.,Petticrew, E.L., McCullough, G.K., Liu, C., Gaspar, L., 2015. Selecting color-based tracers and classifying sediment sources in the assessment of sediment dynamics using sediment source fingerprinting. J. Environ. Qual. 44. 1605-1616.

Benmansour, M., Mabit, L., Nouira, A., Moussadek, R., Bouksirate, H., Duchemin, M., Benkdad, A., 2013. Assessment of soil erosion and deposition rates in a Moroccan agricultural field using fallout ^{137}Cs and $^{210}Pb_{ex}$. J. Environ. Radioact. 115, 97–106.

Berry, J.K., Detgado, J.A., Khosla, R., Pierce, F.J., 2003. Precision conservation for environmental sustainability. J. Soil Water Conserv. 58, 332–339.

Berry, J.K., Delgado, J.A, Pierce, F.J., Khosla, R., 2005. Applying spatial analysis for precision conservation across the landscape. J. Soil Water Conserv. 60, 363–370.

Blake, W.H., Ficken, K.J., Taylor, P., Russell, M.A., Walling, D.E., 2012. Tracing crop-specific sediment sources in agricultural catchments. Geomorphology 139–140, 322–329.

Boley, J.D., Drew, A.P., Andrus, R.E., 2009. Effects of active pasture, teak (Tectona grandis) and mixed native plantations on soil chemistry in Costa Rica. For. Ecol. Manage. 257, 2254-2261.

Bonell, M., Purandara, B.K., Venkatesh, B., Krishnaswamy, J., Acharya, H.A.K., Singh, U.V., Jayakumar, R., Chappell, N., 2010. The impact of forest use and reforestation on soil hydraulic conductivity in the Western Ghats of India: implications for surface and sub-surface hydrology. J. Hydrol. 391, 47-62.

Bourbonniere, R.A., Meyers, P.A., 1996. Sedimentary geolipid records of historical changes in the watersheds and productivities of lakes Ontario and Erie. Am. Soc. Limnol. Oceanogr. 41, 352–359.

Boyd, T.J., Osburn, C.L., Johnson, K.J., Birgl, K.B., Coffin, R.B., 2006. Compound-specific isotope analysis coupled with multivariate statistics to source-apportion hydrocarbon mixtures. Environ. Sci. Technol. 40, 1916–1924.

Brandt, C., Cadisch, G., Nguyen, L.T., Vien, T.D., Rasche, F., 2016. Compound-specific $\delta^{13}C$ isotopes and Bayesian inference for erosion estimates under different land use in Vietnam. Geoderma Reg. 7, 311–322.

Brauman, K.A., Daily, G.C., Duarte, T.K., 2007. The nature and value of ecosystem services: an overview highlighting hydrologic services. Ann. Rev. Environ. Resour. 32, 67-98.

Bravo-Linares, C., Schuller, P., Castillo, A., Ovando-Fuentealba, L., Muñoz-Arcos, E., Alarcón, O., de los Santos-Villalobos, S., Cardoso, R., Muniz, M., Meigikos dos Anjos, R., Bustamante-Ortega, R., Dercon, G.,2018. First use of a compound-specific stable isotope (CSSI) technique to trace sediment transport in upland forest catchments of Chile. Sci. Total Environ. 618, 1114–1124.

Brown, A.G., 1985. The potential use of pollen in the identification of suspended sediment sources. Earth Surf. Process. Landforms 10, 27–32

Cadisch, G., Imhof, H., Urquiaga, S., Boddey, R.M., Giller, K.E., 1996. Carbon turnover ($\delta^{13}C$) and nitrogen mineralization potential of particulate light soil organic matter after rainforest clearing. Soil Biol. Biochem. 28, 1555-1567.

Carle, J.B., Ball, J.B., Del Lungo, A., 2009. The global thematic study of planted forests. Evans, J. (Ed.), Planted Forests: Uses, Impacts and Sustainability, CAB International, FAO, Rome, 33-46.

Chamberlain, C.P., Waldbauer, J.R., Fox-Dobbs, K., Newsome, S.D., Koch, P.L., Smith, D.R., Church, M.E., Chamberlain, S.D., Sorenson, K.J., Risebrough, R.., 2005. Pleistocene to recent dietary shifts in California condors. Proc. Natl. Acad. Sci. 102, 16707–16711.

Chikaraishi, Y., Naraoka, H., 2003. Compound-specific $\delta^{13}C$ analyses of n-alkanes extracted from terrestrial and aquatic plants. Phytochemistry 63, 361–371.

Chouvelon, T., Chappuis, A., Bustamante, P., Lefebvre, S., Mornet, F., Guillou, G., Violamer, L., Dupuy, C., 2014. Trophic ecology of European sardine Sardina pilchardus and European anchovy Engraulis encrasicolus in the Bay of Biscay (north-east Atlantic) inferred from $\delta^{13}C$ and $\delta^{15}N$ values of fish and identified mesozooplanktonic organisms. J. S. Res. 85, 277-291.

Clemens, G., Fiedler, S., Cong, N.D., Van Dung, N., Schuler, U., Stahr, K.., 2010. Soil fertility affected by land use history, relief position, and parent material under a tropical climate in NW-Vietnam. Catena 81, 87-96.

Cobo, J.G., Dercon, G., Cadisch, G., 2010. Nutrient balances in African land use systems across different spatial scales: A review of approaches, challenges and progress. Agric. Ecosyst. Environ. 136, 1–15.

Collins, A.L., Pulley, S., Foster, I.D.L., Gellis, A., Porto, P., Horowitz, A.J., 2017. Sediment source fingerprinting as an aid to catchment management: a review of the current state of knowledge and a methodological decision-tree for end-users. J. Environ. Manage., 194. 86-108.

Collins, A.L., Walling, D.E., 2004. Documenting catchment suspended sediment sources: problems, approaches and prospects. Prog. Phys. Geogr. 28, 159-196.

Collins, A.L., Zhang, Y.S., Duethmann, D., Walling, D.E., Black, K.S., 2013. Using a novel tracing-tracking framework to source fine-grained sediment loss to watercourses at sub-catchment scale. Hydrol. Process. 27, 959-974.

Collins, A.L., Zhang, Y., Walling, D.E., Black, K., 2010. Apportioning sediment sources in a grassland dominated agricultural catchment in the UK using a new tracing framework. In: Sediment Dynamics for a Changing Future. International Association of Hydrological Sciences Publication No. 337, Wallingford, UK, 68-75.

Cooper, R.J., Pedentchouk, N., Hiscock, K.M., Disdle, P., Krueger, T., Rawlins, B.G., 2015. Apportioning sources of organic matter in streambed sediments: An integrated molecular and compound-specific stable isotope approach. Sci. Total Environ. 520, 187–197.

Davidson, A., Csillag, F., 2003. A comparison of nested analysis of variance (ANOVA) and variograms for characterizing grassland spatial structure under a limited sampling budget. Can. J. Remote Sens. 29, 43–56.

Dawson, J.J.C., Smith, P. 2007. Carbon losses from soil and its consequences for land management. Sci.Total Environ.. 382, 165-190.

Dawson, T.D., Mambelli, S., Plamboek, A.H., Templer, P.H., Tu, K.P., 2002. Stable isotopes in plant ecology. Annu. Rev. Ecol. Syst. 33, 507–559.

Delgado, J.A., Berry J. K., 2008. Advances in precision conservation. Adv. Agron 98,1-44.

Dercon, G., Mabit, L., Hancock, G., Nguyen, M.L., Dornhofer, P., Bacchi, O.O.S., Benmansour, M., Bernard, C., Froehlich, W., Golosov, V.N., Haciyakupoglu, S., Hai, P.S., Klik, A., Li, Y., Lobb, D.A., Onda, Y., Popa, N., Rafiq, M., Ritchie, J.C., Schuller, P., Shakhashiro, A., Wallbrink, P., Walling, D.E., Zapata, F., Zhang, X., 2012. Fallout radionuclide-based techniques for assessing the impact of soil conservation measures on erosion control and soil quality: An overview of the main lessons learnt under an FAO/IAEA Coordinated Research Project. J. Environ. Radioact. 107, 78–85.

Diamond, J., 2005. Collapse: How Societies Choose to Fail or Survive, Penguin Books.

Don, A., Schumacher, J., Scherer-Lorenzen, M., Scholten, T., and Schulze, E. D., 2007. Spatial and vertical variation of soil carbon at two grassland sites – implications for measuring soil carbon stocks. Geoderma 141, 272–282.

Douglas, G.B., Gray, C.M., Hart, B.T., Beckett, R., 1995. A strontium isotopic investigation of the origin of suspended particulate matter (SPM) in the Murray-Darling River system, Australia. Geochim. Cosmochim. Acta 59, 3799–3815.

Douglas, G., Palmer, M., Caitcheon, G., 2003. The provenance of sediments in Moreton Bay, Australia: A synthesis of major, trace element and Sr-Nd-Pb isotopic geochemistry, modelling and landscape analysis. Hydrobiologia 494, 145–152.

Droppo, I.G., 2001. Rethinking what constitutes suspended sediment. Hydrological Processes 15, 1551–1564.

Du, P., Walling, D.E., 2012. Using ^{210}Pb measurements to estimate sedimentation rates on river floodplains. J. Environ. Radioact. 103, 59–75.

Dung, N.V., Vien, T.D., Lam, N.T., Tuong, T.M., Cadisch, G., 2008. Analysis of the sustainability within the composite swidden agroecosystem in northern Vietnam: 1. Partial nutrient balances and recovery times of upland fields. Agric. Ecosyst. Environ. 128, 37–51.

Dung, N.V., Vien, T.D., Cadisch, G., Lam, N.T., Patanothai, A., Rambo, T., Tuong, T.M., 2009. A nutrient balance analysis of the sustainability of the composite swiddening agroecosystem. In: Vien, T.D., Rambo, T., Lâm, N.T. (Eds.), Farming with Fire and Water: The Human Ecology of a Composite Swiddening Community in Vietnam's Northern Mountains. Kyoto University Press and Trans Pacific Press, Kyoto, 243–283.

El-Swaify, S.A., Dangler, E.W., Armstrong, C.L., 1982. Soil erosion by water in the tropics. College of Tropical Agriculture and Human Resources, University of Hawaii Research Extension Series 024, Honolulu.

FAO. 2010.Global Forest Resources Assessment 2015. Rome (http://www.fao.org/3/a-i4793e.pdf)

Farquhar, G.D., Ehleringer, J.R., Hubick, K.T., 1989. Carbon isotope discrimination and photosynthesis. Annu. Rev. Plant Physiol. Plant Mol. Biol. 40, 503–537.

Fforde, A., Vylder, S. de, 1996, From Plan to Market: Economic Transition in Vietnam 1979-1994. Boulder: Westview Press.

Fernández-Moya, F., Alvarado, A., Forsythe, W., Ramírez, L., Algeet-Abarquero, N., Marchamalo-Sacristán, M., 2014. Soil erosion under teak (Tectona grandis L.f.) plantations: General patterns, assumptions and controversies, Catena 123, 236-242.

Fernandes, R., Millard, A.R., Brabec, M., Nadeau, M.J., and Grootes, P. 2014. Food reconstruction using isotopic transferred signals (FRUITS): a Bayesian model for diet reconstruction. PLoS ONE, 9*(2):* e87436.

Flanagan, L.B., Ehleringer, J.R.,1998. Ecosystem-atmosphere CO2 exchange: interpreting signals of change using stable isotope ratios. Trends Ecol Evol 13. 10–14.

Fox, J.F., Papanicolaou, A.N., 2008. Application of the spatial distribution of nitrogen stable isotopes for sediment tracing at the watershed scale. J. Hydrol. 358. 46-55.

Gaouzi, F.J.E., Sebilo, M., Ribstein, P., Plagnes, V., Boeckx, P., Xue, D.M., 2013. Using $\delta^{15}N$ and $\delta^{18}O$ values to identify sources of nitrate in karstic springs in the Paris basin (France). Appl. Geochem. 35, 230-243.

Gibbs, M.M., 2008. Identifying source soils in contemporary estuarine sediments: A new compound-specific isotope method. Estuaries and Coasts 31, 344–359.

Gibbs, M.M., 2014. Protocols on the use of Compound-Specific Stable Isotopes to identify and apportion soil sources from land use. Revised 2013. Contract report to Joint FAO/IAEA Division of Nuclear Techniques in Food and Agriculture. 126 p. Available on line at http://www-naweb.iaea.org/nafa/swmn/public/CSSI-technique-protocols-revised-2013.pdf

Gingele, F.X., De Deckker, P., 2005. Clay mineral, geochemical and Sr-Nd isotopic fingerprinting of sediments in the Murray-Darling fluvial system, southeast Australia. Aust. J. Earth Sci. 52, 965-974.

Glaser, B., 2005. Compound-specific stable-isotope (delta C-13) analysis in soil science. J. Plant Nutri. Soil Sci. 1685: 633–648.

Grimshaw, D.L., Lewin, J., 1980. Source identification for suspended sediments 47, 151–162.

Hancock, G., Caitcheon, G., 2010. Sediment sources and transport to the Logan–Albert River estuary during the January 2008 flood event. Water for a Healthy Country National Research Flagship. http://www.clw.csiro.au/publications/waterforahealthycountry/2010/wfhc-Logan-Albert-River-flood.pdf

Hancock, G.J., Revill, A.T., 2013. Erosion source discrimination in a rural Australian catchment using compound-specific isotope analysis (CSIA). Hydrol. Process. 27, 923–932.

Hancock, G.J., Wilkinson, S.N., Read, A., 2007. Sources of sediment and nutrients to the Gippsland Lakes assessed using catchment modeling and sediment tracers. CSIRO Land and Water Science Report 70/07. http://www.clw.csiro.au/publications/science/2007/sr70-07.pdf

Häring, V., Fischer, H., Cadisch, G., Stahr, K., 2013. Implication of erosion on the assessment of decomposition and humification of soil organic carbon after land use change in tropical agricultural systems. Soil Biol. Biochem. 65, 158–167.

Häring, V., Fischer, H., Stahr, K., 2014. Erosion of bulk soil and soil organic carbon after land use change in northwest Vietnam. Catena 122, 111–119.

Hatfield, R.G., Maher, B.A., 2009. Fingerprinting upland sediment sources: particle size specific magnetic linkages between soils, lake sediments and suspended sediments. Earth Surf. Process. Landf. 34, 1359–1373.

Hayes, J.M., Freeman, K.H., Popp, B.N., Hoham, C.H., 1990. Compound-specific isotopic analyses: A novel tool for reconstruction of ancient biogeochemical processes. Organic Geochemistry 16. 1115–1128.

He, Q.,Walling, D.E., 1996. Interpreting particle size effects in the adsorption of ^{137}Cs and unsupported ^{210}Pb by mineral soils and sediments. J. Environ. Radioact. 30, 117-137.

He, Q., Walling, D.E., 1997. The distribution of fallout ^{137} Cs and ^{210} Pb in undisturbed and cultivated soils. Appl. Radiat. Isot., 48, 677–690.

Hien, B.H., Anh, D.T., Tiem, L.V., Thiet, M.V., Trung, N.M., 1995. Etude sur la durabilité de l' agriculture d'une commune de montagne du Nord-Ouest Vietnam. In: Durabilité du Dévelopment Agricole au Nord-Vietnam, Etudes de Cas, INSA, CIRAD URPA (eds). Maison d'Édition de l'Agriculture: Hanoi, 114-172.

Hilger, T., Keil, A., Lippe, M., Panomtaranichagul, M., Saint-macary, C., Zeller, M., Pansak, W., Dinh, T.V., Cadisch, G., 2013. Soil Conservation on Sloping Land: Technical Options and Adoption Constraints. In Stahr, K., n.d. Sustainable Land Use and Rural Development in Southeast Asia: Innovations and Policies for Mountainous Areas.

Hobbs, P.R., 2007. Conservation agriculture: what is it and why is it important for future sustainable food production? J. Agric. Sci. 145, 127–137.

Hobbs, P.R., Sayre, K., Gupta, R., 2008. The role of conservation agriculture in sustainable agriculture. Philos. Trans. R. Soc. London B. Biol. Sci. 363, 543–555.

Hook, P.B., Burke, I.C., 2000. Biogeochemistry in a shortgrass landscape: control by topography, soil texture, and microclimate. Ecology 81, 2686–2703.

Hopkins, J.B. III, Ferguson, J.M., 2012. Estimating the diets of animals using stable isotopes and a comprehensive Bayesian mixing model. PLoS ONE, 7(1): e28478.

Hultine, K.R., Marshall, J.D., 2000. Altitude trends in conifer leaf morphology and stable carbon isotope composition. Oecologia 123, 32–40.

Ibekwe, A.M., Kennedy, A.C., 1999. Fatty acid methyl ester (FAME) profiles as a tool to investigate community structure of two agricultural soils. Plant Soil 206, 151-161.

Ichihara K., Fukubayashi Y., 2010. Preparation of fatty acid methyl esters for gas-liquid chromatography. J. Lipid Res. 51, 635-640.

Ilstedt, U., Malmer, A., Verbeeten, E., Murdiyarso, D., 2007. The effect of afforestation on water infiltration in the tropics: a systematic review and meta-analysis. For. Ecol. Manage. 251, 45-51.

Kaplan, J.O., Krumhardt, K.M., Zimmermann, N., 2009. The prehistoric and preindustrial deforestation of Europe. Quat. Sci. Rev. 28, 3016–3034.

Kloeppel, B.D., Treichel, I.W., Kharuk, S., Gower, S.T., 1998. Foliar carbon isotope discrimination in Larix species and sympatric evergreen conifers: a global comparison. Oecologia 114, 153–159.

Knight, B.L., 2005. Precision conservation. J. Soil Water Conserv. 60, 137A.

Kongkaew, T., 2000. Yield and Nutrient Budgets of Hillside Cropping Systems with Erosion Control in Northern Thailand. Verlag Grauer, Stuttgart, 112.

Körner, Ch., Farquhar, G.D., Wong, S.C., 1991. Carbon isotope discrimination by plants follows latitudinal and altitudinal trends. Oecologia, 88, 30-40.

Kurashige, Y., Fusejima, Y., 1997. Source identification of suspended sediment from grain-size distributions: I. application of nonparametric statistical tests. Catena 31. 39-52.

Kramer, C., Gleixner, G., 2006. Variable use of plant- and soil-derived carbon by microorganisms in agricultural soils. Soil Biol. Biochem. 38, 3267–3278.

Krishnaswami, S., Kirk Cochran, J., 1978. Uranium and thorium series nuclides in oriented ferromanganese nodules: growth rates, turnover times and nuclide behavior. Earth Planet. Sci. Lett. 40, 45–62.

Kürten, B., Al-Aidaroos, A.M., Struck, U., Khomayis, H.S., Gharbawi, W.Y., Sommer, U., 2014. Influence of environmental gradients on C and N stable isotope ratios in coral reef biota of the Red Sea, Saudi Arabia. J. Sea Res. 85, 379-394.

Lam, N.T., Patanothai, A., Limpinuntana, V., Vityakon, P., 2005. Land-use sustainability of composite swiddening in the uplands of northern Vietnam: nutrient balances of swidden fields during the cropping period and changes of soil nutrients over the swidden cycle. Int. J. Agric. Sustain. 3, 1–12.

Lal, R., 2003. Soil erosion and the global carbon budget. Environ. Int. 29, 437-450.

Lal, R., 2004. Soil carbon sequestration to mitigate climate change. Geoderma 123, 1-22.

Lambin, E.F., Turner B.L, Geist, H.J., Agbola, S.B., Angelsen, A., Bruce, J.W, Coomes, O.T., Leemans, R., Li, X., Morna, E.F., Mortimore, M., Ramakrishnan, P.S., Richards, J.F., Skanes, H., Stone, G.D., Svedin, U., Veldkamp, T.A., Vogel, C., Xu, J., 2001. The causes of land-use and landcover change: moving beyond the myths. Global Environ. Change 11, 261-269.

Lippe, M., Marohn, C., Hilger, T., Dung, N. V., Vien, T.D., Cadisch, G., 2014. Evaluating a spatially-explicit and stream power-driven erosion and sediment deposition model in Northern Vietnam. Catena 120, 134–148.

Lippe, M., Thai Minh, T., Neef, A., Hilger, T., Hoffmann, V., Lam, N.T., & Cadisch, G. (2011). Building on qualitative datasets and participatory processes to simulate land use change in a mountain watershed of Northwest Vietnam. Environ. Modell. Softw. 26, 1454-1466.

Leigh, A., Ricker-Gilbert, J., Florax, R.J.G.M., 2014. How does population density influence agricultural intensification and productivity ? Evidence from Ethiopia. Food Policy 48, 142–152.

Mabit, L., Benmansour, M., Walling, D.E., 2008. Comparative advantages and limitations of the fallout radionuclides ^{137}Cs, $^{210}Pb_{ex}$ and ^{7}Be for assessing soil erosion and sedimentation. J. Environ. Radioact. 99, 1799–1807.

Mabit, L., Meusburger, K., Fulajtar, E., Alewell, C., 2013. The usefulness of ^{137}Cs as a tracer for soil erosion assessment : A critical reply to Parsons and Foster (2011). Earth-Sci. Rev. 127, 300–307.

Mabit, L., Benmansour, M., Abril, J.M., Walling, D.E., Meusburger, K., Iurian, A.R., Bernard, C., Tarján, S., Owens, P.N., Blake, W.H., Alewell, C., 2014. Fallout ^{210}Pb as a soil and sediment tracer in catchment sediment budget investigations: A review. Earth-Sci. Rev. 138, 335–351.

Matsumoto, K., Kawamura, K., Uchida, M., Shibata, Y., 2007. Radiocarbon content and stable carbon isotopic ratios of individual fatty acids in subsurface soil: implication for selective microbial degradation andmodification of soil organicmatter. Geochem. J. 41, 493–500.

McKenzie, N.J., Jacquier, D.J., Isbell, R.F., Brown, K.L., 2010, Australian Soils and Landscapes An Illustrated Compendium. CSIRO Publishing: Collingwood, Victoria.

McKenzie, R.H., 2010.Agricultural Soil Compaction : Causes and Management, Alberta Agriculture and Rural Development. 1–10.

Masle, J., Farquhar, G.D., 1988. Effect of soil strength on the relation of water-use efficiency and growth to carbon isotope discrimination in wheat seedlings. Plant Physiol 86, 32-38.

Mead, R., Xu, Y., Chong, J., Jaffé, R. 2005. Sediment and soil organic matter source assessment as revealed by themolecular distribution and carbon isotopic composition of n-alkanes. Org. Geochem. 36, 363–370.

Michener, R.H., Lajtha, K., 2007. Stable isotopes in ecology and environmental science, Ecological methods and concepts series. Blackwell.

Minh, T.T., Neef, A., Hoffmann, V., 2011. Agricultural knowledge transfer and innovation processes in Vietnam's northwestern uplands: State-governed or demand-driven? Southeast Asian Stud. 48, 425–455.

Mirzaeitalarposhti, R., Demyan, M.S., Rasche, F., Poltoradnev, M., Cadisch, G., Müller, T., 2015. MidDRIFTS-PLSR-based quantification of physico-chemical soil properties across two agroecological zones in Southwest Germany: generic independent validation surpasses region specific cross-validation. Nutr. Cycl. Agroecosystems 102, 265–283.

Moench, M., 1991. Soil erosion under a successional agroforestry sequence: a case study from Idukki District, Kerala, India. Agrofor. Syst. 15, 31–50.

Moore, J.W., Semmens, B.X. 2008. Incorporating uncertainty and prior information into stable isotope mixing models. Ecol. Lett. 11: 470–480.

MSEC (Managing Soil Erosion Consortium). 2003. An innovative approach to sustainable land management in Lao PDR. MSEC final report (October 1998–December 2002). Vientiane: MSEC.

Mukundan, R., Walling, D.E., Gellis, A.C., Slattery, M.C., Radcliffe, D.E., 2012. Sediment source fingerprinting: transforming from a research tool to a management tool. J. Am. Water Resour. Assoc. 48, 1241e1257.

Naafs, D.F., van Bergen, P.F., Boogert, S.J., de Leeuw, J.W., 2004. Solvent-extractable lipids in an acid andic forest soil; variations with depth and season. Soil Biol. Biochem. 36, 297–308.

Nagle, G.N., 2001. The Contribution to Agricultural Erosion to Reservoir Sedimentation in the Dominican Republic. Water Policy 3, 491-505.

Noordwijk, M. Van, Poulsen, J.G., Ericksen, P.J., 2004. Quantifying off-site effects of land use change : filters , flows and fallacies. Agric., Ecosyst. Environ. 104, 19–34.

Nosrati, K., Govers, G., Ahmadi, H., Sharifi, F., Amoozegar, M.A., Merckx, R., Vanmaercke, M., 2011. An exploratory study on the use of enzyme activities as sediment tracers: biochemical fingerprints? Int. J. Sediment Res. 26. 136–151.

O'Leary, M.H., 1988. Carbon isotopes in photosynthesis. Bioscience 38, 328–336.

Otto, A., Simpson, M.J., 2006. Sources and composition of hydrolysable aliphatic lipids and phenols in soils fromWestern Canada. Org. Geochem. 37, 385–407.

Owens, P., Blake, W.H., Gaspa, L., Gateuille, D., Koiter, A.J., Lobb, D.A., Petticrew, E.L, Reiffarth, D.G., Smith, H.G., Woodward, J.C. 2016. Fingerprinting and tracing the sources of soils and sediments: earth and ocean science, geoarchaeological, forensic, and human health applications. Earth. Sci. Rev. 162. 1-23.

Pandey, D., Brown, C., 2000. Teak: a global overview. Unasylva 51, 1-15.

Pansak, W., Hilger, T.H., Dercon, G., Kongkaew, T., Cadisch, G., 2008. Changes in the relationship between soil erosion and N loss pathways after establishing soil conservation systems in uplands of Northeast Thailand. Agric. Ecosyst. Environ. 128, 167–176.

Parnell, A., Inger, R., Bearhop, S., Jackson, A.L., 2010. Source partitioning using stable isotopes: coping with too much variation. PLoS ONE, 5(3), e9672.

Parnell, A.C., Inger, R., Bearhop, S., Jackson, A.L., 2010. SIAR: Stable isotope analysis in R, http://cran.r-project.org/web/packages/siar/index.html

Parnell, A.C., Phillips, D.L., Bearhop, S., Semmens, B.X., Ward, E.J., Moore, J.W., Jackson, A.L., Grey, J., Kelly, D.J., Inger, R., 2013. Bayesian Stable Isotope Mixing Models. Environmetrics 24, 387-399.

Phien T, Loan L.D. 2005. From research results to establishment of cultivation model on slopping lands of small households. In: Bo, N.V., Phien, T., Dinh, B.D., Son, T.T., Cung, D.V., Hanh, N.M. (Eds.) Proceeding on National Institute for soil and fertilizer 30 years anniversary Hanoi, Vietnam, pp. 470-484.

Phillips, D.L., Gregg, J.W., 2001. Uncertainty in source partitioning using stable isotopes. Oecologia 127. 171–179.

Phillips, D.L., Gregg, J.W., 2003. Source partitioning using stable isotopes: coping with too many sources. Oecologia 136, 261-269.

Phillips, D.L., Inger, R., Bearhop, S., Jackson, A.L., Moore, J.W., Parnell, A.C., Semmens, B.X., Ward, E.J., 2014. Best practices for use of stable isotope mixing models in food-web studies 835, 823–835.

Phillips, D.L., Koch. P.L., 2002. Incorporating concentration dependence in stable isotope mixing models. Oecologia 130. 114–125.

Pimentel, D., 2006. Soil erosion: A food and environmental threat. Environ. Dev. Sustain. 8, 119–137.

Pingali, P.L., Shah, M., 2001. Policy re-directions for sustainable resource use. J. Crop Produc., 3.103–118.

Podwojewski, P., Orange, D., Jouquet, P., Valentin, C., van Nguyen, T., Janeau, J.L., Tran, D.T. 2008. Land-use impacts on surface runoff and soil detachment within agricultural sloping lands in Northern Vietnam. Catena 74, 109–118.

Poulenard, J., Perrette, Y., Fanget, B., Quetin, P., Trevisan, D., Dorioz, J.M., 2009. Infrared spectroscopy tracing of sediment sources in a small rural watershed (French Alps). Sci. Total Environ. 407, 2808–2819.

Poulenard, J., Legout, C., Némery, J., Bramorski, J., Navratil, O., Douchin, A., Fanget, B., Perrette, Y., Evrard, O., Esteves, M., 2012. Tracing sediment sources during floods using Diffuse Reflectance Infrared Fourier Transform Spectrometry (DRIFTS): A case study in a highly erosive mountainous catchment (Southern French Alps). J. Hydrol. 414–415, 452–462.

Pulley, S., Foster, I., Collins, A.L., 2017. The impact of catchment source group classification on the accuracy of sediment fingerprinting outputs. J. Environ. Manag. 194, 16–26.

Putthacharoen, S., Howeler, R.H., Jantawat, S., Vichukit, V., 1998. Nutrient uptake and soil erosion losses in cassava and six other crops in a Psamment in eastern Thailand. Field Crops Res. 57, 113-126.

Rambo, A.T., Vien, T..D., 2001. Social Organization and the Management of Natural Resources : A Case Study of Tat Hamlet, a Da Bac Tay Ethnic Minority Settlement in Vietnams Northwestern Mountains. Southeast Asian Stud. 39, 299–324.

Ratnayake, R.R., Seneviratne, G., Kulasooriya, S.A. 2011. The effect of cultivation on organic carbon content in the clay mineral fraction of soils. Int. J. Soil Sci. 6, 217–223.

Raudsepp-Hearne, C., Peterson, G.D., Bennett, E.M., 2010. Ecosystem service bundles for analyzing tradeoffs in diverse landscapes. Proc Natl Acad Sci. 107, 5242-7.

Ravenzwaaij, D. Van, Cassey, P., Brown, S.D., 2018. A simple introduction to Markov Chain Monte – Carlo sampling. Psychol. Bull.2143–154.

Reiffarth, D., Petticrew, E.L., Owens, P.N., Lobb, D.A., 2016. Identification of sources of variability in fatty acid (FA) biomarkers in the application of compound-specific stable isotopes (CSSIs) to soil and sediment fingerprinting and tracing: a review. Sci. Total Environ. 565, 8–27.

Reid, L.M., Dune, T., 1996. Rapid Evaluation of Sediment Budgets, 1996. Catena Verlag Gmbh, Reiskirchen, Germany. 200 pp.

Reina-Pinto, J.J., Yephremov, A., 2009. Surface lipids and plant defenses. Plant Physiol. Biochem. 47, 540–549.

Rowan, J.S., Black, S., Franks, S.W., 2012. Sediment fingerprinting as an environmental forensics tool explaining cyanobacteria blooms in lakes. Appl Geogr 32. 832–843.

Rustomji., P., Caitcheon, G., Hairsine, P., 2008. Combining a spatial model with geochemical tracers and river station data to construct a catchment sediment budget. Water Resour Res 44, 16.

Savage, C., Leavitt, P.R., Elmgren, R., 2010. Effects of land use, urbanization, and climate variability on coastal eutrophication in the Baltic Sea. Limnol. Oceanogr. 55, 1033–1046.

Scherr, S.J., 1999. Soil degradation: A threat to developing country food security by 2020? [Policy Brief], 2020 Vision.

Scherr, S.J., McNeely, J.A., 2008. Biodiversity conservation and agricultural sustainability: towards a new paradigm of “ecoagriculture”landscapes. Philos. Trans. R. Soc. B Biol. Sci. 363, 477–494.

Schimmack, W., Auerswald, K., Bunzl, K., 2002. Estimation of soil erosion and deposition rates at an agricultural site in Bavaria, Germany, as derived from fallout radiocesium and plutonium as tracers. Naturwissenschaften 89, 43–46.

Schmitter, A.P., Fröhlich, H.L., Dercon, G., Hilger, T., Thanh, N.H., Lam, N.T., Vien, D., Cadisch, G., July, N., 2017. Redistribution of carbon and nitrogen through irrigation in intensively cultivated tropical mountainous watersheds. Biogeochemistry 109, 133–150.

Shafi, M., Bakht, J., Jan, M.T., Shah, Z., 2007. Soil C and N dynamics and maize (Zea may L.) yield as affected by cropping systems and residue management in North-western Pakistan. Soil Till. Res. 94, 520–529.

Shakhashiro, A., Mabit, L., 2009. Results of an IAEA inter-comparison exercise to assess ^{137}Cs and total ^{210}Pb analytical performance in soil, Appl. Radiat. Isot. 67, 139–146.

Shoji, S., Dahlgren, R., Nanzyo, M., 1993. Terminology, concepts and geographic distribution of volcanic ash soils. Dev. Soil Sci. 21, 1–5.

Sidle, R.C., Ziegler, A.D., Negishi, J.N., Rahim Nik, A., Siew, R., Turkelboom, F., 2006. Erosion processes in steep terrain—truths, myths, and uncertainties related to forest management in southeast Asia. For. Ecol. Manage. 224, 199-225.

Sikor, T., 2001. The allocation of forestry land in Vietnam: Did it cause the expansion of forests in the northwest? For. Policy Econ. 2, 1–11.

Sikor, T., Truong, D.M., 2002. Agricultural Policy and Land Use Changes in a Black Thai Commune of Northern Vietnam, 1952–1997. Mt. Res. Dev. 22, 248–255.

Sikor, T., 2004. Conflicting Concepts: Contested Land Relations in North-western Vietnam. Conserv. Soc. 2, 75-95.

Simoneit, B.R.T., 2005. A review of current applications ofmass spectrometry for biomarker/molecular tracer elucidations. Mass Spectrom. Rev. 24, 719–765.

Sinclair, F.L., 1999. A general classification of agroforestry practice. Agrofor. Syst. 46, 161–180.

Smith, B.N., Epstein, S., 1971. Two categories of 13C/12C ratios for higher plants. Plant Physiology 47. 380–384.

Smith, P., 2008. Land use change and soil organic carbon dynamics. Nutr. Cycl. Agroecosyst. 81169–178

Smith, J.A., Mazumder, D., Suthers, I.M., Taylor, M.D., 2013. To fit or not to fit: evaluating stable isotope mixing models using simulated mixing polygons. Methods Ecol. Evol. 4, 612-618.

Soil and Water Conservation Society. 2003. Conservation Implications of Climate Change: Soil Erosion and Runoff from Cropland. Ankeny, IA: Soil and Water Conservation Society.

Stock, B. C., Semmens, B.X. 2013. MixSIAR GUI User Manual. Version 3.1. https://github.com/brianstock/MixSIAR/. doi:10.5281/zenodo.47719.

Sulzman, E. W., 2008. Stable Isotope Chemistry and Measurement: A Primer. In Stable Isotopes in Ecology and Environmental Science (eds R. Michener and K. Lajtha).

Sutherland, R.A., 1991. Examination of caesium-137 areal activities in control (uneroded) locations. Soil Technol. 4, 33-50.

Thao, L.B., 1997. Viet Nam: the country and its geographical regions. The Gioi Publishers, Ha Noi, 617 pp.

Torres, A.I., Gil, M.N., Amin, O., Esteves, J.L., 2009. Environmental characterization of a eutrophicated semi-enclosed system: nutrient budget (Encerrada Bay, Tierra del Fuego Island, Patagonia, Argentina). Water Air Soil Poll. 204, 259-270.

Treignier, C., Tolosa, I., Grover, R., Reynaud, S, Ferrier-Page, C., 2009. Carbon isotope composition of fatty acids and sterols in the scleractinian coral Turbinaria reniformis: Effect of light and feeding. Limnol. Oceanogr. 54, 1933-1940.

Tuan, V.D., Hilger, T., MacDonald, L., Clemens, G., Shiraishi, E., Vien, T.D., Stahr, K., Cadisch, G., 2014. Mitigation potential of soil conservation in maize cropping on steep slopes. Field Crop. Res. 156, 91–102.

UNSCEAR (United Nations Scientific Committee on the Effects of Atomic Radiation), 2000. Sources and Effects of Ionizing Radiation, 2000 Report to the General Assembly. UNSCEAR, New York. Visited 30.06.2017. www.unscear.org.

Upadhayay, H.R., Bodé, S., Griepentrog, M., Huygens, D., Bajracharya, R.M., Blake,W.H., Dercon, G., Mabit, L., Gibbs, M., Semmens, B.X., Stock, B.C., Cornelis, W., Boeckx, P., 2017. Methodological perspectives on the application of compound-specific stable isotope fingerprinting for sediment source apportionment. J. Soils Sediments 1–17.

USEPA (U.S. Environmental Protection Agency), 1999. Protocol for Developing Sediment TMDLs, First Edition. https://nepis.epa.gov/Exe/ZyPDF.cgi/20004P3U.PDF?Dockey=20004P3U.PDF

USGS (U.S. Geological Service), 1999. Mineral Commodity Summaries, Helium, January 1999. https://minerals.usgs.gov/minerals/pubs/commodity/helium/330399.pdf

USGS (U.S. Geological Service), 2018. Mineral Commodity Summaries, Helium, January 2018. https://minerals.usgs.gov/minerals/pubs/commodity/helium/mcs-2018-heliu.pdf

Vågen, T. G., L. Winowiecki, J. E. Tondoh. 2013. Land Degradation Surveillance Framework (LSDF): field guide. International Center for Tropical Agriculture, World Agroforestry Centre, and the Earth Institute at Columbia University.

Valentin, C., Agus, F., Alamban, R., Boosaner, A., Bricquet, J.P., Chaplot, V., de Guzman, T., de Rouw, A., Janeau, J.L., Orange, D., Phachomphonh, K., Do Duy Phai, Podwojewski, P., Ribolzi, O., Silvera, N., Subagyono, K., Thiébaux, J.P., Tran Duc Toan, Vadari, T., 2008. Runoff and sediment losses from 27 upland catchments in Southeast Asia: Impact of rapid land use changes and conservation practices. Agric. Ecosyst. Environ. 128, 225–238.

Van De, N., Douglas, I., Mcmorrow, J., Lindley, S., Thuy Binh, D.K.N., Van, T.T., Thanh, L.H., Tho, N., 2008. Erosion and nutrient loss on sloping land under intense cultivation in Southern Vietnam. Geogr. Res. 46, 4–16.

van Dijk, A.I.J.M., Keenan, R.J., 2007. Planted forests and water in perspective. Forest Ecol. Manag. 251, 1-9.

Van De Water, P.K., Leavitt, S.W. & Betancourt, J.L., 2002. Leaf $\delta^{13}C$ variability with elevation, slope aspect, and precipitation in the southwest United States. Oecologia, 132, 332–343.

van der Waal, B., Rowntree, K., Pulley, S., 2015. Flood bench chronology and sediment source tracing in the upper Thina catchment, South Africa: the role of transformed landscape connectivity. J. Soils Sediments 15. 2398-2411.

Van den Bygaart, A. J., Kay, B. D. 2004. Persistence of soil organic carbon after plowing a long-term no-till field in southern Ontario, Canada. Soil Sci. Soc. Amer .68, 1394–1402.

Verburg, P., 2007. The need to correct for the Suess effect in the application of δ13C in sediment of autotrophic Lake Tanganyika, as a productivity proxy in the Anthropocene. J. Paleolimnol., 37. 591–602.

Wagner, H. H., Fortin, M., J., 2005. Spatial analysis of landscapes: concepts and statistics. Ecology 86, 1975-1987.

Wang, Y.J., Zhao, G.C., Xia, X.P., Zhang, Y.H., Fan, W.M., Li, C., Bi, X. W., Li, S. Z., 2009. EarlyMesozoic unroofing pattern of the detrital zircon geochronology and Si-in-white mica analysis of synorogenic sediments in the Jianghan Basin. Chem Geol 266. 231–241.

Wang, G., Zhou, L., Liu, M., Han, J., Guo, J., Faiia, A., Su, F., 2010. Altitudinal trends of leaf δ13C follow different patterns across amountainous terrain in North China characterized by a temperate semi-humid climate. Rapid Commun. Mass Spectrom. 24, 1557–1564.

Wallbrink, P.J., Murray, A.S., Olley, J.M., 1999. Relating suspended sediment to its original soil depth using fallout radionuclides. Soil Sci. Am. J. 63, 369-378.

Walling, D.E., 2005. Tracing suspended sediment sources in catchments and river systems. Sci. Total Environ. 344, 159–184.

Walling, D.E., Collins, A.L., Stroud, R.W., 2008. Tracing suspended sediment and particulate phosphorus sources in catchments. J. Hydrol. 350, 274–289.

Walling, D. E., He, Q., Appleby, P.G. 2003. Conversion models for use in soil-erosion, soil-redistribution and sedimentation investigations. Handbook for the Assessment of Soil Erosion and edimentation Using Environmental Radionuclides, 111–164. Springer.

Walling, D.E., He, Q., Blake, W., 1999. Use of ^{7}Be and ^{137}Cs measurements to document short- and medium-term rates of water induced soil erosion on agricultural land. Water Resour. Res. 35, 3865–3874.

Walling, D.E., Owens, P.N., Leeks, G.J.L., 1999. Fingerprinting suspended sediment sources in the catchment of the River Ouse, Yorkshire, UK. Hydrol. Process 13, 955e975.

Walling, D.E., Quine, T.A., 1995. The use of fallout radionuclides in soil erosion investigations. In: Nuclear Techniques in Soil–Plant Studies for Sustainable Agriculture and Environmental Preservation. International Atomic Energy Agency Publication ST1/PUB/947.

Walling, D.E., Woodward, J.C., 1992. Use of radiometric fingerprints to derive information on suspended sediment sources. In: Bogen, J., Walling, D.E., Day, T.J. (Eds.), Erosion and Sediment Transport Monitoring Programmes in River Basins. IAHS Publ., Oslo, 153-164 no. 210.

Ward, E.J., Semmens, B.X., and Schindler, D.E. 2010. Including source uncertainty and prior information in the analysis of stable isotope mixing models. Environ. Sci. Technol. 44: 4645–4650.

Wei, K., Jia, G., 2009. Soil n-alkane δ13C along amountain slope as an integrator of altitude effect on plant species δ13C. Geophys. Res. Lett. 36

Weltje, G., 2012. Quantitative models of sediment generation and provenance: state of the art and future developments. Sediment. Geol. 280. 4-20.

Wezel, A., Luibrand, A., Thanh, L.Q., 2002. Temporal changes of resource use, soil fertility and economic situation in upland Northwest Vietnam. L. Degrad. Dev. 13, 33–44.

Wiesenberg, G.L.B., Gocke, M., Kuzyakov, Y., 2010. Fast incorporation of root-derived lipids and fatty acids into soil - Evidence from a short term multiple $^{14}CO_2$ pulse labelling experiment. Org. Geochem. 41, 1049–1055.

Wiesenberg, G.L.B., Schneckenberger, K., Schwark, L., Kuzyakov, Y., 2012. Use of molecular ratios to identify changes in fatty acid composition of Miscanthus × giganteus (Greef et Deu.) plant tissue, rhizosphere and root-free soil during a laboratory experiment. Org. Geochem. 46, 1–11.

Wiesenberg, G.L.B., Schwarzbauer, J., Schmidt, M.W.I., Schwark, L., 2004. Source and turnover of organic matter in agricultural soils derived from n-alkane/n-carboxylic acid compositions and C-isotope signatures. Org. Geochem. 35, 1371–1393.

Wilkinson, S.N., Olley, J.M., Furuichi, T., Burton, J., Kinsey-Henderson, A.E., 2015. Sediment source tracing with stratified sampling and weightings based on spatial gradients in soil erosion. J. Soils Sediments 15. 2038–2051.

Williams, M.A., Myrold, D.D., Bottomley, P.J., 2006. Carbon flow from ^{13}C-labeled straw and root residues into the phospholipid fatty acids of a soil microbial community under field conditions. Soil Biol. Biochem. 38, 759-768.

WWAP (World Water Assessment Programme). 2012. The United Nations World Water Development Report 4: Managing Water under Uncertainty and Risk. Paris, UNESCO.

Xue, D.M., De Baets, B., Van Cleemput, O., Hennessy, C., Berglund, M., Boeckx, P., 2012. Use of a Bayesian isotope mixing model to estimate proportional contributions of multiple nitrate sources in surface water. Environ. Pollut. 161, 43-49.

Yen, B.T., Visser, S.M., Hoanh, C.T., Stroosnijder, L., 2013. Constraints on Agricultural Production in the Northern Uplands of Vietnam. Mt. Res. Dev. 33, 404–415.

Young A. 1997. Agroforestry for Soil Management, 2nd edition. CAB International, Wallingford, UK (in association with ICRAF, Nairobi, Kenya). 320 pp. ISBN 0 85199 189 0.

Yu, L., Oldfield, F., 1989. Amultivariate mixing model for identifying sediment sources from magnetic measurements. Quaternary Res 32.168–181.

Yu, L.Z., Oldfield, F., 1993. Quantitative sediment source ascription using magnetic measurements in a reservoir-catchment system near Nijar, Se Spain. Earth Surf. Proc. Land 18. 441–454.

Zhang, Y., Collins, A.L., Horowitz, A.J., 2012. A preliminary assessment of the spatial sources of contemporary suspended sediment in the Ohio River basin, United States, using water quality data from the NASQAN programme in a source tracing procedure. Hydrol. Process. 26. 326–334.

Zhang, W., Xing, Y., Yu, L., Feng, H., Lu, M., 2008. Distinguishing sediments from the Yangtze and Yellow Rivers, China: a mineral magnetic approach. Holocene 18, 1139-1145.

Zapata, F., 2003. The use of environmental radionuclides as tracers in soil erosion and sedimentation investigations: Recent advances and future developments. Soil Tillage Res. 69, 3–13.

Ziegler, A.D., Giambelluca, T.W., Sutherland, R.A., Nullet, M.A., Yanarsan, S., Pinthong, J., Preechpanya, P., Jaiaree, S., 2004. Toward understanding the cumulative impacts of roads in upland agricultural watersheds of northern Thailand. Agric. Ecosyst. Environ. 104, 145–158.

Apendices

Appendix A: Correlation Matrix

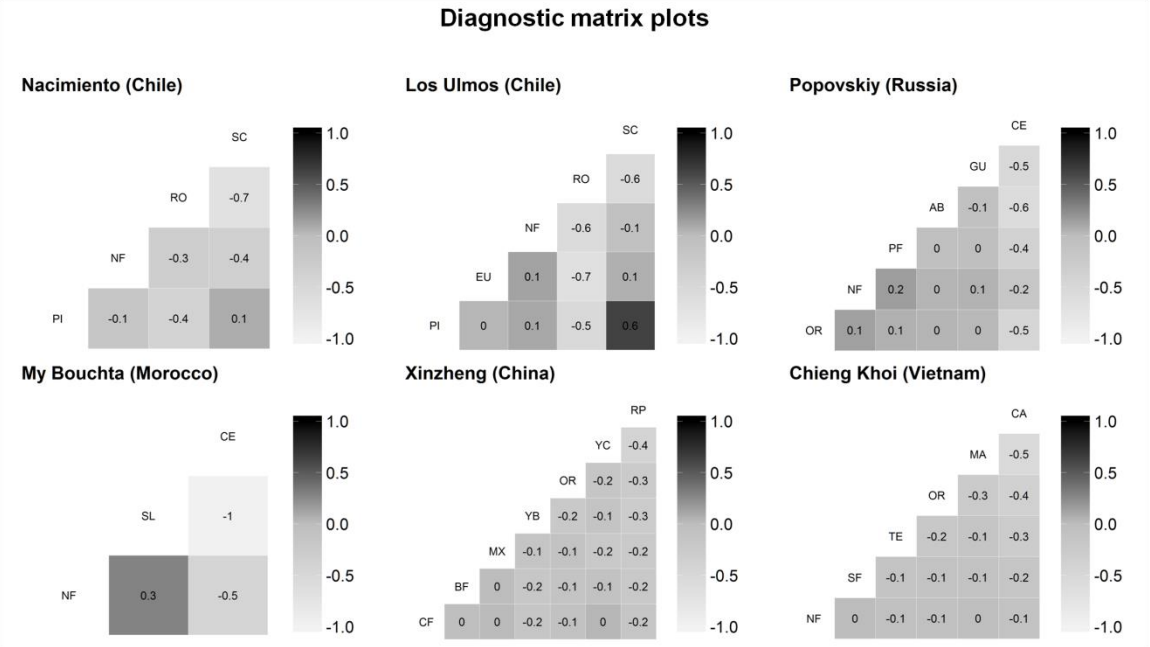

Figure A1. Correlation matrix of estimates of each source proportion calculated in the mixing models from the SIAR package output. Correlation values between sources are inside the boxes. Well separated sources are characterized by weak correlation values. Sources close to each other resulted in strong correlations. Increased correlation among sources will increase the level of uncertainty in the model output.

Appendix B: Proportional soil contribution table

Table B1. Estimated proportional soil contributions of land use specific soils in percent (%).

CAT	LUC	LUT	Proportional soil contributions (%)					
			Min	Q1	Mdn	M	Q3	Max
NAC	FO	PI	< 0.1	2.5	5.7	7.2	10.4	45.7
	NC	RO	< 0.1	10.1	20.2	21.8	31.8	77.0
	FO	NF	< 0.1	3.4	7.9	10.8	15.3	67.3
	NC	SC	6.4	51.9	60.6	60.3	69.1	98.3
LOS	FO	PI	< 0.1	4.4	6.3	6.6	8.4	27.9
	FO	EU	< 0.1	10.0	14.6	16.7	21.1	79.7
	NC	RO	< 0.1	48.2	61.2	57.2	70.2	96.0
	FO	NF	< 0.1	3.7	8.3	10.6	15.2	80.5
	NC	SC	< 0.1	2.9	6.5	8.8	12.4	61.3
POP	NC	AB	< 0.1	4.3	9.9	12.8	18.9	74.6
	NC	GU	< 0.1	4.9	10.8	12.8	19.2	78.5
	CL	CE	0.1	44.7	57.6	56.7	70.1	95.6
	CL	OR	< 0.1	2.3	5.6	7.8	11.4	52.1
	FO	NF	< 0.1	3.3	7.6	10.0	14.5	99.3
	FO	PF	< 0.1	4.6	9.2	10.0	14.0	66.3
CHK	FO	NF	< 0.1	1.0	2.3	3.0	4.4	20.5
	FO	SF	< 0.1	2.4	5.7	6.9	10.3	38.5
	CL	MA	< 0.1	18.5	26.5	26.5	33.8	81.0
	CL	CA	< 0.1	22.2	32.3	31.5	40.7	91.3
	CL	TE	< 0.1	6.2	12.4	13.2	19.1	59.6
	CL	OR	< 0.1	10.5	18.8	18.9	26.3	71.6
XIN	CL	OR	< 0.1	7.4	13.8	14.1	19.7	50.5
	CL	RP	< 0.1	13.2	22.8	22.7	31.9	63.9
	CL	MX	< 0.1	6.9	11.8	12.1	16.4	53.5
	CL	YB	< 0.1	6.8	13.7	14.2	20.8	53.3
	CL	YC	< 0.1	15.5	22.2	21.8	28.2	55.4
	FO	CF	< 0.1	2.6	5.2	5.6	8.1	25.1
	FO	BF	< 0.1	4.7	9.1	9.5	13.5	48.1
MYB	CL	CE	< 0.1	58.1	71.0	67.6	81.2	99.8
	FO	NF	< 0.1	1.3	3.0	3.9	5.5	46.1
	NC	SL	< 0.1	15.6	25.7	28.5	37.7	97.9

Abbreviations: Min: minimum value; Q1: 1st quartile; Mdn: median; M: mean; Q3: 3rd quartile; Max: maximum value

Appendix C: Tables for mean top soil SOC (%) and $\delta^{13}C$ (‰) values of six catchments

Table C1. Chile, Nacimiento catchment. Mean topsoil (0-2 cm) SOC (%) and $\delta^{13}C$ (‰) values for soil bulk carbon and topsoil-derived $\delta^{13}C$-FAME values (‰) for identified fatty acids for each soil source, i.e. land use type of each catchment. Mean (M) and standard error (SE) are included.

	Chile – Nacimiento							
	PI		RO		NF		SC	
Fatty Acid (‰)	M	SE	M	SE	M	SE	M	SE
C (%)	5.9	0.3	3	0.6	5.5	0.5	9	0.2
Bulk δ13C	-27.3	0.1	-27.2	0.3	-27.1	0.1	-27.5	0.2
Me C12:0	-32.1	0.3	-32	0.5	-33.9	0.5	-34	0.4
Me C14:0	-33.7	0.1	-33.3	0.2	-33.3	0.2	-34.2	0.3
Me i-C15:0	-25.6	0.1	-26.5	0.2	-26.2	0.1	-26.9	0.1
Me a-C15:0	-25.3	0.3	-26.4	0.3	-25.7	0.2	-26.8	0.2
Me C15:0	-29.4	0.9	-30.5	0.4	-30.4	0.5	-28.8	0.3
Me C16:0	-30.6	0.1	-30.5	0.3	-30.3	0.2	-30.3	0.1
Me 10 Me C16:0	-29.1	1.1	-28.1	0.4	-28.4	0.6	-27.9	0.9
Me C16:1w9	-27.5	0.6	-27.6	0.4	-28.2	0.5	-26.9	0.7
Me C16:1w7	-28.6	0.3	-29.8	0.4	-29	0.3	-31	0.4
Me C16:1w5	-27.7	0.5	-28.8	0.3	-28.8	0.5	-29.3	0.3
Me C17:0 cy	-30.8	0.3	-32.8	2.1	-31	0.3	-30.1	0.3
Me C18:0	-28.6	0.2	-29.3	0.2	-28.6	0.2	-30.6	0.2
Me 10 Me C18:0	-39.6	1.9	-38.7	1.4	-36.3	1.3	-32.6	0.8
Me C18:1w9c	-30	0.1	-29.8	0.5	-29.7	0.5	-29.4	0.2
Me C18:1w7c	-29.3	0.2	-28.1	0.6	-28.7	0.4	-30.2	0.2
Me C18:2(n6)	-31.6	0.2	-31.2	0.4	-31.9	0.5	-31.1	0.6
Me C19:0 cy	-32	0.8	-32	2	-29.7	1	-31.4	0.6
Me C18:3(n3)	-35.2	0.2	-36.1	0.4	-36	0.4	-36.4	0.5
Me C20:0	n.a.	n.a.	-30.9	1.8	n.a.	n.a.	n.a.	n.a.
Me C20:1w9c	-37.8	0.7	n.a.	n.a.	n.a.	n.a.	n.a.	n.a.
Me C21:0	-33.2	0.7	-32.9	0.7	-33.9	0.7	-34.1	0.5
Me C22:0	-30.5	0.1	-31	0.7	-32	0.2	-33	0.1
Me C23:0	-33.3	0.3	-34.6	0.5	-34.8	0.2	-35	0.3
Me C24:0	-31	0.1	-31.1	0.8	-32.4	0.3	-32.8	0.2
Me C26:0	-33.5	1	-35	0.6	-35	0.7	-35.9	0.3

Table C2. Chile, Los Ulmos catchment. Mean topsoil (0-2 cm) SOC (%) and $\delta^{13}C$ (‰) values for soil bulk carbon and topsoil-derived $\delta^{13}C$-FAME values (‰) for identified fatty acids for each soil source, i.e. land use type of each catchment. Mean (M) and standard error (SE) are included.

	Chile – Los Ulmos									
	PI		EU		RO		NF		SC	
Fatty Acid (‰)	M	SE	M	SE	M	SE	M	SE	M	SE
C (%)	19.2	0	13.9	0.1	2.8	0	10	0	6.8	0.2
Bulk δ13C	-26.5	0	-26.9	0.1	-26.9	0	-27.3	0	-27.6	0
Me C12:0	-33.9	0.1	-32.8	1.2	-32.1	1.3	-35.4	0.2	-30.4	1.5
Me C14:0	-35.3	0.1	-36.3	1	-34.3	0.4	-32.9	0.2	-33.8	0.3
Me i-C15:0	-28	0.5	-28	0.9	-27.6	0.2	-28.6	0.1	-29.3	0.2
Me a-C15:0	-28.8	1	-28	2	-26.2	0.1	-29.7	0.4	-30.2	0.1
Me C15:0	-32.8	0.4	-32.7	0	-31.6	0.1	-31.8	0.1	-32.1	0
Me C16:0	-30.7	0.3	-30.5	0	-30.2	0.1	-29.2	0.1	-30.1	0.1
Me 10 Me C16:0	-27	0.5	-30.3	0.1	-28.4	0.8	-27.2	3	-29.9	0.1
Me C16:1w9	-26.6	0.2	-25.2	0.6	-24.8	0.5	-25	0.6	-26.4	0.1
Me C16:1w7	-30.1	0.3	-30.8	0.2	-30.7	0.3	-30	0.3	-32	0.2
Me C16:1w5	-30.3	0.7	-29.7	0.2	-29.6	0.4	-30.6	0.5	-30.8	0
Me C17:0 cy	-31.3	0.6	-32.3	0.1	-31.5	0.2	-30.3	0.6	-30.3	0.3
Me C18:0	-29.2	0	-29.5	1	-29.4	0.5	-28.9	0.5	-30.3	0.2
Me 10 Me C18:0	n.a.	n.a.	-52.3	5.2	-39.9	3.5	-37.6	4.1	-31.7	0.4
Me C18:1w9c	-32.3	0.1	-32.1	0.2	-30.7	0.2	-30.1	0.5	-31.5	0.3
Me C18:1w7c	-31.8	0	-30.1	0.4	-29.9	1	-30.5	0.1	-30.9	0.2
Me C18:2(n6)	-34.7	0.4	-33.4	0.1	-32.6	0.1	-32.5	0.1	-32.2	0.2
Me C19:0 cy	-31.8	0	-32.3	0.6	-29.7	0.4	-31.7	0.5	-32	0.1
Me C18:3(n3)	-37.3	0.3	-36.8	0	-37.6	0.1	-36.4	0.2	-36.6	0.1
Me C20:0	-36.8	0.6	-32.7	1.9	-29.5	0.1	n.a.	n.a.	-28.3	1.6
Me C20:1w9c	-40.7	6.5	-47.2	8.5	-50.4	0.4	-46.6	3.9	-43.4	0.1
Me C21:0	-37.6	2	-36.5	0.1	-35.8	1.2	-34.8	1.1	-34.1	0.8
Me C22:0	-30.8	0.2	-29.7	0.1	-31.6	0	-30.9	0.1	-29.9	0.2
Me C23:0	-34.3	0.9	-34.5	0.8	-34.1	0.1	-34.1	0.2	-33.8	0.1
Me C24:0	-32.8	0.1	-30.9	0.1	-30.7	0.1	-32.1	0.4	-30.6	0.6
Me C26:0	-34.9	1.2	-36.1	0.3	-35.4	1.2	-33.6	1.6	-35.2	0.8

Table C3. Russia, Popovskiy Pond catchment. Mean topsoil (0-2 cm) SOC (%) and $\delta^{13}C$ (‰) values for soil bulk carbon and topsoil-derived $\delta^{13}C$-FAME values (‰) for identified fatty acids for each soil source, i.e. land use type of each catchment. Mean (M) and standard error (SE) are included.

	Russia - Popovskiy Pond											
	AB		GU		CE		OR		NF		PF	
Fatty Acid (‰)	M	SE	M	SE	M	SE	M	SE	M	SE	M	SE
C (%)	1.6	0.1	2.1	0.3	1.3	0	2.7	0.1	4.2	0.3	2.9	0.2
Bulk δ13C	-26.5	0.1	-22.3	1.4	-25.2	0.1	-26.8	0.1	-25.9	0.2	-26.2	0.2
Me C12:0	-34.4	1.1	-34.6	1.2	-35.6	1	-33.8	1.5	-32.8	2.1	-29.5	2.1
Me C14:0	-31.2	0.1	-30.7	0.2	-30.8	0.4	-31.4	0.3	-31.2	0.5	-32.7	0.5
Me i-C15:0	-26.9	0.2	-26.4	0.1	-22.9	0.9	-26.7	0.2	-26.2	0.1	-26.7	0.2
Me a-C15:0	-27.4	0.3	-26.4	0.2	-22.7	1.8	-26.9	0.4	-25.9	0.3	-26.9	0.5
Me C15:0	-30.3	0.2	-30.2	0.2	-30.2	0.3	-30.1	0.6	-29.2	0.3	-29.9	0.6
Me C16:0	-28.4	0.5	-30.5	0.3	-27.5	0.6	-29.7	0.2	-29.2	0.4	-29.2	0.1
Me 10 Me C16:0	-32.1	1.2	-28.7	0.4	-29.6	0.8	-37.8	3.1	-28.8	0.5	-29.2	0.6
Me C16:1w9	-24.3	2.1	-25.4	0.4	-22.8	1.5	-29.3	1.7	-27.7	0.9	-24	1.5
Me C16:1w7	-30.4	0.2	-30.3	0.3	-28	0.8	-31.8	0.4	-30	0.4	-30.9	0.6
Me C16:1w5	-29.8	0.4	-29.5	0.3	-25.1	0.9	-30.6	0.2	-29.6	0.2	-30.2	0.5
Me C17:0 cy	-35.5	4.8	-32.9	1.1	-33	0.7	-32.6	4.2	-31.7	1	-31.5	0.8
Me C18:0	-30.3	0.1	-31.7	0.3	-28.3	0.8	-29.7	0.6	-31.2	0.5	-30.5	0.2
Me 10 Me C18:0	-30.7	0.2	-31.4	0.7	-30.6	1	-28	2.2	-29.7	0.8	-30.5	0.5
Me C18:1w9c	-29.7	0.2	-30	0.3	-24.7	1.2	-29.9	0.2	-29.7	0.5	-29.4	0.2
Me C18:1w7c	-34.3	3.7	-28.9	0.4	-32.2	0.8	-29.5	0.5	-29.1	0.6	-28.3	0.6
Me C18:2(n6)	-30	0.3	-33.2	0.2	-26.3	0.7	-34	0.5	-31.1	0.4	-30.8	0.1
Me C19:0 cy	-41.9	3.6	-39.5	1.8	n.a.	n.a.	-71.9	28	-49.3	13.9	-35.5	1.1
Me C18:3(n3)	-38.9	0.2	-39	0.4	-34.7	0.8	-37.7	0.4	-39.1	0.4	-36.4	0.3
Me C20:0	-29	0.9	-31.4	1.2	n.a.	n.a.	n.a.	n.a.	-27.2	1.6	-25.3	1.8
Me C20:1w9c	-42.9	1.8	n.a.	n.a.	-43.5	4.7	-40.1	6.2	-43.5	3.6	-43.7	3.8
Me C21:0	-33.1	0.6	-34.7	0.5	-29.3	0.7	-34.6	0.3	-35.2	0.5	-34.7	1
Me C22:0	-34.8	0.3	-35	0.5	-32.5	0.5	-35.1	0.2	-34.6	0.3	-33.9	0.4
Me C23:0	-34.7	0.2	-35	0.4	-31.7	0.4	-35.2	0.3	-35.6	0.3	-35.3	0.5
Me C24:0	-34.3	0.3	-33.2	0.2	-31.4	0.5	-34.9	0.6	-33.1	0.4	-32.7	0.3
Me C26:0	-35.5	0.4	-34.4	0.2	-32.9	0.6	-35.6	0.5	-35.6	0.5	-35	0.3

Table C4. Vietnam, Chieng Khoi catchment. Mean topsoil (0-2 cm) SOC (%) and $\delta^{13}C$ (‰) values for soil bulk carbon and topsoil-derived $\delta^{13}C$-FAME values (‰) for identified fatty acids for each soil source, i.e. land use type of each catchment. Mean (M) and standard error (SE) are included.

	Vietnam - Chieng Khoi											
	NF		SF		MA		CA		TE		OR	
Fatty Acid (‰)	M	SE	M	SE	M	SE	M	SE	M	SE	M	SE
SOC (%)	2.9	0.3	1.6	0.1	0.8	0.1	0.7	0.1	1.2	0.1	0.9	0.1
Bulk $\delta^{13}C$	-26.8	0.1	-27.6	0.2	-24.0	0.3	-24.8	0.3	-26.3	0.2	-26.1	0.3
Me C12:0	-30.2	0.4	-29.1	0.1	-28.1	0.4	-27.2	0.5	-28.0	0.3	-28.3	0.1
Me C13:0	-27.6	0.5	-27.9	0.5	-27.4	0.6	-24.3	0.1	-25.3	0.6	-27.3	0.8
Me C14:0	-31.9	0.6	-31.0	0.3	-28.3	0.3	-28.4	0.4	-29.4	0.4	-29.0	0.3
Me C14:1	-27.9	0.3	-28.4	0.6	-24.7	0.6	-24.5	0.5	-26.9	0.4	-26.4	0.3
Me C15:0	-30.2	1.1	-29.4	0.3	-27.6	0.5	-27.5	0.8	-29.0	0.9	-28.2	0.3
Me C15:1	-29.3	0.8	-30.0	0.0	-28.7	0.4	-26.2	0.9	-31.2	1.4	-28.0	0.3
Me C16:0	-31.3	0.4	-32.8	0.8	-27.5	0.4	-26.9	0.4	-29.7	1.0	-27.3	0.2
Me C16:1	-28.4	0.3	-30.1	1.0	-25.8	0.6	-30.8	1.1	-28.7	0.4	-28.7	1.2
Me C17:0 cy	-28.1	0.1	-29.0	0.2	-24.8	1.0	-26.5	2.1	-27.9	0.6	-29.1	0.7
Me C18:0	-29.7	0.3	-32.9	1.0	-27.1	0.3	-26.8	0.3	-28.9	0.5	-27.5	0.2
Me C18 comb	-29.6	0.2	-29.8	0.5	-27.4	0.5	-30.2	0.5	-29.1	0.2	-28.1	0.4
Me C20:0	-34.1	0.8	-33.0	1.0	-28.5	0.6	-28.4	0.4	-32.4	0.7	-30.7	0.4
Me C22:0	-34.2	0.4	-33.1	0.9	-29.5	0.4	-29.7	0.6	-33.1	0.8	-32.3	0.3
Me C24:0	-34.7	0.8	-33.4	1.0	-29.2	0.7	-29.7	0.6	-33.4	0.7	-31.8	0.4

Table C5. China, Xinzheng catchment. Mean topsoil (0-2 cm) SOC (%) and $\delta^{13}C$ (‰) values for soil bulk carbon and topsoil-derived $\delta^{13}C$-FAME values (‰) for identified fatty acids for each soil source, i.e. land use type of each catchment. Mean (M) and standard error (SE) are included.

	China – Xinzheng													
	OR		RP		MX		YB		YC		CF		BF	
Fatty Acid (‰)	M	SE	M	SE	M	SE	M	SE	M	SE	M	SE	M	SE
SOC (%)	1.7	0.3	1.0	0.1	2.3	1.1	1.4	0.5	1.3	0.2	4.2	0.5	2.5	0.9
Bulk $\delta^{13}C$	-25.6	0.6	-26.2	0.3	-23.6	2.3	-25.9	0.4	-23.4	1.1	-26.7	0.3	-26.1	0.4
Me C12:0	-33.4	0.3	-28.3	0.4	-28.8	0.6	n.a.	n.a.	-26.8	0.7	-31.4	0.2	n.a.	n.a.
Me C13:0	-29.8	0.4	-26.8	0.4	-25.6	0.3	-26.7	0.1	-29.2	0.3	-28.1	0.8	-26.7	0.2
Me C14:0	-33.0	0.9	-31.3	0.7	-28.1	0.6	-30.7	0.7	-28.8	1.1	-33.2	0.4	-30.0	0.7
Me C14:1	n.a.	n.a.	-30.4	0.3	-27.4	0.5	n.a.	n.a.	-23.1	1.4	-27.8	0.4	n.a.	n.a.
Me C15:0	-30.0	1.0	-29.6	0.4	-28.5	0.5	n.a.	n.a.	-21.8	0.3	-34.7	1.9	n.a.	n.a.
Me C15:1	-29.4	0.4	-33.1	0.2	-27.8	0.4	n.a.	n.a.	-24.7	1.9	-33.0	1.3	-30.0	0.1
Me C16:0	-31.1	0.9	-31.3	1.9	-26.9	0.4	-29.9	1.1	-20.8	0.6	-32.3	0.6	-32.6	0.2
Me C16:1	n.a.	n.a.	n.a.	n.a.	n.a.	n.a.	n.a.	n.a.	n.a.	n.a.	n.a.	n.a.	n.a.	n.a.
Me C17:0 cy	n.a.	n.a.	n.a.	n.a.	n.a.	n.a.	n.a.	n.a.	n.a.	n.a.	n.a.	n.a.	n.a.	n.a.
Me C18:0	-30.3	1.0	-28.7	0.7	-24.3	0.5	-27.4	1.4	n.a.	n.a.	n.a.	n.a.	-32.0	0.2
Me C18 comb	-33.8	1.6	-29.8	1.1	-29.8	0.6	n.a.	n.a.	-22.3	2.6	n.a.	n.a.	-32.6	2.0
Me C20:0	-35.0	1.1	-32.9	0.9	-29.0	0.7	-31.0	1.5	n.a.	n.a.	-32.7	0.7	-33.5	1.8
Me C22:0	-34.5	1.3	-34.7	0.8	-31.8	0.4	-33.3	1.2	-31.0	2.8	-35.5	0.2	-33.2	0.7
Me C24:0	-34.3	0.7	-32.7	0.5	-32.0	0.4	-36.6	0.6	-29.8	2.3	-35.4	0.7	-34.6	0.8

Table C5. Morocco, My Bouchta catchment. Mean topsoil (0-2 cm) SOC (%) and $\delta^{13}C$ (‰) values for soil bulk carbon and topsoil-derived $\delta^{13}C$-FAME values (‰) for identified fatty acids for each soil source, i.e. land use type of each catchment. Mean (M) and standard error (SE) are included.

	Morocco - My Bouchta					
	CE		NF		SL	
Fatty Acid (‰)	M	SE	M	SE	M	SE
SOC (%)	0.4	0.1	4.6	0.6	1.1	0.7
Bulk $\delta^{13}C$	-26.9	0.3	-27.9	0.3	-25.0	2.8
Me C12:0	-31.0	0.6	-30.7	0.5	-30.9	0.9
Me C13:0	-29.5	0.7	-29.0	0.9	-29.2	1.0
Me C14:0	-30.6	0.9	-32.9	0.7	-31.3	0.6
Me C14:1	-28.2	1.2	-27.2	1.4	-27.1	0.8
Me C15:0	-26.1	0.6	-25.6	2.1	-26.4	1.0
Me C15:1	-28.5	0.7	-28.1	0.3	-29.0	0.4
Me C16:0	-30.1	0.7	-29.3	0.7	-30.0	0.8
Me C16:1	-28.8	0.5	-27.9	0.9	-28.6	0.4
Me C17:0 cy	-27.9	2.4	n.a.	n.a.	n.a.	n.a.
Me C18:0	-29.2	0.4	n.a.	n.a.	-29.9	0.5
Me C18 comb	-28.1	0.4	-28.1	0.3	-28.8	0.2
Me C20:0	-32.0	0.6	-31.9	1.0	-31.6	1.1
Me C22:0	-32.3	0.4	-32.6	1.0	-31.7	1.3
Me C24:0	-33.3	0.4	-32.7	0.9	-34.1	1.1

*C18 comb' comprises of C18:1 (Oleic acid) and C18:2 (Linoleic acid) whose individual $\delta^{13}C$ signatures could not be completely resolved for every sample.

Christian Brandt

Address	Steinpilzweg 27, 70599 Stuttgart
Phone	+49(0)1782888776
e-mail	christian.brandt@uni-hohenheim.de
Date of birth	1977-09-09

Experience

2009-07-present

Research scientist

University of Hohenheim, Institute of Agricultural Sciences in the Tropics and Subtropics (Hans-Ruthenberg-Institute), Stuttgart, Germany

Key responsibilities

- Research on integrated isotopic approaches for an area-wide precision conservation to control the impacts of agricultural practices on land degradation and soil erosion (FAO/IAEA Coordinated Research Project)
- Proposal establishment for third-party funds (e.g. DFG, BMBF, FAO/IAEA)
- Lecturing responsibilities in Bachelor and Master courses Mentoring students in the planning, execution and writing of their master's thesis

2005-07-2008-04

Research scientist

Institute of Crop and Resource Conservation, Department of Plant Nutrition, University of Bonn, Germany

Key responsibilities

- Planning, organizing and realizing of argo-ecological studies (plant nutrition, stress physiology and soil sciences) in the resource management project: “Closing Nutrient Cycles in Decentralised Water Treatment Systems in the Mekong-Delta”. Stationed in Can Tho, Vietnam (30 months)
- Planning and establishment of a constructed and planted wetland for wastewater treatment, Can Tho University, Vietnam
- Coordination with project partners and management of activities related to my sub-projects
- Organizing and conducting field trips and stakeholder meetings

Education

2009-07-present	**University of Hohenheim, Faculty of Agriculture, Stuttgart, Germany** PhD candidate
2003-09-2004-07	**Julius Maximilians University of Würzburg, Germany** Diploma thesis: "Local food and medicinal plants of the Serranía de Cuenca (Casilla-La Mancha, Spain) and phytochemical investigation of *Merendera montana* (L.) Lange (Colchicaceae)"
2003-09-2004-06	**Centre for Pharmacognosy and Phytotherapy, School of Pharmacy, University of London, London, UK** Laboratory work for diploma thesis
2001-03-2004-09	**Julius Maximilians University of Würzburg, Germany, Biology (Dipl.) (*Hauptstudium*)** Title of qualification awarded: Diplom-Biologist Univ. Principal subjects: Molecular plant physiology and biophysics Pharmaceutical biology Animal ecology and tropical biology
1998-03-2001-02	**Johannes Gutenberg University of Mainz, Germany, Biology (Dipl.) (*Grundstudium*)**

Publications

Brandt, C., Dercon, G., Cadisch, G., Nguyen, L.T., Schuller, P., Bravo Linares, C., Castillo Santana, A., Golosov, V., Benmansour, M., Amenzou, N., Xinbao, Z., Rasche, F., 2018. Towards global applicability – Erosion source discrimination across catchments using compound-specific $\delta^{13}C$ isotopes. Agriculture, Ecosystems and Environment 256, 114-122.

Brandt, C., Benmansour, M., Walz, L., Nguyen, L.T., Cadisch, G., Rasche, F., 2018. Integrating compound-specific $\delta^{13}C$ isotopes and fallout radionuclides to retrace land use type specific net erosion rates in a small tropical catchment exposed to intense land use change. Geoderma 310, 53-64.

Brandt, C., Cadisch, G., Nguyen, L.T., Vien, T.D., Rasche, F., 2016. Compound-specific $\delta^{13}C$ isotopes and Bayesian inference for erosion estimates under different land use in Vietnam. Goderma Regional 7, 311–322.

Stuttgart, April 3, 2018. Christian Brandt